Evaluation of Failure Criteria for Continuous Fiber Reinforced Composites

by

REIDAR KVALE JOKI

THESIS

for the degree of

MASTER OF SCIENCE

(Master i Anvendt matematikk og mekanikk)

Faculty of Mathematics and Natural Sciences
University of Oslo

May 27, 2011

Det matematisk- naturvitenskapelige fakultet
Universitetet i Oslo

Forword This thesis is written for the degree of Master of Science, at the University of Oslo, department of Mathematics, Mechanics division. The work with this thesis has been carried out at SINTEF Materials and Chemistry, department of Synthesis and Properties in Oslo.

During this one year dissertation I have learned a lot on material testing, the interpretation of test results, the complexity of laminated composite materials and the problems associated with determining the properties of these materials. The numerous hours spent developing and meshing Finite Element models, troubleshooting, studying theory manuals and making the results understandable and suited for presentation, has gained me valuable insights into the world of Finite Element Method. This work, as part of an ongoing research project at SINTEF, has introduced me to the working life of a researcher, by preparing presentations and collaborating in project meetings. The task of preparing a conference article, the process of undergoing peer review and holding a conference speech, has also given me new insights.

I am indebted to my supervisor Dr. Frode Grytten at SINTEF, for the numerous hours he has spent by my side explaining the bits and bolts of LS-DYNA and LS-OPT. I would not have been able to scope the entirety of this work with out his guidance. My supervisor at the University of Oslo, Associated Professor Harald Osnes, has my deepest gratitude for thorough guidance in writing this thesis and for always taking the time to counsel me. I would also like to thank Dr. Einar L. Hinrichsen at SINTEF for including me as a contributing partner in the COMPACT project, and finding me suited for a post-graduate fellowship.

Finally I would like to direct my sincere gratitude to my wife, Anne Kvale Joki, and my two sons Alexander and Philip for their patience and all the encouragement they have given me.

Abstract This thesis gives an overview of in-plane failure mechanisms in fiber reinforced polymer composite laminates. Three different failure criteria are evaluated, and the Puck failure criterion is described and evaluated thoroughly. A progressive failure analysis is developed based on the Puck failure criterion and optimized to fit experimental observations using the optimization tool LS-OPT. The material model is implemented in the LS-DYNA finite element code, and all numerical analyses in this thesis are modeled and simulated using this finite element code. Results from the numerical analyses have been compared with material test results and other published numerical results. Material tests have been carried out, and material properties have been extracted from material tests. The implemented material model is shown to produce damage behavior in good agreement with experimental observations, and the localization and mode of failure and fracture are also shown to be in good agreement with that of material test results and other published numerical results.

Contents

List of Figures

List of Tables

Symbols

A	Area
$\mathbf{A}$	Extensional stiffness matrix
α	angle
$\mathbf{B}$	Coupling stiffness matrix
$\mathbf{D}$	Bending stiffness matrix
δ	any elongation
E_c	Young modulus in composite
E_f	Young modulus in fiber
E_m	Young modulus in matrix
E_1	Young modulus in fiber direction
E_2	Young modulus in transverse direction
e	Various failure parameters
ϵ_1	Strain in fiber direction
ϵ_2	Strain in transverse direction
ϵ_c	Strain in composite
ϵ_f	Strain in fiber
ϵ_m	Strain in matrix
$\epsilon_u c$	Ultimate strain in compression
$\epsilon_u t$	Ultimate strain in tension
ϵ_{12}	Shear strain
F	Strength tensor
FF	Fiber failure
$f(\sigma)$	Failure surface in the stress space
G_{12}	Shear modulus
γ_{12}	Engineering shear strain
γ_{12}^u	Ultimate engineering shear strain
IFF	Inter fiber failure
k	curvature
$\mathbf{K}$	Global stiffness matrix
$\mathbf{k}$	Element stiffness matrix
M	Bending moments
$m_{\sigma f}$	Stress magnification factor
$\mathbf{N}$	Shape function vector

N	Normal forces
ν_{12}	Major Poisson's factor
ν_{21}	Minor Poisson's factor
P	Any applied force
$\mathbf{Q}$	Single ply stiffness matrix (material coordinates)
$\bar{\mathbf{Q}}$	Single ply stiffness matrix (global koordinates)
$\mathbf{R}$	Global forces
$\mathbf{r}$	Global displacements
ρ_c	Composite density
ρ_f	Fiber density
ρ_m	Matrix density
S	Ply shear strength
σ_1	Stress in fiber direction
σ_2	Stress in transverse direction
σ_c	Stress in composite
σ_f	Stress in fiber
σ_m	Stress in matrix
$\sigma_u t$	Ultimate stress in tension
$\sigma_u c$	Ultimate stress in compression
τ_{u12}	Ultimate shear stress
τ_{12}	Shear stress
θ	Material orientation
θ_{fp}	Angle of failure plane - arbitrary loading
θ^0_{fp}	Angle of failure plane - pure transverse compressive loading
u	Energy per unit area
$\mathbf{u}$	Displacement vector
V_f	Fiber volume fraction
v_f	Fiber volume
V_m	Matrix volume fraction
v_m	Matrix volume
W_f	Fiber weight fraction
w_f	Fiber weight
W_m	Matrix weight fraction
w_f	Matrix weight
ξ	Reinforcement factor
X_t	Longitudinal strength in tension
X_c	Longitudinal strength in compression
Y_t	Transverse strength in tension
Y_c	Transverse strength in compression
z_k	Distance from laminate mid surface to ply k
$(10\gamma_{21})^2$	empirical factor used in Puck failure criteria
$\perp$	Referes to transverse

$\parallel$	Referes to parallel

Chapter 1

Introduction

1.1 General background

The simplest definition of a composite material is a material with two or more distinct constituents. One example is Fiber Reinforced Polymer Composites, or FRPC. These composites are being used in many applications varying from sporting goods, sailboats and cabin cruisers to naval vessels and the aircraft and aerospace industry. FRPC materials are increasingly being used in all these applications due to their favorable combination of low weight, good mechanical properties and absence of corrosion. The use of composites have been pioneered by industries where performance is more important than costs. Examples of this can be seen in Figure 1.1, where the F1 represents the state of the art in raceing cars, and the Oracle trimaran sailboat represents the ultimate performance sail boat with a mainsail twice the size of a Boing 747 wing and a top speed of more than 40 knots. In the military industry, performance is literally a question of life and death. In Figure 1.2, the Joint Strike Fighter has a fuselage made up of a combination of aluminum and laminated composites, and the Skjold Class Fast Patrol Boat is one of many naval vessels constructed with composite materials.

The use of composites as engineering materials is an old technology. One early example of the use of a composite is the reinforcement of clay bricks with straw, in order to reduce shrinkage during drying and to improve their fracture toughness[8]. Today we achieve similar favorable features by distributing aggregates in a cement matrix giving concrete its favorable material properties. There are many natural structures and materials which make use of the symbiotic relationships possible from the combination of several different constituents. Examples in our own body are bone and muscle, and in nature there are numerous examples from specific sedimentary rocks to wood. Wood achieves its impressive variety of mechanical properties by the formations of cells which combine the strength of cellulose fibers, see Figure 1.3, with the ductility of a lignin matrix.

Composite materials have replaced more traditional materials in many ap-

Figure 1.1: On the left: The BMW Saubar F1 Racecar[1], Ragasco LPG cylinder [2], The BMW Oracle [3]

Figure 1.2: On the left: The Joint Strike Fighter [4], the Skjold Class FPB [5]

plications. Unlike isotropic materials (which means the material-properties are the same in all directions), composites can have different material-properties in different directions. This makes it possible for the mechanical properties to be engineered for specific loading conditions, and the structure to behave in specific ways when laded. The blades of wind turbines are an example of this[7].

The electricity producing generator in the windmill has an upper and lower limit for rotating speeds, but the rotating speed of a fixed-bladed wind turbine will vary due to changes in wind velocity. Engineering the blades with laminates of continuous fiber reinforced polymer organized in a specific way allows the blades to twist with increasing rotational speed, decreasing the wind lift on the blade [12]. This, in addition to mechanically pitching of the whole blade, enables the windmill to generate electricity from a wider range of wind velocities. Even though this is a remarkable attribute, the main driver for the use of FRP in wind energy systems is the need to optimize stiffness-to-weight as wind turbine designers increase blade length to make turbines more cost-effective.

Unlike ductile metals that can absorb large amounts of energy via plasticity without loss of strength, brittle composites absorb energy by elastic deformation and irreversible damage mechanisms. This makes composites sensitive to impact loading. The design of composite to resist impact or crash events represents a difficult task for the composite engineer. The combination of a fundamental knowledge of the behavior of composite laminates subjected to impact loading, and advanced modeling tools that can predict impact behavior, will substantially

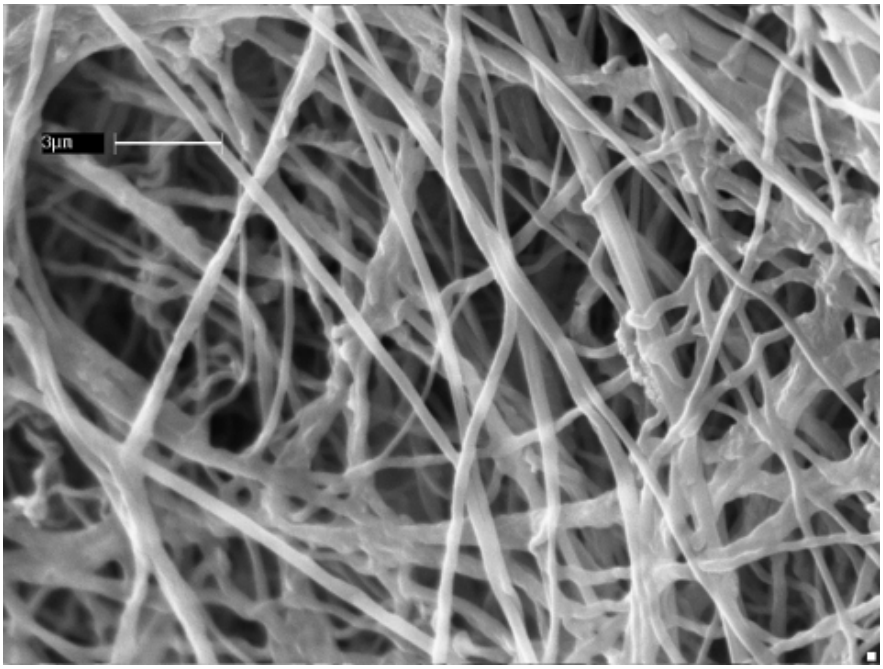

Figure 1.3: Microscopic view of cellulose nanofibers [6]

add to the designers toolbox.

1.2 Specification of the thesis

The content of the thesis is limited to cover continuous fiber reinforced composites subjected to in-plane quasi-static loads.

- The candidate will carry out mechanical testing on industrial relevant laminates to determine the necessary input parameters for numerical modeling (FEM). This includes elastic parameters and strength parameters for use in material models describing damage (in-plane).

- The numerical modeling should also be verified with regard to accuracy and resilience by appropriate mechanical testing.

- The candidate will establish numerical models of the mechanical tests using a commercial finite element program.

- The different failure criteria available in the finite element program is to be evaluated.

Figure 1.4: Blade production for the Gamesa G8X 2-MX wind turbine [7]

1.3 Organization of the thesis

In Chapter 2 the basics of composite materials will be presented. First the properties of composite plies will be presented, before the theories governing laminates of composite material are described.

Chapter 3 covers failure criteria for composite material. Here the criteria readily available in the commercial finite element program will be presented, as well as the implemented Puck failure criterion.

Chapter 4 describes the material testing carried out. The standards used for the material testing, the testing equipment and the test specimen are also presented.

Chapter 5 is dedicated to finite element analysis. The LS-DYNA finite element code is briefly presented. Some aspects of the finite element method applied to composite material will be described.

In Chapter 6, *Case study 1: Puck failure criteria* is presented. The study describes the implementation of a material model using the criterion in the LS-DYNA finite element code, verification of the material model and comparison of the model to other available material models in LS-DYNA.

In Chapter 7, *Case study 2: Pinhole loaded FRPC plate* is presented. The study describes the effects of different laminate layups. The results are compared to other results found in literature.

In Chapter 8, *Case study 3: Shear test Geometry* is presented. The objective

of the study is to describe a stress concentration in a specific specimen geometry subjected to the V-notched rail shear test, ASTM D7078, found in material tests conducted at SINTEF in Oslo.

Final discussions and conclusions are presented in Chapter 9. Some thoughts regarding this thesis in a larger perspective are presented and some directions for further work based on the findings are also pointed out.

In the Appendix, an article subjected to the MekIT'11 conference in Trondheim in May 2011 is included. The article describes some of the work carried out in Case study 1. Also included in the Appendix, are some of the input files for the work carried out in Matlab and LS-DYNA.

Chapter 2

Composite Materials

2.1 Basic mechanical properties

Composite materials are primarily divided into two groups, fiber reinforced composites and particle reinforced composites. The fiber reinforced composites are divided into single layer and multilayered composites. The single layer composites are subsequently divided into continuous- and discontinuous fiber reinforced composites. The continuous fiber reinforced composites can be unidirectional or bidirectional (woven reinforcement). The current study addresses continuous fiber reinforced composites, and the other kinds of composites mentioned will not be further discussed in this thesis.

The mechanical properties of a unidirectional fiber reinforced composite is governed by the properties of the fiber and the matrix, the volume fraction of the two and the bond between them. Their properties depend on the direction in which they are measured. The direction of the fibers is defined as the longitudinal direction (denoted as 1-direction), and the two directions transverse to the fibers as the transverse directions, one in-plane (denoted as 2-direction) and one out of plane (denoted as 3-direction). The longitudinal properties are fiber dominated, and the properties in the two transverse directions are matrix dominated. Thus the mechanical properties of FRP composites are defined by three orthogonal directions, 1,2 and 3. These composites are said to be orthotropic. If the properties in all directions transverse to the fibers are identical, the material is defined as transversely isotropic. This is one of the basic assumptions made by most failure criteria presented in this thesis.

2.1.1 Volume and weight fractions

One of the most important factors determining the properties of composites is the relative proportions of the matrix and the fibers. The relative proportions can be given as weight fractions or volume fractions. The basic relationship between composite, matrix and fiber are described by the following: $v_c = v_f + v_m$ and

$w_c = w_m + w_f$. Where v_c, v_m and v_f are the volume of the composite, the matrix and the fiber, respectively, and w_c, w_m and w_f are the corresponding weights of the constituents. From this the volume fractions can be derived

$$V_f = \frac{v_f}{v_c} \ and \ V_m = \frac{v_m}{v_c} \tag{2.1}$$

and the weight fractions

$$W_f = \frac{w_f}{w_c} \ and \ W_m = \frac{w_m}{w_c}. \tag{2.2}$$

If the density is taken into account, the weight relationships can be rewritten using the accompanying volumes

$$\rho_c v_c = \rho_f v_f + \rho_m v_m, \tag{2.3}$$

where ρ is the density. By dividing both sides with c_v, an expression for the density of the composite emerges

$$\rho_c = \rho_f \frac{v_f}{v_c} + \rho_m \frac{v_m}{v_c} = \rho_f V_f + \rho_m V_m, \tag{2.4}$$

or by weight fractions

$$\rho_c = \frac{1}{\frac{W_f}{\rho_f} + \frac{W_m}{\rho_m}}. \tag{2.5}$$

Now the link between weight fractions and volume fractions can be derived

$$W_f = \frac{w_f}{w_c} = \frac{\rho_f v_f}{\rho_c v_c} = \frac{\rho_f}{\rho_c} V_f \tag{2.6}$$

and

$$W_m = \frac{\rho_m}{\rho_c} V_m. \tag{2.7}$$

2.1.2 Longitudinal stiffness and strength

The fibers are assumed to be uniform in properties and diameter, continuous, and parallel throughout the composite and that there exists a perfect bond between the matrix and the fibers so that no slippage can occur at the interface. When subjected to longitudinal loading the elongation in this direction will be the same for all the constituents, i.e. $\epsilon_f = \epsilon_m = \epsilon_c$. The longitudinal loading, P, will be divided between fiber and matrix.

$$P_c = P_f + P_m, \tag{2.8}$$

$$P_c = \sigma_c A_c = \sigma_f A_f + \sigma_m A_m, \tag{2.9}$$

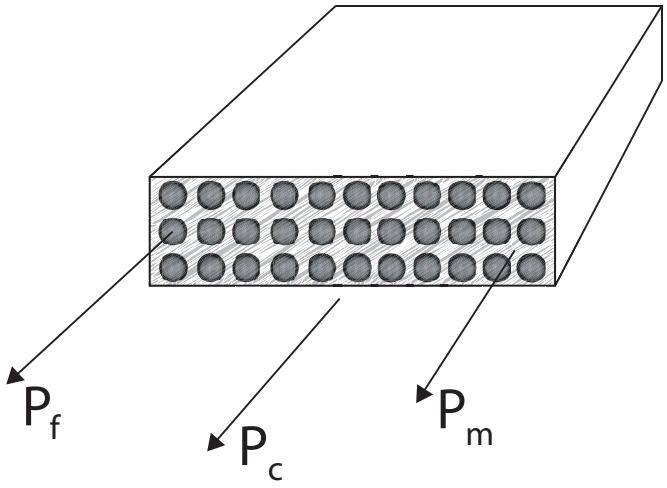

Figure 2.1: An illustration of the cross section of a continuous fiber reinforced composite

where σ is the stress and A is the corresponding cross section area on which the stress is applied

$$\sigma_c = \sigma_f \frac{A_f}{A_c} + \sigma_m \frac{A_m}{A_c}. \tag{2.10}$$

By assuming a proportional relationship between the volume and the cross sectional area

$$\frac{A_f}{A_c} = \frac{v_f}{v_c} = V_f \tag{2.11}$$

$$\frac{A_m}{A_c} = \frac{v_m}{v_c} = V_m, \tag{2.12}$$

the level of stress in the fibers or in the matrix can be extracted

$$\sigma_c = \sigma_f V_f + \sigma_m V_m. \tag{2.13}$$

With this relationship and the assumptions made above regarding the stress in matrix and fiber being the same as for the whole composite, the Young's modulus for the composite in longitudinal tension can be derived.

$$E_c = E_f V_f + E_m V_m \tag{2.14}$$

In a unidirectional composite subjected to a longitudinal load, failure initiates when the fibers are strained to their fracture strain. It is assumed that the failure strain of the fibers is less than of the matrix [13]. For theoretical predictions it is also assumed that all the fibers fail at the same time, and that the matrix is not able to support the entire load when all the fibers break. Composite failure will then take place instantly. Under these conditions the ultimate longitudinal

tensile strength of the composite can be assumed equal to the composite stress at the fiber fracture strain ϵ_f^*. The rule of mixture therefore can be used to obtain

$$\sigma_{cu} = \sigma_{fu} V_f + (\sigma_m)_{\epsilon_f^*} V_m \tag{2.15}$$

where σ_{cu} is the longitudinal strength of the composite, σ_{fu} is the ultimate strength of the fibers, and $(\sigma_m)_{\epsilon_f^*}$ is the matrix stress at the fiber fracture strain ϵ_f^*.

If the fiber volume fraction is small, that is, below a given V_{min} the matrix will be able to support the entire composite load when all the fibers break. It is assumed that the fibers do not support any load at composite strains higher than the fiber fracture strain. The composite eventually fails when the matrix stress equals its ultimate strength. This yields an ultimate strain of the composite when the fiber volume fraction less than V_{min}

$$\sigma_{cu} = \sigma_{mu} V_m. \tag{2.16}$$

The minimum fiber volume fraction that ensures fiber-controlled composite failure, V_{min}, is defined as

$$V_{min} = \frac{\sigma_{mu} - (\sigma_m)_{\epsilon_f^*}}{\sigma_{fu} + \sigma_{mu} - (\sigma_m)_{\epsilon_f^*}}. \tag{2.17}$$

While deriving the expressions for longitudinal stiffness and strength, many simplifying assumptions regarding the physical variables of the system were made. Only some of these assumptions were stated explicitly, whereas others were implied. The factors influencing the stiffness and strength of composites are (1) missorientation of fibers, (2) fibers of nonuniform strength, (3) discontinuous fibers, (4) interfacial conditions, and (5) residual stresses.

2.1.3 Transverse stiffness and strength

A simple mathematical model may be constructed for studying the transverse properties of composites in the same manner as the one constructed earlier for studying the longitudinal properties in Section 2.1.2. The fibers are assumed to be uniform in properties and diameter, continuous and parallel through the composite. The composite is subjected to tensile loading in the transverse direction, i.e. the direction perpendicular to the parallel fibers. In this model we think of the fibers and matrix as layers side by side, bonded together. This is illustrated in Figure 2.2. Each layer is perpendicular to the direction of the loading and has the same area on which the load acts. This meaning that every layer carries the same load and experience equal stress, i.e.

$$\sigma_f = \sigma_m = \sigma_c. \tag{2.18}$$

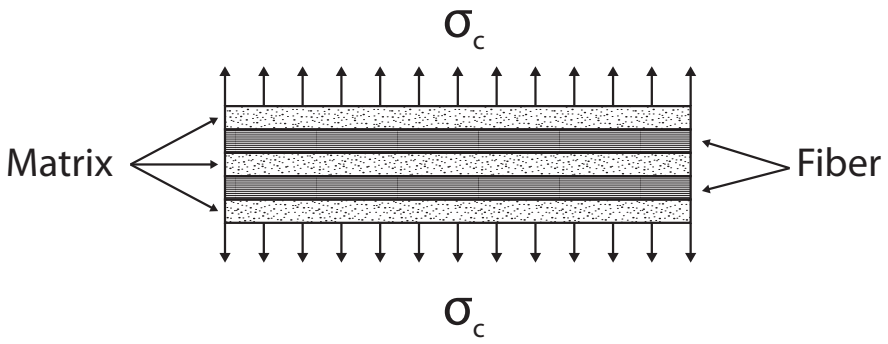

Figure 2.2: An illustration of the cross section of a continuous fiber reinforced composite

The elongation of the composite δ_c is the sum of the elongation of the matrix δ_m and the fiber δ_f, i.e.

$$\delta_c = \delta_m + \delta_f. \tag{2.19}$$

The elongation is the product of the strain and the width. Based on this, the previous equation can be rewritten

$$\epsilon_c t_c = \epsilon_m t_m + \epsilon_f t_f. \tag{2.20}$$

The thickness is proportional to the volume, and by dividing both sides by the thickness of the composites, the composite strain can be expressed by summing up the products of strain and volume fraction of the matrix and the fibers

$$\epsilon_c = \epsilon_m V_m + \epsilon_f V_f. \tag{2.21}$$

The strains can be expressed as the stress divided by the Young's modulus

$$\frac{\sigma_c}{E_c} = \frac{\sigma_m}{E_m} V_m + \frac{\sigma_f}{E_f} V_f. \tag{2.22}$$

Given the relationship in Equation (2.18), this equation can be written as

$$\frac{1}{E_c} = \frac{1}{E_m} V_m + \frac{1}{E_f} V_f, \tag{2.23}$$

which gives an expression for the Young's modulus in the transverse direction of the composite,

$$E_c = \frac{1}{\frac{V_f}{E_f} + \frac{V_m}{E_m}}. \tag{2.24}$$

The simplifications made while deriving the expressions for the transverse stiffness makes the model insufficient in predicting true values. Consequently the transverse modulus derived from this equation does not correspond to the results

from material testing. Halpin and Tsai [14] have developed simple and generalized equations to approximate the results of more exact micro mechanical analyses. The equations are quite accurate if the fiber volume fraction does not approach 1.

$$\frac{E_T}{E_m} = \frac{1 + \xi\eta V_f}{1 - \eta V_f} \tag{2.25}$$

where

$$\eta = \frac{(E_f/E_m) - 1}{(E_f/E_m) + \xi} \tag{2.26}$$

ξ is a measure of reinforcement and depends on the fiber geometry, packing geometry and loading conditions. The values of ξ is obtained by comparing Equation (2.25) and (2.26) with exact elasticity solutions through curve-fitting techniques. Halpin and Tsai have suggested that a value of $\xi = 2$ may be used for fibers with circular or square cross sections. For rectangular cross-section fibers, ξ may be calculated as

$$\xi = 2\frac{a}{b} \tag{2.27}$$

where a/b is the rectangular cross-section aspect ratio with the dimension a taken in the direction of the loading.

When a unidirectional composite is subjected to transverse loads, the fibers, as a result of the geometry, are unable to take the same proportion of the load as they do in the case of longitudinal loading. The high-modulus fibers serve as effective constraints on the deformation of the matrix, which results in the transverse composite modulus being higher than the matrix modulus, although only marginally unless the fiber volume fraction is very high. In the terms of the transverse strength, the constraints placed on the matrix by the fibers cause strain and stress concentrations in the matrix adjacent to the fibers and thus results in composite failure at a much lower macroscopic strain than the strain at which the unrestrained matrix material fails. Therefore, unlike the longitudinal strength and stiffness and transverse modulus, the transverse strength is reduced because of the presence of the fibers.

2.1.4 Shear properties

Assuming the same model as used for prediction the transverse properties, the shear stress on the fibers and the matrix are equal. Thus

$$\tau_c = \tau_m = \tau_f. \tag{2.28}$$

The total shear deformation of the composite δ_c is the sum of the shear deformation in the fibers δ_f and in the matrix δ_m

$$\delta_c = \delta_m + \delta_f. \tag{2.29}$$

The shear deformation in each material can be written as the product of the thickness and the shear strain

$$\begin{aligned} \delta_c &= \gamma_c t_c, \\ \delta_m &= \gamma_m t_m, \\ \delta_f &= \gamma_f t_f. \end{aligned} \tag{2.30}$$

Substituting this into Equation (2.29) gives

$$\delta_c t_c = \delta_m t_m + \delta_f t_f. \tag{2.31}$$

Dividing both sides with the thickness of the composite, (t_c) and recognizing that the thickness is proportional to the volume fraction, yields

$$\begin{aligned} \gamma_c &= \gamma_m \frac{t_m}{t_c} + \gamma_f \frac{t_f}{t_m} \\ &= \gamma_m V_m + \gamma_f V_f. \end{aligned} \tag{2.32}$$

If the shear stress-shear strain relationship of fiber and matrix is assumed linear, the shear strains can be replaced by the shear strain divided by the shear modulus as follows:

$$\frac{\tau_c}{G_c} = \frac{\tau_m}{G_m} V_m + \frac{\tau_f}{G_f} V_f. \tag{2.33}$$

The relationship in Equation (2.28) allows for the following simplification

$$\frac{1}{G_c} = \frac{1}{G_m} V_m + \frac{1}{G_f} V_f. \tag{2.34}$$

From this an expression for the in-plane shear modulus can be derived

$$G_c = \frac{G_f G_m}{G_m V_f + G_f V_m}. \tag{2.35}$$

2.1.5 Poisson's ratio

For in-plane loading of a unidirectional composite two Poisson's ratios are defined. The first of these relates the longitudinal stress to the transverse strain. This will be denoted as ν_{12}, normally referred to as major Poisson's ratio. The second, ν_{21}, relates the transverse stress to longitudinal strain, normally referred to as minor Poisson's ratio.

The major Poisson's ratio can be predicted using the same model as that used for predicting the Young's modulus in the longitudinal direction. Only this time the load is applied in transverse direction. The model yields

$$\nu_{12} = \nu_f V_f + \nu_m V_m, \tag{2.36}$$

which is the rule of mixtures for the major Poisson's ratio of a unidirectional composite. The minor Poisson's ratio can be obtain from the following relation

$$\frac{\nu_{12}}{E_1} = \frac{\nu_{21}}{E_2}, \tag{2.37}$$

where E_1 is the Young's modulus in the longitudinal direction for the composite and E_2 is the Young's modulus in the transverse direction for the composite.

2.2 Mechanical properties of a single lamina

In the following longitudinal direction will be denoted as 1, and transverse in plane direction will be denoted as 2. For a lamina loaded either parallel or perpendicular to the fiber direction, the equations below may be used to describe the in-plane stress-strain relationship. They are known as the constitutive equations

$$\begin{aligned} \epsilon_1 &= \frac{\sigma_1}{E_1} - \nu_{21}\frac{\sigma_2}{E_2}, \\ \epsilon_2 &= \frac{\sigma_2}{E_2} - \nu_{12}\frac{\sigma_1}{E_1}, \\ \gamma_{12} &= \frac{\tau_{12}}{G_{12}}. \end{aligned} \tag{2.38}$$

With the relationship between the major and the minor Poisson's ratio shown in Equation (2.37) the four parameters required to characterize the in-plane elastic behavior of a continuous fiber reinforced composite are E_1, E_2, ν_{12} and G_{12}.

When a unidirectional lamina is loaded at an angle other than one of the principal directions, the analysis is more complicated. Initially the stresses are resolved into the principal directions using Mohr's circle, where θ is the angle between the fibers and the loading direction,

$$\begin{aligned} \sigma_1 &= \sigma_x \cos^2\theta + \sigma_y \sin^2\theta + \tau_{xy} 2\sin\theta\,\cos\theta, \\ \sigma_2 &= \sigma_x \sin^2\theta + \sigma_y \cos^2\theta - \tau_{xy} 2\sin\theta\,\cos\theta, \\ \tau_{12} &= -\sigma_x \sin\theta\,\cos\theta + \sigma_y \sin\theta\,\cos\theta + \tau_{xy}(\cos^2\theta - \sin^2\theta), \end{aligned} \tag{2.39}$$

where σ_1, σ_2 and τ_{12} are the in-plane stresses parallel and perpendicular to the fiber direction and σ_x, σ_y and τ_{xy} are the in-plane stresses resolved to the lamina orientation. This may be expressed in matrix form

$$\begin{bmatrix} \sigma_1 \\ \sigma_2 \\ \tau_{12} \end{bmatrix} = \begin{bmatrix} \cos^2\theta & \sin^2\theta & 2\sin\theta\,\cos\theta \\ \sin^2\theta & \cos^2\theta & -2\sin\theta\,\cos\theta \\ -\sin\theta\,\cos\theta & \sin\theta\,\cos\theta & \cos^2\theta - \sin^2\theta \end{bmatrix} \begin{bmatrix} \sigma_x \\ \sigma_y \\ \tau_{xy} \end{bmatrix}, \tag{2.40}$$

or in reduced form, where $[T]$ is given above

$$\begin{bmatrix} \sigma_1 \\ \sigma_2 \\ \tau_{12} \end{bmatrix} = [T] \begin{bmatrix} \sigma_x \\ \sigma_y \\ \tau_{xy} \end{bmatrix}, \tag{2.41}$$

and by inverting

$$\begin{bmatrix} \sigma_x \\ \sigma_y \\ \tau_{xy} \end{bmatrix} = [T]^{-1} \begin{bmatrix} \sigma_1 \\ \sigma_2 \\ \tau_{12} \end{bmatrix}, \tag{2.42}$$

where T^{-1} is the inverse of T

$$[T]^{-1} = \begin{bmatrix} \cos^2\theta & \sin^2\theta & -2\sin\theta\,\cos\theta \\ \sin^2\theta & \cos^2\theta & 2\sin\theta\,\cos\theta \\ \sin\theta\,\cos\theta & -\sin\theta\,\cos\theta & \cos^2\theta - \sin^2\theta \end{bmatrix}. \tag{2.43}$$

It is possible to use the same notation to relate the strains

$$\begin{bmatrix} \epsilon_1 \\ \epsilon_2 \\ \frac{1}{2}\gamma_{12} \end{bmatrix} = [T] \begin{bmatrix} \epsilon_x \\ \epsilon_y \\ \frac{1}{2}\gamma_{xy} \end{bmatrix}, \tag{2.44}$$

$$\begin{bmatrix} \epsilon_x \\ \epsilon_y \\ \frac{1}{2}\gamma_{xy} \end{bmatrix} = [T]^{-1} \begin{bmatrix} \epsilon_1 \\ \epsilon_2 \\ \frac{1}{2}\gamma_{12} \end{bmatrix}. \tag{2.45}$$

It should be pointed out that we multiply the shear strains with $\frac{1}{2}$ because engineering strains are being calculated rather than tensorial strains. This allows Equation (2.38) to be rewritten as

$$\begin{bmatrix} \sigma_1 \\ \sigma_2 \\ \tau_{12} \end{bmatrix} = \begin{bmatrix} Q_{11} & Q_{12} & 0 \\ Q_{12} & Q_{22} & 0 \\ 0 & 0 & Q_{66} \end{bmatrix} \begin{bmatrix} \epsilon_1 \\ \epsilon_2 \\ \gamma_{12} \end{bmatrix}, \tag{2.46}$$

where

$$\begin{aligned} Q_{11} &= \frac{E_1}{(1-\nu_{12}\,\nu_{21})}, \\ Q_{22} &= \frac{E_2}{(1-\nu_{12}\,\nu_{21})}, \\ Q_{11} &= \frac{\nu_{12}\,E_2}{(1-\nu_{12}\,\nu_{21})}, \\ Q_{66} &= G_{12}. \end{aligned} \tag{2.47}$$

The substitution of Equations (2.44) and (2.46) into Equation (2.42) gives the following expression

$$\begin{bmatrix} \sigma_x \\ \sigma_y \\ \tau_{xy} \end{bmatrix} = \begin{bmatrix} \bar{Q}_{11} & \bar{Q}_{12} & \bar{Q}_{16} \\ \bar{Q}_{12} & \bar{Q}_{22} & \bar{Q}_{26} \\ \bar{Q}_{16} & \bar{Q}_{26} & \bar{Q}_{66} \end{bmatrix} \begin{bmatrix} \epsilon_x \\ \epsilon_y \\ \gamma_{xy} \end{bmatrix}, \tag{2.48}$$

where

$$\begin{bmatrix} \bar{Q}_{11} & \bar{Q}_{12} & \bar{Q}_{16} \\ \bar{Q}_{12} & \bar{Q}_{22} & \bar{Q}_{26} \\ \bar{Q}_{16} & \bar{Q}_{26} & \bar{Q}_{66} \end{bmatrix} = [T]^{-1} \begin{bmatrix} Q_{11} & Q_{12} & 0 \\ Q_{12} & Q_{22} & 0 \\ 0 & 0 & Q_{66} \end{bmatrix} [T]. \tag{2.49}$$

2.3 Mechanical properties of laminates

A laminated composite is made up of several lamina or plies stacked on-top of each other. A laminate is considered to be thin from a mathematical point of view. That is, its length and width is significantly greater than its thickness. Even though a laminate is thin (e.g. 5 mm) it can consist of a great number of plies. In order to simplify the description of the laminates, a notation is derived for the lay-up and stacking sequence. A laminate with lamina orientations in 0°, 90°, 90° and 0°, may be described as $[0/90_2/0]$ where the subscript 2 indicates that there are two plies with the 90° orientation. The same laminate may also be described as $[0/90]_s$ where the subscript s denotes a symmetric stacking sequence. Laminates with this lay-up are referred to as cross-ply laminates. A laminate containing plies with angles other than 0° and 90° is called a angle-ply laminate. A laminate with a lay-up like $[0/90/\pm 45]_s$ where there are equal quantities of material in each of the four directions and it is both balanced (i.e. each positive ply has an equal and opposite negative ply) and symmetric, is referred to as quasi-isotropic. The $\pm$ symbol means that there is an adjacent $-45°$ ply for every $+45°$ ply.

When examining the stress and strain distribution within a laminate the simplest technique is to use laminated plate theory. The analysis of laminates has to include out of plane loads and deformations, that is moments, curvature and twisting.

The stress state for the K^{th} ply within a laminate containing n plies subjected to a force per unit width and moment per unit width may be described by

$$\begin{bmatrix} \sigma_x \\ \sigma_y \\ \tau_{xy} \end{bmatrix}_K = \begin{bmatrix} \bar{Q}_{11} & \bar{Q}_{12} & \bar{Q}_{16} \\ \bar{Q}_{12} & \bar{Q}_{22} & \bar{Q}_{26} \\ \bar{Q}_{16} & \bar{Q}_{26} & \bar{Q}_{66} \end{bmatrix}_K \begin{bmatrix} \epsilon_1 \\ \epsilon_2 \\ \gamma_{12} \end{bmatrix}_K . \tag{2.50}$$

The matrix for the entire laminate stack is assembled by examining the corresponding matrix for each layer, and then adding them together

$$[A_{ij}]_1 = \sum_{k=1}^{n} (\bar{Q}_{ij})_k (z_k - z_{k-1}), \tag{2.51}$$

where A_{ij} is the extensional stiffness matrix for the laminate, $\bar{Q}_{ij}$ is the transformed reduced stiffness matrix of each lamina and $(z_k - z_{k-1})$ is the distance from the bending plane of the lamina to the neutral axis of the laminate. To account for out-of-plane forces and deformations, and coupling between in- and out-of-plane forces and deformations we use the following

$$[B_{ij}]_1 = \frac{1}{2} \sum_{k=1}^{n} (\bar{Q}_{ij})_k (z_k^2 - z_{k-1}^2), \tag{2.52}$$

$$[D_{ij}]_1 = \frac{1}{3} \sum_{k=1}^{n} (\bar{Q}_{ij})_k (z_k^3 - z_{k-1}^3). \tag{2.53}$$

The full matrix is given by

$$\begin{bmatrix} N_x \\ N_y \\ N_{xy} \\ M_x \\ M_y \\ M_{xy} \end{bmatrix} = \begin{bmatrix} A_{11} & A_{12} & A_{16} & B_{11} & B_{12} & B_{16} \\ A_{12} & A_{22} & A_{26} & B_{12} & B_{22} & B_{26} \\ A_{16} & A_{26} & A_{66} & B_{16} & B_{26} & B_{66} \\ B_{11} & B_{12} & B_{16} & D_{11} & D_{12} & D_{16} \\ B_{12} & B_{22} & B_{26} & D_{12} & D_{22} & D_{26} \\ B_{16} & B_{26} & B_{66} & D_{16} & D_{26} & D_{66} \end{bmatrix} \begin{bmatrix} \epsilon_x^0 \\ \epsilon_y^0 \\ \epsilon_{xy}^0 \\ k_x \\ k_y \\ k_{xy} \end{bmatrix}, \tag{2.54}$$

where N_x, N_y and N_{xy} are the in-plane forces per unit width and M_x, M_y and M_{xy} are the applied moments per unit width. In Figure 2.3 the behavioral effects of the different factors is illustrated. These factors allow the designers to tailor the behavior of a laminate to their specific requirements. In Figure 2.3. the coupling

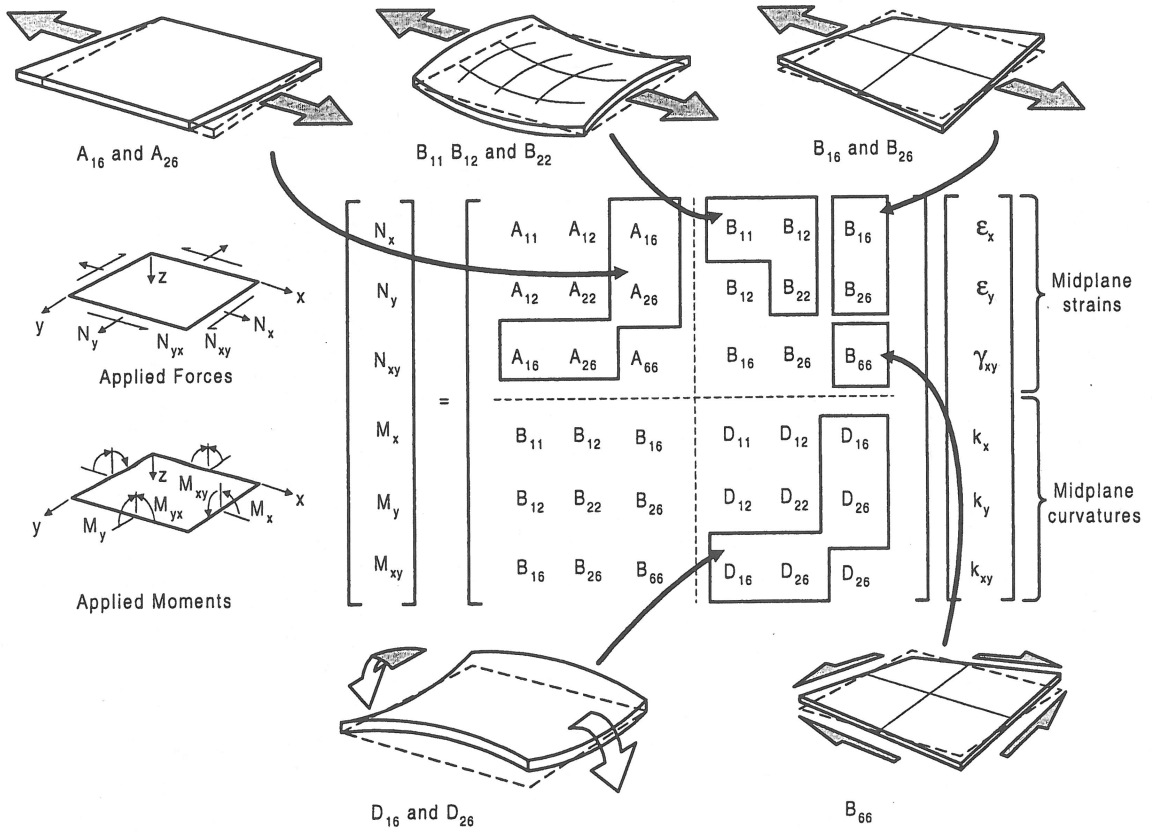

Figure 2.3: An illustration of coupling phenomena in laminated composite plates. [8]

effects mentioned in Chapter 1, is evident.

We can make the following associations:

- A_{16} and A_{26} relate in-plane direct forces to in-plane shear strain, or in-plane shear forces to in-plane direct strains.

- B_{11}, B_{12} and B_{22} relate in-plane direct forces to plate curvatures, or bending moments to in-plane direct strains.
- B_{16} and B_{26} relate in-plane direct forces to plate twisting, or torque to in-plane direct strains.
- B_{66} relates in-plane shear force to plate twisting, or torque to in-plane shear strain.
- D_{16} and D_{26} relate bending moments to plate twisting, or torque to plate curvature.

In certain circumstances some of the couplings listed above can be undesirable. They can be eliminated by appropriate construction of the laminate.

If $A_{16} = A_{26} = 0$ there will be no coupling between direct stress and shear strains, or shear stress and direct strains. This can be achieved if we have a laminate in which all plies have 0° and/or 90° fiber orientation (a unidirectional or cross-ply laminate), or if the lay up is balanced, i.e. for every layer with a $+\theta$ orientation there is an identical lamina with a $-\theta$ orientation.

Bending-stretching coupling occurs due to a non zero B matrix. This coupling can be eliminated if the laminate construction reduces each element of the B matrix to zero. In Equation (2.52), it is shown that the contribution by each ply to a particular term in the B matrix is given by the square of the z coordinate of the top and bottom of each ply. The contribution of a ply above the midplane can be nullified by placing an identical (in properties and orientation) ply an equal distance below the midplane. The B matrix is identical to zero for laminates in which for each ply above the midplane there is an identical ply placed an equal distance below the midplane. Laminates that are constructed in this way are referred to *symmetric laminates* These laminates are commonly constructed because bending-stretching coupling is eliminated, which in non symmetric laminates cause warping due to in-plane plane loads. Temperature changes will also cause warping of non symmetric laminates. When these laminates are fabricated at an elevated temperature, warping will result when they are cooled to room temperature.

The bending-stretching coupling effect can be minimized for non symmetric laminates if the plies are relatively thin compared to the laminate thickness and the non symmetric stacking sequence is repeated many times through the thickness of the laminate. This will not result in a non zero **B**-matrix, but it will approach zero as the repetitions of the stacking sequence increase.

The phenomenon of bending-twisting coupling is eliminated if $D_{16} = D_{26} = 0$. This is achieved with unidirectional or cross-ply laminates, or with balanced anti symmetric lay ups, i.e. for every layer at $+\theta$ orientation and a given distance above the mid-plane there is a layer with identical thickness and properties oriented at $-\theta$ and the same distance below the mid-plane. Such a lay up is not

symmetrical, i.e. $B \neq 0$. The preference for symmetrical laminates mean D_{16} and $D_{26} \neq 0$. However, these terms tend to zero for thick multilayer symmetric laminates.

For some lay-ups in-plane behavior of the laminate is such that it appears to be isotropic. It is then called quasi-isotropic. Examples are $[0/90/\pm 45^\circ]$ and $[0 \pm 60^\circ]$ lay-ups. For such laminates, $A_{11} = A_{22}$, $A_{11} - A_{12} = 2A_{66}$ and $A_{16} = A_{26} = 0$.

Chapter 3

Failure criteria - strength predictions

When a solid is subjected to any kind of loading, static or dynamic, it can absorb energy by two basic mechanisms: material deformation and creation of new surfaces. The material deformation occurs first. If the loading supplies a sufficient amount of energy, a crack may initiate and propagate, creating new surfaces, which is the second source of energy absorption. The material deformation continues ahead of the crack tip during crack propagation. The more brittle a material is, the less energy it can absorb in material deformation before additional energy initiate fracture. The energy associated with fracture surface creation is thus relatively low for brittle materials. They are said to have low energy-absorbing capability or low toughness. Ductile materials on the other hand can absorb a lot of energy by plastic deformation. They are said to have high energy-absorbing capability or high toughness. This shows that the energy absorbing capability or toughness of a material can be enhanced by increasing its plastic deformation capability or by increasing the creation of new surfaces during fracture [13].

3.1 Failure in composite material

When a fiber reinforced polymer composite fracture, a wide range of different energy-absorbing mechanisms and failure modes are involved. The failure modes are generally divided into failure in fiber, failure in matrix and delamination. In Figure 3.1, a variety of failure-modes are illustrated [9]. In the following, different failure-modes and associated energies are discussed. Delamination is not covered in this thesis and will not be discussed.

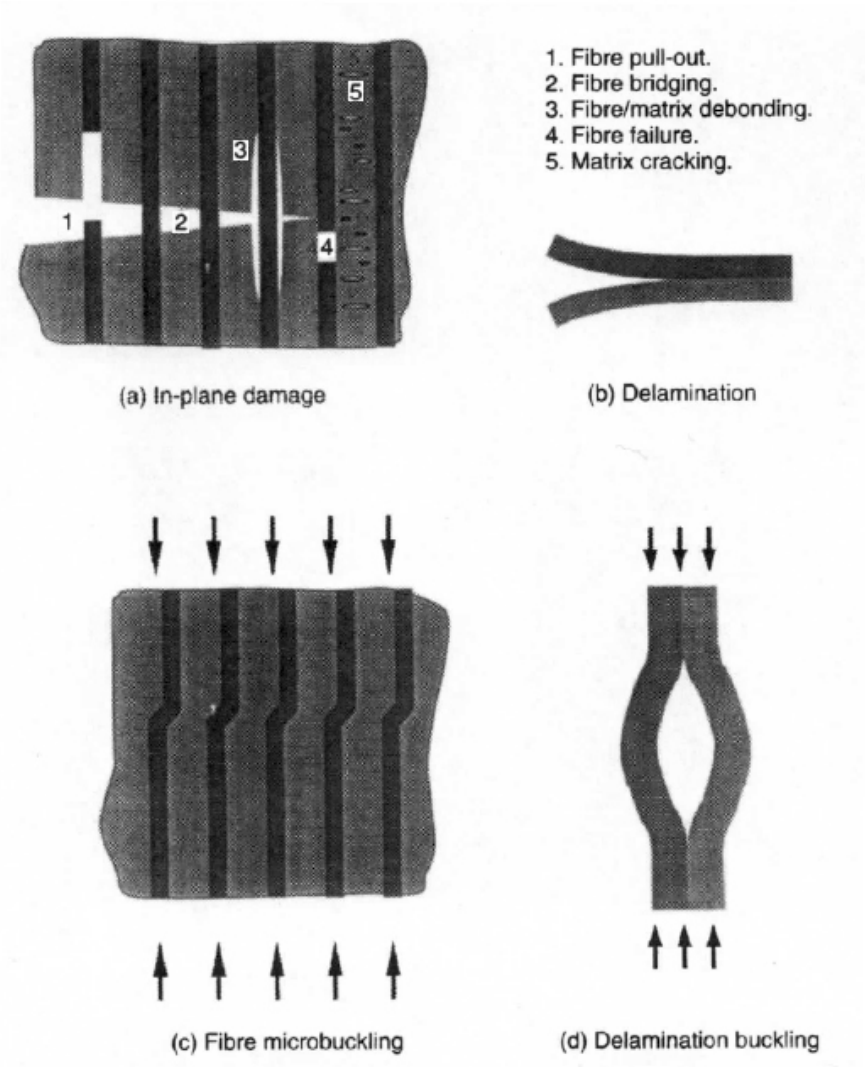

Figure 3.1: Four different failure-modes illustrated. The failure-modes are described in detail in [9].

3.1.1 Failure in fibers

Whenever a crack has to propagate in the direction normal to the fibers, fiber breakage will eventually occur for complete separation of the global fracture of the laminate. In such cases, the fibers cracks when their fracture strain is reached. Brittle fibers have a low fracture strain and hence have a low energy-absorbing capability. The energy required per unit area of the composite for fracture of fibers in tension is given by the following expression [15]

$$u = \frac{V_f \sigma_{fu}^2 l}{6E_f}, \tag{3.1}$$

where V_f is the fiber volume fraction, σ_{fu} is the ultimate stress of the fibers, E_f is the fiber modulus, and l is the fiber length. For composites with continuous fibers, it is more suitable to use the critical fiber length[16] (i.e. the minimum length of fiber needed for the matrix to be able to transfer the ultimate strain of the fiber to the fiber). Although the fibers are responsible for imparting high strength to the composites, the fracture of the fibers account for only a very small fraction of the total energy absorbed. It has been observed experimentally [16] that the number of fibers fractured has little influence on the total impact energy. The presence of fibers, however, significantly influences the failure modes and in that way the total energy absorbed.

3.1.2 Matrix deformation and cracking

The matrix material surrounding the fibers has to fracture to complete the failure of the composite. Thermosetting resins, such as epoxies and polyesters, are brittle materials and can undergo only a limited deformation prior to fracture. The work done in deforming the matrix is proportional to the work done in deforming the matrix to rupture per unit volume U_m times the volume of the matrix deformed per unit area of the crack surface [17]. Based on the equation derived by Cooper and Kelly [18] for the volume of matrix affected by fracture, the energy required for matrix fracture per unit area of composite is given by

$$u = \frac{(1 - V_f)^2}{V_f} \frac{\sigma_{mu} d}{4\tau} U_m, \tag{3.2}$$

where σ_{mu} is the tensile strength of the matrix, d is the fiber diameter, and τ is the interfacial shear stress. The total energy absorbed by matrix cracking is equal to the product of the surface energy and the new area produced by the crack. When a crack propagates in a single direction, the new area produced is small, producing small fracture energy. Large crack areas may be produced by crack branching, in which case the crack runs in the direction normal to the general direction of the fracture. For example, when a matrix crack encounters a strong fiber placed perpendicular, or at a large angle to the direction of the crack propagation, the crack may branch and run parallel to the fiber as well. In many cases the surface area produced by the secondary cracks (the branches) is much larger than the surface area of the primary cracks.

3.1.3 Strength of a single unidirectional ply

When calculating the strength of a composite, it is convenient to begin with an analysis of a single ply. One of the most basic theories to use for calculating the strength is the maximum stress criterion. It assumes that failure occurs when the stress, either parallel or perpendicular to the fibers, reaches a critical value.

The critical values are given as

$$\begin{aligned} |\sigma_1| &\geqslant \sigma_{1u}, \\ |\sigma_2| &\geqslant \sigma_{2u}, \\ \tau_{12} &\geqslant \tau_{12u}, \end{aligned} \tag{3.3}$$

where σ_{1u} is the failure stress parallel to the fibers, σ_{2u} is the failure stress perpendicular to the fibers and τ_{12u} is the shear strength of the lamina. By comparing these with equation (2.39) it is possible to resolve the stresses in a ply into principal direction and predict the failure mode for the lamina. These expressions are given as

$$\begin{aligned} \sigma_{f_1} &= \frac{\sigma_{1u}}{\cos^2\theta}, \\ \sigma_{f_2} &= \frac{\sigma_{2u}}{\sin^2\theta}, \\ \tau_{f_{12}} &= \frac{\tau_{12u}}{\sin\theta\,\cos\theta}, \end{aligned} \tag{3.4}$$

where $\sigma_{f_1}, \sigma_{f_2}$ and $\tau_{f_{12}}$ are the failure stresses for each mode at an angle θ to the fiber direction of the lamina. The failure mode is determined at a specific angle when the lowest of these failure stresses is exceeded. This is illustrated in Figure 3.2. This is quite a rough approach to reality, and results will most

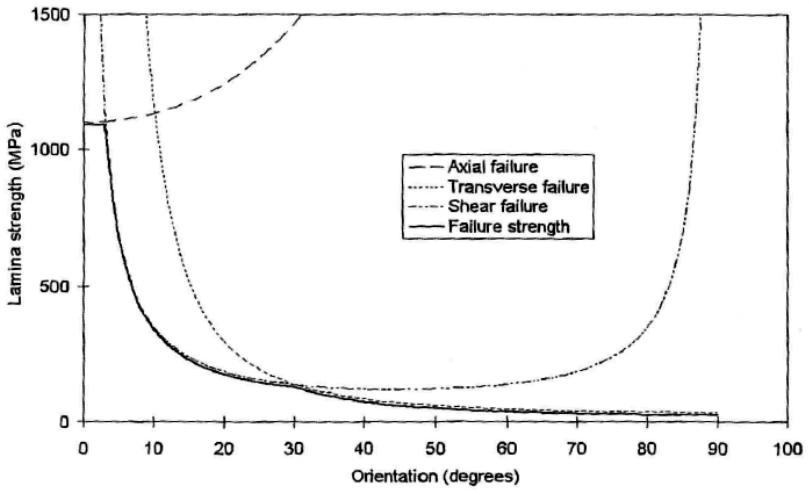

Figure 3.2: Variation of lamina failure strength with orientation (θ) for the three failure modes of the maximum stress failure criteria [8].

likely diverge increasingly for experiments when the loading conditions or the

material lay up and geometry gets more complicated. A lot of work has been carried out in the field of finding a set of failure criteria that predicts failure in composite materials. When composites are exposed to loading combinations of normal- and shear stress, most criteria fail to predict the outcome correctly. This is an ongoing process, and in the latter years, considerable progress in this field has been obtained. In the following some failure criteria are presented.

3.2 Failure criteria

3.2.1 Tsai-Wu failure model

The Tsai-Wu criterion [19] is purely empirical. The basic assumption is that a failure surface exists in the stress space on the following form

$$f(\sigma) = F_i\sigma_i + F_{ij}\sigma_i\sigma_j = 1, \tag{3.5}$$

where F_i and F_{ij} are strength tensors of first and second order, respectively. If we confine ourselves to unidirectional layers oriented at various angles through a rotation about the 3-axis from the specially transverse isotropic orientation, the strength tensors in terms of engineering strengths are as follows

$$F_i = \begin{bmatrix} \frac{1}{X_t} - \frac{1}{X_c} \\ \frac{1}{Y_t} - \frac{1}{Y_c} \\ \frac{1}{Y_t} - \frac{1}{Y_c} \\ 0 \\ 0 \\ 0 \end{bmatrix}, \tag{3.6}$$

$$F_{ij} = \begin{bmatrix} \frac{1}{X_tX_c} & F_{12} & F_{12} & 0 & 0 & 0 \\ & \frac{1}{Y_tY_c} & F_{23} & 0 & 0 & 0 \\ & & \frac{1}{Y_tY_c} & 0 & 0 & 0 \\ & & & 2\left(\frac{1}{Y_tY_c} - F_{23}\right) & 0 & 0 \\ & & & & \frac{1}{S_{12}^2} & 0 \\ & & & & & \frac{1}{S_{12}^2} \end{bmatrix}. \tag{3.7}$$

A plane stress representation of the general quadratic criterion reads

$$\frac{\sigma_1^2}{X_tX_c} + \frac{2F_{12}^*\sigma_1\sigma_2}{\sqrt{X_tX_cY_tY_c}} + \frac{\sigma_2^2}{Y_tY_c} + \frac{\tau_{12}^2}{S_{12}^2} + \left[\frac{1}{X_tX_c} - \frac{1}{X_c}\right]\sigma_1 + \left[\frac{1}{Y_tY_c} - \frac{1}{Y_c}\right]\sigma_2 = 1, \tag{3.8}$$

where X_t andX_c are the longitudinal tensile and compressive strengths, Y_t and Y_c are the transverse tensile and compressive strengths, S_{12} is the longitudinal shear strength and F_{12}^* is the normalized interaction term. The interaction term has a value $-1 > F_{12}^* > 1$, and can be determined by combined stress test. A value of $F_{12}^* = -1/2$ is referred to as the generalized von Mises model, and is claimed to be reasonable for most materials [20].

3.2.2 Chang-Chang failure model

Chang and Chang [21] consider three different in-plane failure modes: matrix failure, fiber failure and a third condition they have defined as fiber-matrix shearing. Fiber-matrix shearing is the condition that causes fiber pull-out, and fiber-matrix debonding. These mechanisms are illustrated in Figure 3.1. The criterion for matrix failure reads

$$\left(\frac{\sigma_2}{Y_t}\right)^2 + \frac{\int_0^{\gamma_{12}^{\text{current}}} \tau_{12} d\gamma_{12}}{\int_0^{\gamma_{12}^u} \tau_{12} d\gamma_{12}} = e^2, \tag{3.9}$$

where σ_2 is the transverse tensile stress and τ_{12} is the shear stress, while Y_t is the transverse tensile strength and γ_{12}^u is the ultimate shear strain. For laminates with linear elastic behavior this can be reduced to

$$\left(\frac{\sigma_2}{Y_t}\right)^2 + \frac{\tau_{12}}{S_{12}} = e^2, \tag{3.10}$$

where S_{12} is the shear strength. In both cases, failure occurs when $e^2 \geqslant 1$

Compressive failure in the matrix is predicted by

$$\left(\frac{\sigma_2^c}{2S_c}\right)^2 + \left[\left(\frac{Y_c}{2S_c}\right)^2 - 1\right]\frac{\sigma_2^c}{Y_c} + \frac{\int_0^{\gamma_{12}^{\text{current}}} \tau_{12} d\gamma_{12}}{\int_0^{\gamma_{12}^u} \tau_{12} d\gamma_{12}} = e^2. \tag{3.11}$$

For laminates with linear elastic behavior this is reduced to

$$\left(\frac{\sigma_2^c}{2S_c}\right)^2 + \left[\left(\frac{Y_c}{2S_c}\right)^2 - 1\right]\frac{\sigma_2^c}{Y_c} + \frac{\tau_{12}}{S_c} = e^2, \tag{3.12}$$

where Y_c is the transverse compressive strength and σ_2^c is the transverse compressive stress. For this failure mode, failure also occurs when $e^2 \geqslant 1$.

The following equation predicts both fiber failure and the fiber-matrix shearing condition,

$$\left(\frac{\sigma_1^t}{X_t}\right)^2 + \frac{\int_0^{\gamma_{12}^{\text{current}}} \tau_{12} d\gamma_{12}}{\int_0^{\gamma_{12}^u} \tau_{12} d\gamma_{12}} = e^2. \tag{3.13}$$

3.2.3 Puck failure model

The Puck failure criterion is based on a phenomenological model. In [10], Puck describes five different failure modes divided into 2 groups; fiber failure (FF) and interfiber failure (IFF). The longitudinal stress in the fiber under combined loading is obtained as

$$\sigma_{f1} = \epsilon_1 E_{f1} + \nu_{f12} m_{\sigma f} \sigma_2, \tag{3.14}$$

where the factor $m_{\sigma f}$ accounts for a *stress magnification effect* caused by the different moduli of fibers and matrix. When the tensile stress in the fibers reaches

the level that gave failure for uniaxial loading, it is assumed that failure occurs. Therefore, the tensile failure condition for the fibre (tensile FF) is

$$\frac{1}{\epsilon_{1T}}\left(\epsilon + \frac{\nu_{f12}}{E_{f1}} m_{\sigma f}\sigma_2\right) = 1. \tag{3.15}$$

Experimental results show that the compressive strength parallel to the fibers is reduced when a shear stress τ_{12} is imposed [10]. Puck therefore suggests an empirical shear correction, and the proposed failure condition in compression is

$$\frac{1}{\epsilon_{1T}}\left|\left(\epsilon + \frac{\nu_{f12}}{E_{f1}} m_{\sigma f}\sigma_2\right)\right| + (10\gamma_{21})^2 = 1, \tag{3.16}$$

where the compressive fracture strain ϵ_{1C} is given as a positive value, and $(10\gamma_{21})^2$ is a purely empirical term.

The Puck IFF criterion is based on a Mohr Columb friction type of failure. The underlying assumption is that a failure surface exists that is governed by the normal force and two orthogonal shear forces at the failure surface, one parallel, and the other normal to the fibers. In [10], Puck gives an analytical solution to IFF by dividing the criterion into three different modes, namely A, B and C. These three modes are illustrated i Figure 3.3. Mode A can be viewed as a tensile matrix mode, and mode B and C as compressive matrix modes. IFF mode A occurs when $\sigma_2 \geqslant 0$, and the condition is

$$\sqrt{\left(\frac{\tau_{21}}{S_{21}}\right)^2 + \left(1 - p^{(+)}_{\perp||}\frac{Y_t}{S_{21}}\right)^2\left(\frac{\sigma_2}{Y_t}\right)^2} + p^{(+)}_{\perp||}\frac{\sigma_2}{S_{21}} = 1 - \left|\frac{\sigma_1}{\sigma_{1D}}\right|, \tag{3.17}$$

where S_{21} is the in-plane shear strength of a unidirectional layer, Y_t is the transverse tensile strength and $p^{(+)}_{\perp||} = -\frac{\delta\tau_{21}}{\delta\sigma_2}|_{\sigma_2=0}$ is the slope of the $\sigma_2 - \tau_{21}$ curve for $\sigma_2 \geqslant 0$ at $\sigma_2 = 0$. Finally σ_{1D} is a stress value for linear degradation.

IFF mode B occur when $\sigma_2 \leqslant 0$ and $\left|\frac{\sigma_2}{\tau_{21}}\right| \leqslant \frac{R^A_{\perp\perp}}{S_{21}\sqrt{1+2p^{(-)}_{\perp\perp}}}$. The condition is

$$\frac{1}{S_{21}}\left(\sqrt{\tau_{21}^2 + \left(p^{(-)}_{\perp||}\sigma_2\right)^2} + p^{(-)}_{\perp||}\sigma_2\right) = 1 - \left|\frac{\sigma_1}{\sigma_{D1}}\right|, \tag{3.18}$$

where $p^{(-)}_{\perp||} = -\frac{\delta\tau_{21}}{\delta\sigma_2}|_{\sigma_2=0}$ is the slope of the $\sigma_2 - \tau 21$ curve for $\sigma_2 \leqslant 0$ at $\sigma_2 = 0$.

IFF mode C occur when $\sigma_2 \leqslant 0$ and $\left|\frac{\sigma_2}{\tau_{21}}\right| \geqslant \frac{R^A_{\perp\perp}}{S_{21}\sqrt{1+2p^{(-)}_{\perp\perp}}}$. The condition is

$$\left[\left(\frac{\tau_{21}}{1 + \left(p^{(-)}_{\perp\perp}S_{21}\right)}\right)^2 + \left(\frac{\sigma_2}{Y_c}\right)^2\right]\frac{-Y_c}{\sigma_2} = 1 - \left|\frac{\sigma_1}{\sigma_{D1}}\right|, \tag{3.19}$$

where $p_{\perp\perp}^{(-)} = \frac{1}{2}\left(\sqrt{1 + 2p_{\perp\parallel}^{(-)}\frac{Y_c}{S_{21}}} - 1\right)$, and Y_c is the transverse compressive strength. The difference between the two compressive matrix modes is the angle of the fracture plane. Mode B will as mode A have a fracture plane with an angle, $\theta_{fp} = 0$. The angle of the fracture plane in mode C will be non zero, and it is given by $\cos\theta_{fp} = \sqrt{\frac{f_w Y_c}{2\sigma_2\left(1+p_{\perp\perp}^{(-)}\right)}}$ where $f_w = 1 - \left|\frac{\sigma_1}{\sigma_{D1}}\right|$.

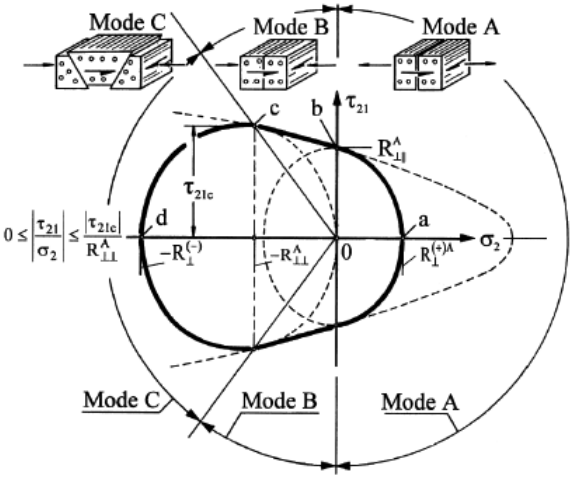

Figure 3.3: Puck's IFF locus for vanishing longitudinal stress. The figure is picked from [10].

This analytical solution to the failure criterion is only applicable to in-plane loading conditions (in two dimensional analysis). When taking into account out of plane effects and loading conditions in three dimensions, the Puck IFF criterion has no analytical solution. The full 3-D formulation of the Puck IFF criterion is formulated as follows

$$e^2 = \left(\frac{\sigma_n}{R_n}\right)^2 + \left(\frac{\tau_{n1}}{R_{n1} - p_{n1}\sigma_n}\right)^2 + \left(\frac{\tau_{nt}}{R_{nt} - p_{nt}\sigma_n}\right)^2 = 1 \text{ for } \sigma_n \geqslant 0, \quad (3.20)$$

$$e^2 = \left(\frac{\tau_{n1}}{R_{n1} - p_{n1}\sigma_n}\right)^2 + \left(\frac{\tau_{nt}}{R_{nt} - p_{nt}\sigma_n}\right)^2 = 1 \text{ for } \sigma_n < 0,$$

where the stress components σ_n, τ_{n1} and τ_{nt} are the stresses acting on the fracture surface as illustrated in Figure 3.4 and defined by the angle of the fracture surface, θ_{fp}, in Equation (3.23). The parameter R_n describes the resistance of the fracture plane against normal failure induced by σ_n. The parameters R_{n1} and R_{nt} are the resistance of the fracture plane against shear, and finally, p_{n1} and p_{nt} are the slope parameters representing internal friction effects (Mohr-Coulomb type of failure)

[22]. In [23], Puck suggests the following values for these parameters

$$\begin{aligned} R_n &= Y_t, \\ R_{n1} &= S_{12}, \\ R_{nt} &= \frac{Y_c}{2tan(\theta^0_{fp})}, \end{aligned} \tag{3.21}$$

$$\begin{aligned} p_{nt} &= -\frac{1}{tan(2\theta^0_{fp})}, \\ p_{n1} &= p_{nt}\frac{R_{n1}}{R_{nt}}. \end{aligned} \tag{3.22}$$

Here, Y_t and Y_c are the transverse strengths in tension and compression, respectively, and S_{12} is the shear strength. The angle θ^0_{fp} is the angle at which a specimen loaded in uniaxial compression in the transverse fiber direction fracture due to shear failure. When subjected to in-plane loading, IFF is provoked by σ_{22} and τ_{12}. The shape of the failure envelope depends strongly on θ^0_{fp}, which is illustrated in Figure 3.5. This angle can be viewed upon as a material property and has a constant value for a given material. It should be emphasized that this is not the same angle as the fracture angle defining the action plane of an arbitrary loading condition θ_{fp}.

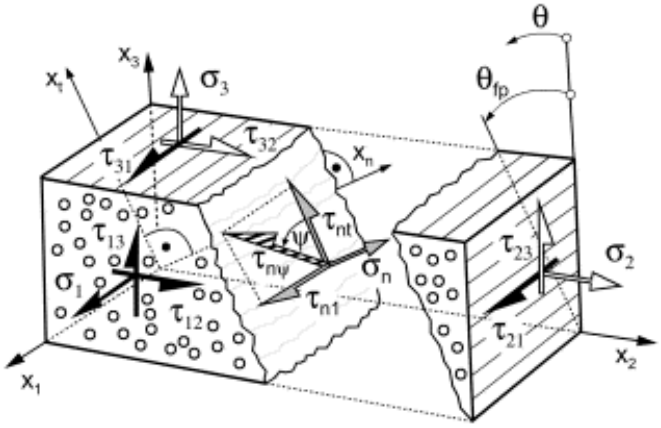

Figure 3.4: Illustration of the the fracture surface and the stress components acting on the surface [10].

$$\begin{aligned} \sigma_n &= \sigma_{22}cos^2\theta_{fp} + \sigma_{33}sin^2\theta_{fp} + 2\sigma_{23}cos\theta_{fp}sin\theta_{fp}, \\ \tau_{n1} &= \sigma_{12}cos\theta_{fp} + \sigma_{13}sin^2\theta_{fp}, \\ \tau_{nt} &= -\sigma_{22}sin\theta_{fp}cos\theta_{fp} + \sigma_{33}sin\theta_{fp}cos\theta_{fp} + \sigma_{23}(cos^2\theta_{fp} - sin^2\theta_{fp}). \end{aligned} \tag{3.23}$$

Because no analytical solution to the criterion is possible, one needs to search through all the possible failure surfaces to find the one in where the criterion

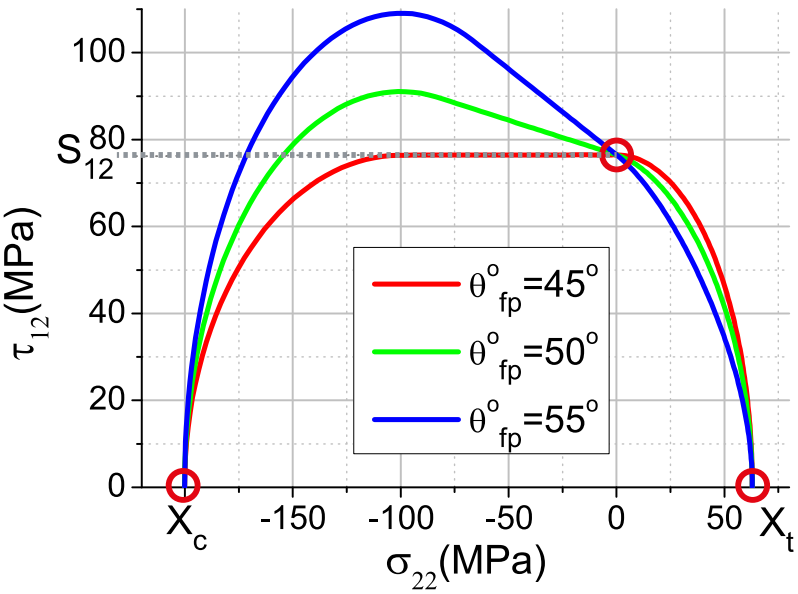

Figure 3.5: Failure envelope for the Puck IFF criterion for different values of θ^0_{fp}.

has its maximum value. The criterion is defined by the failure surface stress components σ_n, τ_{n1} and τ_{nt}, and consequently they have to be calculated for every search angle. Because of symmetry, the search for the action plane can be limited to the range $-90° \geqslant \theta \geqslant 90°$. A cost effective methodology is the Golden Section Search[22]. This procedure has been proven to be an effective tool when searching for the action plane using the Puck criterion by Wiegand et al. in [22].

3.2.4 Comparison of the different criteria

As mentioned above when a composite material is loaded purely in the fiber direction, transverse direction or in shear, the different criteria give the same results. Failure initiates when first ply failure stress/strain-level is reached. The different failure models diverges when the specimen is subjected to combined loading, e.g. a transverse loading combined with shear lading. This is illustrated in figure 3.6.

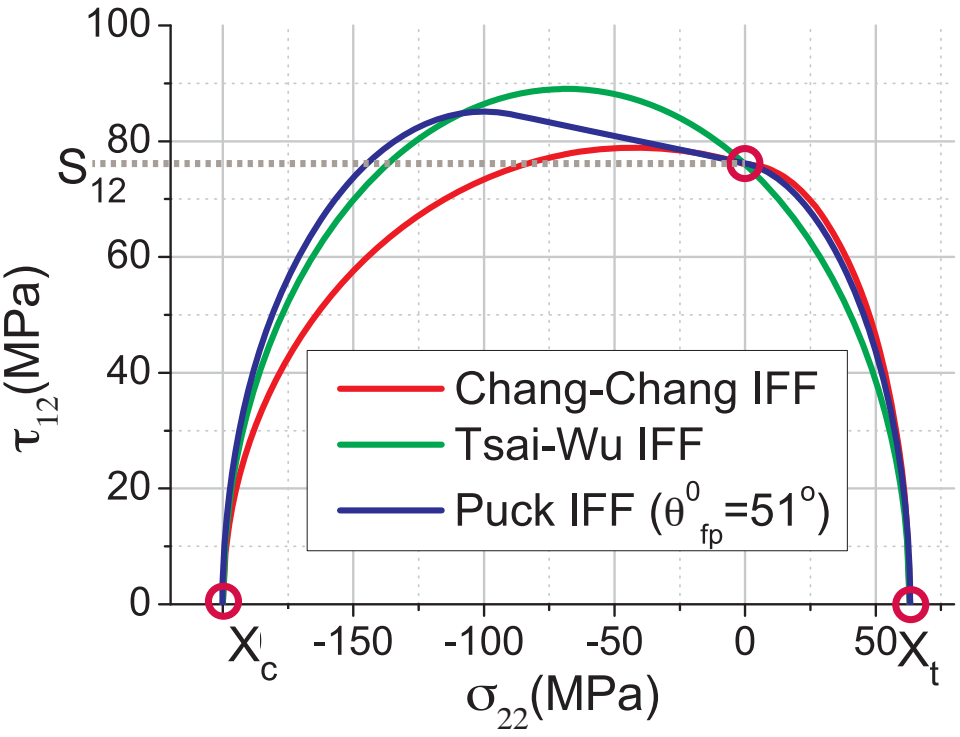

Figure 3.6: Failure locus for the transverse and shear loading domain, showing the difference between the Chang-Chang, Tsai-Wu and Puck interfiber failure criterion. It can be seen that they give the same results for pure loading conditions (red circles), but that there are some divergence for combined loading conditions. Especially they produce different failure levels for combined transverse compression and shear loading. It should also be noted that the shape of the curves are different.

Chapter 4

Material testing

The material tests evaluated in this study are divided into tests used as sources for definition of material properties to be implemented in the material model, and tests that are used in validation of the material model. When defining the material properties for composite laminates, the properties are defined for a unidirectional ply. The properties of the laminate are then calculated in the finite element code using classical laminate theory. This makes it easy to variate the laminate lay up without the need for gathering of new material properties.

When analyzing materials and making predictions on how they behave under various loading conditions it is curtail to have the correct inputs for the analysis. If the material properties used in the model diverge from those of the real construction, the model will probably not predict the actual behavior no matter how realistic or accurate the modeling has been conducted. It is easy to come to the conclusion that when a behavior has been shown by experiments, this is how the tested construction will behave in situ. It is important to keep in mind that the outcome of material testing is vastly dependent on the testing conditions. Test fixture, temperature variations, material imperfections, how the deformation is measured and how the properties are extrapolated from the test results all influence the outcome. The same test conducted at different locations by different personnel on the same test material will most likely have some divergence in the results. The difference may not be significant but it is important to keep it in mind. This has spawned the development of general rules describing how tests should be conducted.

4.1 Standards

ASTM International has worked out such a set of rules. ASTM International (originally known as the American Society for Testing and Materials) was established more than a century ago, when a group of engineers and scientists came together to address frequent rail breaks in the burgeoning railroad indus-

try. Their work led to standardization on the steel used in rail construction, ultimately improving railroad safety to the public. ASTM has continued to develop international standards, and today provide standards for a wide range of industries, including many standards on composite materials. The international organization for standardization (ISO) also provides standards for the testing of composite materials, but these will not be further discussed in this thesis.

4.2 Elastic constants and strength

Elastic constants and strength are basic mechanical material properties. For a unidirectional lamina or composite, there are four independent in-plane elastic constants - the elastic moduli (E_1 and E_2) in longitudinal and the transverse directions respectively, the shear modulus (G_{12}), and the Poisson's ratio (ν_{12}) - and five independent in-plane strengths, namely, tensile and compressive strengths (σ_{u1t}, σ_{u2t}, σ_{u1c}, σ_{u2c}) in the longitudinal and transverse direction and in-plane shear strength (τ_{u12}). In addition to these five ultimate strengths, there are also five corresponding elastic strengths. These represent the stress at which the stress-strain relationship cease to be linear. These strengths represent first ply failure for composite laminates. For composite laminates there is also the interlaminar shear strength which determines an important mode of failure, namely, failure by delamination. This will not be discussed further, since delamination is not covered by this thesis. It is desirable that all the properties be established for a single ply or lamina of the composite material that is the basic building block for the composite laminate. Then the laminate theory can be used to calculate the properties of the whole laminates. Practical considerations often prevent the construction of single-layer test specimens. Thus it becomes necessary to conduct tests on multilayer specimens and use the laminate theory to reduce the results in terms of lamina properties.

4.3 Tensile testing

The data recording in a tension test consists of measuring the applied load and strain both parallel and perpendicular to the load. The applied load is usually measured by a load cell that generally is provided with the testing machine. The strains can be measured by means of extensometer or an electrical-resistance strain gauge. Extentsiometers, mechanically attached, tend to slip at times, although they are said to be quite simple to use. Strain gauge may be used for a more accurate measurement of strains. From these data taken until, failure, a stress-strain curve can be plotted for the material and the required material properties determined. When the applied load is in the longitudinal direction of a UD-laminate, the initial slope (linear elastic region) of the stress-strain curve

gives the longitudinal modulus (E_1). Similarly, the transverse modulus (E_2) can be determined by applying the load in transverse direction. The ultimate longitudinal and transverse tensile strength (σ_{u1t} and σ_{u2t}) is obtained from the knowledge of load at fracture in the two tests. The Poisson's ratio (ν_{12}) is obtained from the strains parallel and perpendicular to the load measured at the same axial load.

While testing unidirectional composites in the longitudinal direction, it should be ensured that the load direction does coincide with the fiber direction. Misalignment by only a few degrees may result in considerably lower values of elastic modulus and ultimate tensile strength[13]. This problem is not as critical for tests in the transverse direction. The material properties deduced from tests

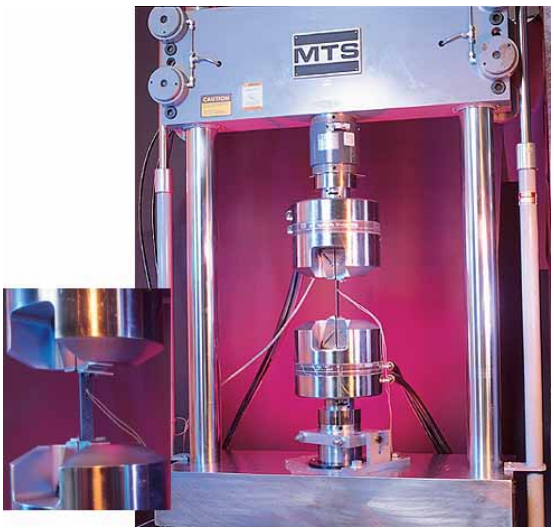

Figure 4.1: An illustration of the ASTM d3039 test setup

on UD laminates should be used with care when describing plies of the same material and orientations situated in laminates with plies in multiple directions. Experimental observations studied in the work with this thesis indicate that the ultimate strength in the fiber direction can be as much as 60% higher for a ply situated in a laminate with plies in multiple directions than for a UD laminate oriented in the same direction.

4.4 Shear testing

There are several published test methods for establishing the in-plane shear properties of composite laminates. Most of these methods have been subjected to quite extensive research during recent years, and have resulted in a lot of publications. The most recent and perhaps best documented method is the standard test method for shear properties of composite materials by V-notched rail shear

method (ASTM D7078/7078M-05). In Figure 4.2 the V-notched rail shear test fixture with the test specimen installed (not visible), is illustrated. The purpose of the test is to obtain the shear properties of the material. This is achieved at the specimen mid-length by application of two counteracting moments produced by two force couples. In the middle section of the test specimen, a shear force of magnitude P is induced. The bending moments exactly cancel at the mid-length of the specimen, producing a state close to pure shear. The test fixture is designed to restrain each end of the test specimen from rotating. The 90° notches on each edge of the specimen(see Figure 4.3 and 4.5) produce a more constant shear-stress distribution between the two notches instead of parabolic shear-stress distribution for a constant-cross-section beam. Therefore, the value of shear stress τ for the test shown in Figure 4.2 is given by the shear force divided by the net cross-section area:

$$\tau = \frac{P}{wt}, \tag{4.1}$$

where w is the net width between the two notches, and t is the thickness of the test specimen. A state of evenly distributed shear is not possible. The shear stress at the ends will always be equal to zero, and usually there will be some concentrations of shear stresses near the edges. A curve displaying a typical shear distribution is shown in Figure (4.4).

Even though specimens with $[0]_N$ or $[90]_N$ fiber lay-ups can be used, the standard (ASTM D7078) recommends using specimens with $[0/90]_{NS}$ lay-ups.

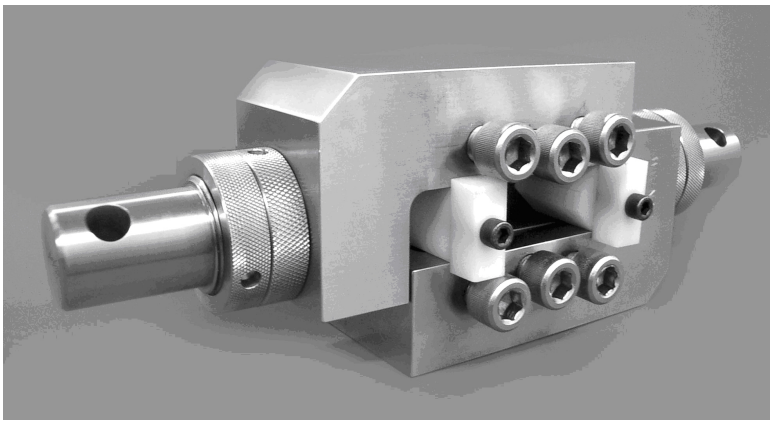

Figure 4.2: The v-notched rail shear test fixture, ASTM D7078

The rail shear test can determine both shear modulus and shear strength. However, for highly orthotropic materials (i.e. large value of E_1/E_2), there is a non uniformity in the stress distribution in the test section, which introduces an error in the determination of property values. Adams and Walrath [24] suggested using cross-ply laminate, $[0/90]_S$, instead of a unidirectional composite. In theory, shear properties of the cross-ply laminate are the same as those of the unidirectional composite.

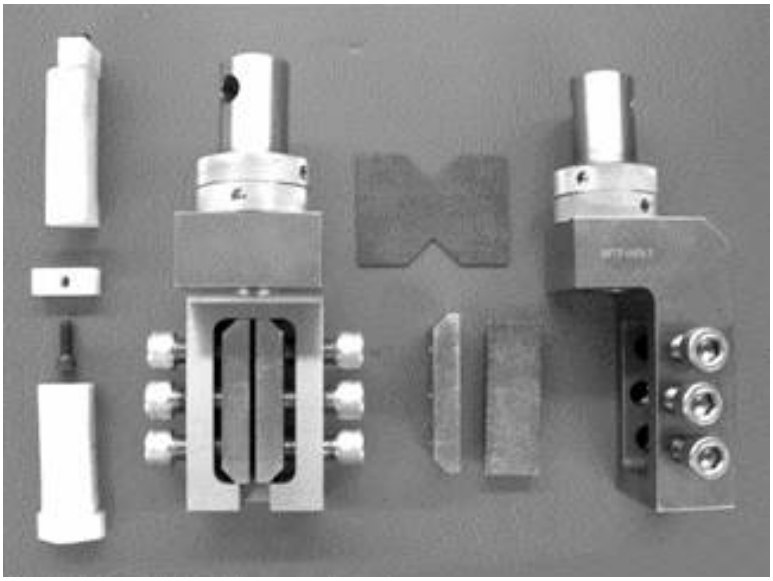

Figure 4.3: The v-notched rail shear test fixture shown with a standard v-notched specimen and with one pair for grip plates removed

The shear modulus (G_{12}) can also be obtained by a standard coupon test of a cross-ply laminate elongated in 45° of the fibers. This method is quite suitable for determination of shear modulus, but not for shear strength (τ_{u12}) because the lamina is in a state of combined stress rather than pure shear. [13]

4.5 Digital Image Correlation - DIC

The term *digital image correlation* refers to the class of non-contact methods that acquire images of an object, store images in digital form and perform image analysis to extract full-field shape, deformation and motion measurements. Digital image registration has been performed with many types of object-based patterns, including lines, grids, dots and random arrays. One of the most commonly used approaches employs random patterns and compares sub-regions throughout the image to obtain a full-field of measurements.

The method used in the work with this thesis, seen in Figure 4.6, is based on *Three-Dimensional Computer Vision*. The projection captured through a standard video camera lens, captures the world as if seen through a pinhole. Such a projection transforms a 3D object point into a 2D image point, thereby removing the third dimension in an irreversible manner. As shown in Figure 4.7, the two 3D points Q and R are imaged onto the same image-point p as they are lying on the same projective ray (C,p), illustrating that there exists an infinite number of 3D points that correspond to the image point p. As it is shown in Figure 4.8, it is possible to recover three-dimensional position of the true object

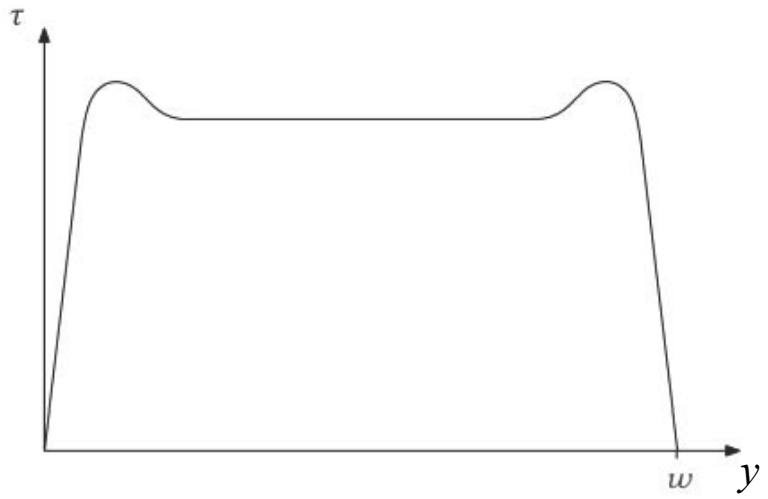

Figure 4.4: The distribution of the shear stress along the shortest direct line, w between the two notches

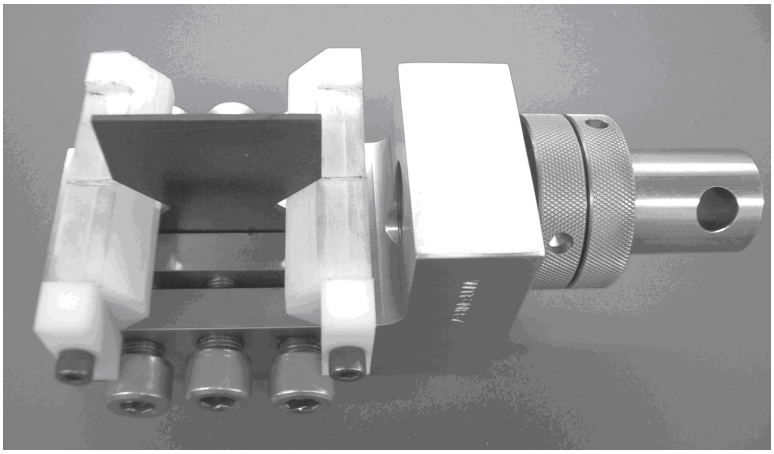

Figure 4.5: Half the rail shear test fixture removed, test specimen sticking out.

points by using two cameras to record simultaneous image points of the same object. If the two image points are (p,q'), then the unique 3D point is Q. If the corresponding image points are (p,r'), then the unique 3D point is R.

These stereo vision systems, seen in Figure 4.6 and shown schematically in Figure 4.8, using multiple cameras are able to measure a tree-dimensional displacement field such that the in-plane components of the displacement are independent of the out of plane motions.

Prior to performing test measurements, each stereo vision system needs to be calibrated. Calibration of the is performed using images of a translated and rotated planar dot pattern with reasonably well known spacing. A planar target plate with the dot pattern is held i front of the cameras at the approximate

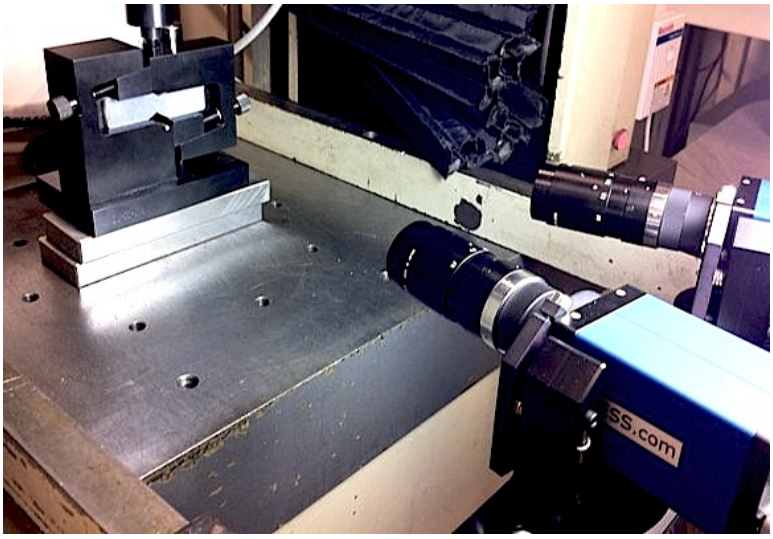

Figure 4.6: Isopesque shear test experiment on an epoxy specimen with a DIC setup recording of the in- and out of plane displacements in the test specimen with two cameras providing stereovision.

location where the test specimen is to be located during the measurement. The target plate is tilted and rotated into different orientations while images are acquired. Each captured orientation of the target plate produce a pari of images. The difference in the two images of every pair, arises from the different perspective of the two cameras. Typical image pairs obtained during a calibrating process can be seen in Figure 4.9.

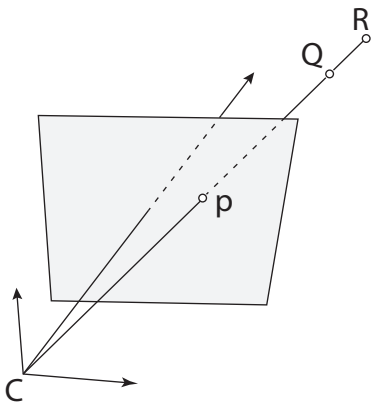

Figure 4.7: Perspective of a single camera.

After the test is captured by the cameras, the data needs to be processed in order to provide the strain measurements. First the area of interest is defined on the test specimen in the recorded images. Then a subset (also called aperture or

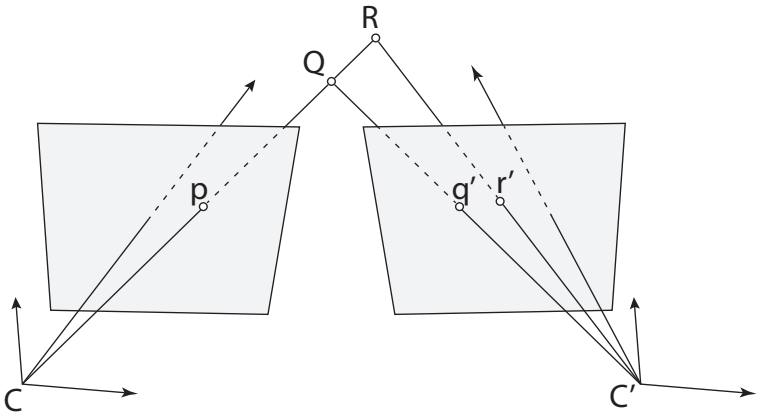

Figure 4.8: Perspective of two cameras.

window) in that area is defined. This subset defines an area of pixels that are used to define a single data point in the strain measurements. A subset is needed to be defined in order to make it possible for the processing to recognize the same point in the images from both cameras, and whereabouts of that data point after deformation. The area of interest is divided into subsets defining the data points used in the strain measurements of the whole area of interest. The smaller the subsets are, the finer the strain measurements gets, but the more difficult it will be for the recognition of datapoint after deformation.

To ensure that the specimen remains in focus during the measured test, the aperture settings on the lenses are reduced to maximize the depth field. The illumination of the specimen is increased in order to compensate for the reduced aperture and to maintain adequate contrast throughout the experiment.

All the DIC measurements carried out in the work with this thesis have been conducted using the VIC-3D[25] system. The VIC-3D is a complete system, including all necessary hardware and software for obtaining full-field, 3-dimensional measurements of shape, displacement and strain. Actual object movements are measured and the Lagrangian strain tensor is made available at every point on the specimenâs surface.

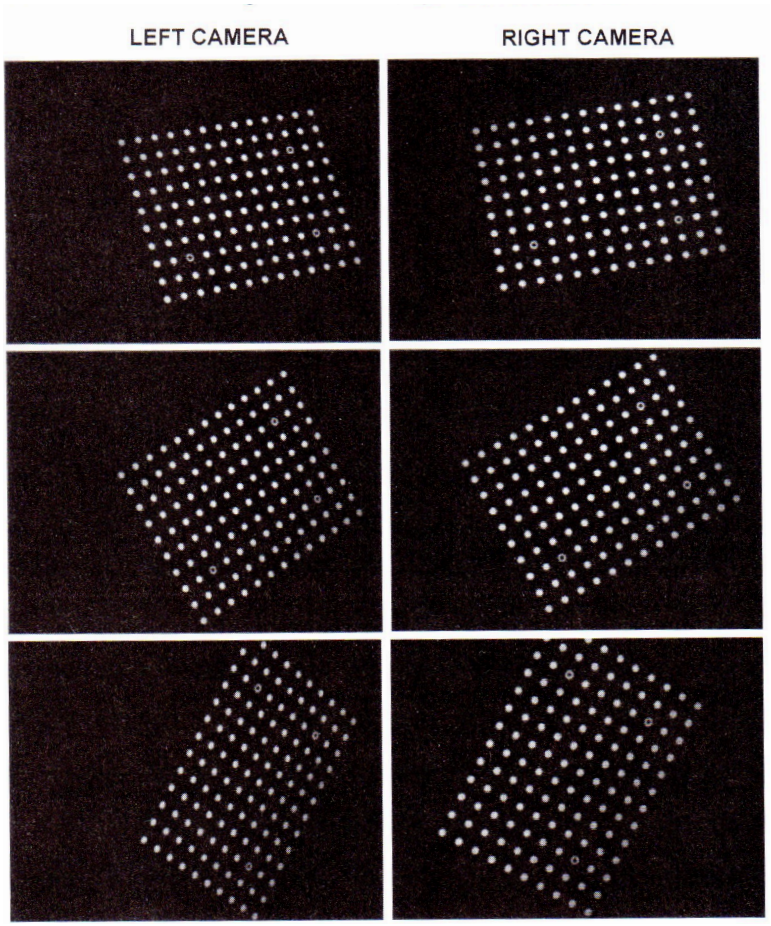

Figure 4.9: Typical image pairs obtained during calibration process[11].

Chapter 5

Finite Element Analysis

When conducting a finite element analysis the structure that is subject to the analysis is divided into a finite number of elements. In each element a displacement field is assumed, i.e. $\mathbf{u} = \mathbf{N}\mathbf{d}$, where $\mathbf{u}$ is the displacement vector, $\mathbf{N}$ contains the shape functions and $\mathbf{d}$ lists the nodal displacement degree of freedom of an element.

Compatibility is then applied exactly

$$\epsilon = \partial^{\mathbf{t}}\mathbf{u} = \mathbf{B}\mathbf{d}, \tag{5.1}$$

where matrix $\mathbf{B}$ is called the *strain-displacement matrix* and is found by the equation $\mathbf{B} = \partial^{\mathbf{t}}\mathbf{N}$. The stress-strain law is also exact

$$\sigma = \mathbf{E}\epsilon. \tag{5.2}$$

The principle of virtual displacement then satisfies equilibrium *approximately*, leading to an *element* stiffness matrix $\mathbf{k}$ and converting the applied loads to kinematically equivalent forces $\mathbf{P}$. The principle of virtual displacement is now summed over the entire structure which produces a global stiffness matrix $\mathbf{K}$ relating the global displacements $\mathbf{r}$ to the global forces $\mathbf{R}$.

The equations $\mathbf{K}\mathbf{r} = \mathbf{R}$ are solved, and on back-substituting $\mathbf{r} \rightarrow \mathbf{d} \rightarrow \epsilon$ we recover the strains and stresses in every element.

Special shape functions are used for beams, plates, shells, solids, etc. Generating the model and solving for the displacements and stresses is made straightforward by most commercial codes. Normally, numerical integration of element stiffness coefficients cannot provide exact results. Accuracy of integration can be increased by using more integration points, but this may not increase the accuracy of the computed FE results. The FE results may actually become more accurate if the order of quadrature is reduced. *Full integration* is defined at a quadrature rule of sufficient accuracy to exactly integrate all stiffness coefficients k_{ij}, of the stiffness matrix $\mathbf{k}$, of an undistorted element[26]. In this thesis, four-node shell elements with only one integration point located at the center of the element has

been widely used. These elements uses an integration rule that is less than full order, this is called *under*-integration or *reduced*-integration. Under-integration reduces computation time, which is an important in consideration in analyses that are nonlinear and dynamic. Under integration introduces the defect variously known as spurious mode, singular mode, zero-energy deformation mode, hourglass mode, kinematic mode, instability and mechanism. An element whose stiffness matrix incorporates a spurious mode has no resistance to nodal loads that tend to activate the mode. For the four-node under integrated element, these types of modes are illustrated in Figure 5.1.

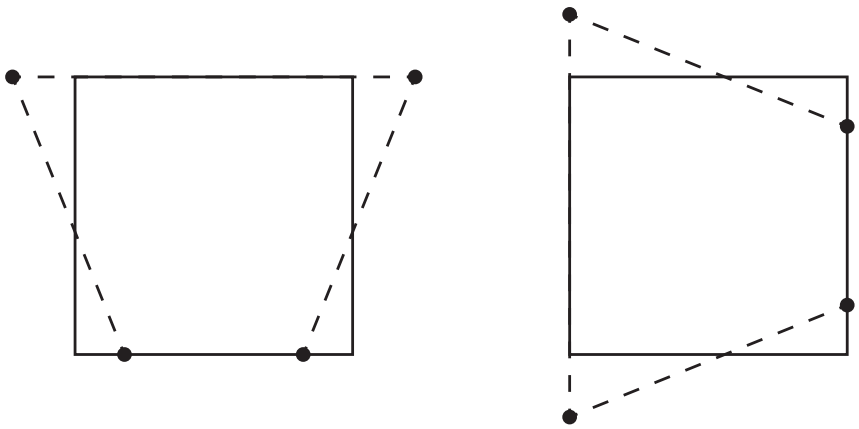

Figure 5.1: Spurious modes for four-node under-integrated shell elements.

5.1 Nonlinear Finite Element Analysis

Nonlinear behavior admits a wide variety of phenomena, possibly interacting with one another, and each perhaps difficult to formulate. The difficulty lies in finding realistic mathematical and numerical models describing the phenomena, and solving the nonlinear equations that result. In structural mechanics, types of nonlinearity include the following:

- *Material nonlinearity*, in which material properties are functions of the state of stress or strain. Examples include nonlinear elasticity, plasticity, creep and failure.

- *Contact nonlinearity*, in which a gap between adjacent parts may open or close, the contact area between parts changes, or there is sliding contact with frictional forces.

- *Geometric nonlinearity*, in which deformation is large enough that equilibrium equations must be written with respect to the deformed structural

geometry. Also, loads may change direction as they increase, as when pressure inflates a membrane.

Problems in these categories are nonlinear because stiffness, and perhaps loads as well, become functions of displacement or deformation. Thus, in structural equations $\mathbf{KD} = \mathbf{R}$, coefficient matrix $\mathbf{K}$ and perhaps load vector $\mathbf{R}$ become functions of $\mathbf{D}$. We cannot immediately solve $\mathbf{D}$ because information needed to construct $\mathbf{K}$ and $\mathbf{R}$ is not known in advance. An iterative process is required to obtain $\mathbf{D}$ and its associated $\mathbf{K}$ and $\mathbf{R}$ such that the product $\mathbf{KD}$ is in equilibrium with $\mathbf{R}$.

When conducting failure analysis, geometric nonlinearity is most certainly going to be present. Geometric nonlinearity arises when deformations are large enough to alter the distribution or orientation of applied loads, or the orientation of initial resisting forces and moments. The essential difficulty of geometrically nonlinear analysis is that equilibrium must be written with respect to the deformed geometry, which is not known in advance.

The elements described in this thesis use a corotational formulation. Corotational coordinates are also called *convected coordinates*. A local coordinate system is attached to each element, and translates and rotates with the element as deformation proceeds. The global coordinate system remains fixed. Element deformation is decomposed into a rigid-body component, which is identical to rigid-body motion of the local system, and a straining component that can be described by degrees of freedom measured in the local system. Having separated the components, they can be addressed independently.

5.2 Finite Element Analysis - Dynamics and Vibrations

The dynamic equilibrium of a multi-element structure can be expressed with one of the following equations

$$\mathbf{M}\ddot{\mathbf{D}}_n + \mathbf{C}\dot{\mathbf{D}}_n + \mathbf{R}_n^{int} = \mathbf{R}_n^{ext}, \tag{5.3}$$

or

$$\mathbf{M}\ddot{\mathbf{D}}_n + \mathbf{C}\dot{\mathbf{D}}_n + \mathbf{K}\mathbf{D}_n = \mathbf{R}_n^{ext}, \tag{5.4}$$

where $\mathbf{M}$ is the mass matrix, $\mathbf{C}$ is the damping matrix, $\mathbf{K}$ is the stiffness matrix and $\ddot{\mathbf{D}}$, $\dot{\mathbf{D}}$ and $\mathbf{D}$ are the accelerations, velocities and displacements of the nodal degrees of freedom respectively. $\mathbf{R}^{ext}$ is the external applied forces working on the structure.

In this thesis two direct integration solution methodologies have been used, implicit- and explicit time integration. Direct integration method refers to calculation of response history using step-by-step integration in time, without first

changing the form of dynamic equations. Response is evaluated at instants separated by time increments Δt, so we compute structural displacements at times Δt, $2\Delta t$, $3\Delta t$, ..., $n\Delta t$, and so on. For nonlinear problems Equation (5.3) may be the better approach since $\mathbf{K}$ may change from one time step to the next. We assume that $\mathbf{M}$ is positive definite, but that $\mathbf{K}$ need only be positive semidefinite. Thus the structure is allowed to have rigid body motions as part of its response. Similarly, a mechanism can be present, provided that it is not without mass.

Methods of direct integration calculate conditions at time step $n + 1$ from the equation of motion, a difference expression, and known conditions at one or more preceding time steps. Algorithms can be classified as explicit or implicit. An explicit algorithm uses a different expression of the general form

$$\mathbf{D}_{n+1} = f(\mathbf{D}_n, \dot{\mathbf{D}}_n, \ddot{\mathbf{D}}_n, \mathbf{D}_{n-1}, ...), \tag{5.5}$$

which contains only historical information on its right-hand side. An implicit algorithm uses a difference expression of the general form

$$\mathbf{D}_{n+1} = f(\dot{\mathbf{D}}_{n+1}, \ddot{\mathbf{D}}_{n+1}, \mathbf{D}_n, \dot{\mathbf{D}}_n, \ddot{\mathbf{D}}_n, ...), \tag{5.6}$$

which is combined with the equation of motion at time step $n + 1$.

When choosing whether to use implicit or explicit algorithm there are some differences one needs to evaluate. Each increment in an implicit analysis consists of at least one iteration, but usually more than one. Each iteration requires the solution of a set of simultaneous equations. The CPU cost per iteration is roughly proportional to the number of degrees of freedom in the model squared. Each increment in an explicit analysis consists of one group of equations, there are no iterations. The CPU cost per increment is directly proportional to the number of degrees of freedom in the model. As the size of the model increases, there is a point at which explicit may become more cost effective than implicit for simulations that could be solved with either.

5.3 LS-DYNA

LS-DYNA is a commercially available software which include a general purpose finite element code for analyzing the large deformation static and dynamic response of structures including structures coupled to fluids. The main solution methodology is based on explicit time integration. An implicit solver is also available.

When solving dynamic responses in the explicit solver, the LS-DYNA code simplifies the mass matrix by assuming that the distributed mass of the elements can be lumped at the nodes [27]. With lumped mass idealization of the finite element, the mass matrix becomes diagonal. The off diagonal terms of the mass matrix are zero because an acceleration of any point mass produces inertia force

only for that degree of freedom at which the mass is situated. And further more, because the mass is lumped in one dimensional points at the nodes, the mass has no inertia to the rotational degree of freedom. The values along the diagonal of the mass matrix associated with these degrees of freedom are therefor also zero. A dynamic analysis using a consistent mass matrix is considerably more computational costly because it has off-diagonal values in the mass matrix. Also, the rotational degrees of freedom can be eliminated by static condensation from the equation of motion for a lumped mass system, whereas all degrees of freedom must be retained in a consistent mass system [28].

5.4 Finite Element Analysis and Composite Materials

When analyzing composite materials, LS-DYNA provides a large variety of options. One can use thin or thick (solid) shell elements or solid continuum elements. Within each element formulation there are numerous integration options, and there are a variety of different material models describing the anisotropy of composite materials, some include failure criteria. The material models we have used are described in detail in Section 5.5.

In this thesis, 4-node shell elements have been widely used. The nodes of these elements have 6 degrees of freedom, translation in three directions, and drilling degrees of freedom about the same directions. The elements have centered integration points through the thickness. Each integration point define a layer in the composite laminate lay-up. We define the material properties for a unidirectional ply in the material model, and then specify what material model, the ply orientation and ply thickness for each integration point. The element formulation is based on a co-rotational and a rate of deformation formulation. The details of these formulations are beyond the scope of this thesis, but can be further investigated in the *LS-DYNA theory manual* [27].

5.5 Material models

LS-DYNA has a variety of material models describing composite materials. In this thesis, the focused has been directed at material models applicable to unidirectional composites (in contrast to woven composites), and shell elements. In addition to the material models incorporated in LS-DYNA, a model based on the Puck failure model [10] has been implemented. This implementation is currently being optimized at SINTEF.

5.5.1 Material 22 - Composite failiure

Material model 22 is based on the Chang-Chang composite failure model [21]. The material model is found in the LS-DYNA material model catalogue under the name *Material 22: Chang-Chang Composite Failure Model*. Five material parameters are used in the three failure criteria. These are:

- X_t, longitudinal tensile strength
- Y_t, transverse tensile strength
- S_{12}, shear strength
- Y_c, transverse compressive strength
- α, nonlinear shear stress parameter.

X_t, Y_t, S_{12} and Y_c are obtained from material strength measurement. α is defined by material shear stress-strain measurements. In-plane stress, the strain is given in terms of the stress, in the *LS-DYNA Theory manual* [27], as

$$\epsilon_1 = \frac{1}{E_1}(\sigma_1 - \nu_{12}\sigma_2), \tag{5.7}$$

$$\epsilon_2 = \frac{1}{E_2}(\sigma_2 - \nu_{21}\sigma_1), \tag{5.8}$$

$$\gamma_{12} = 2\epsilon 12 = \frac{1}{G_{12}}\tau_{12} + \alpha\tau_{12}^3. \tag{5.9}$$

The third equation defines the nonlinear shear stress parameter α. A fiber-matrix shearing term arguments each damage mode:

$$\bar{\tau} = \frac{\frac{\tau_{12}^2}{2G_{12}} + \frac{3}{4}\alpha\tau_{12}^4}{\frac{S_{12}^2}{G_{12}} + \frac{3}{4}\alpha S_{12}^4}, \tag{5.10}$$

which is the ratio of the shear stress to the shear strength. The matrix failure criterion is determined from

$$F_{matrix} = \left(\frac{\sigma_2}{Y_t}\right)^2 + \bar{\tau}, \tag{5.11}$$

where failure is assumed whenever $F_{matrix} > 1$. If $F_{matrix} > 1$, then the material constants E_2, G_{12}, ν_{12} and ν_{21} are set to zero. The compression failure criterion is given as

$$F_{comp} = \left(\frac{\sigma_2}{2S_{12}}\right)^2 + \left[\left(\frac{Y_c}{2S_{12}}\right)^2 - 1\right]\frac{\sigma_2}{Y_c} + \bar{\tau}, \tag{5.12}$$

where failure is assumed whenever $F_{comp} > 1$. If $F_{comp} > 1$, then the material constants E_2, ν_{12} and ν_{21} are set to zero. The final failure mode is due to fiber failure.

$$F_{fiber} = \left(\frac{\sigma_1}{X_t}\right)^2 + \bar{\tau}. \tag{5.13}$$

Failure is assumed whenever $F_{fiber} > 1$. If $F_{fiber} > 1$, then the material constants $E_1, E_2, G_{12}, \nu_{12}$ and ν_{21} are set to zero.

5.5.2 Material 54 - Enhanced composite damage

Material model 54 is a model that allows to describe anisotropic, linear elastic behavior if the material is undamaged, which is valid for many composites. The model uses the linear elastic version of the Chang-Chang failure criterion, as for *Material 22 - Composite failure*. This criterion introduce a nonlinearity into the material model. The material model is found in the LS-DYNA material model catalogue[29] under the name *Material 54: Enhanced Composite Damage Model*. The failure modes are: Tensile fiber mode, Compressive fiber mode, Tensile matrix mode and compressive matrix mode. They are given as follows:

- tensile fiber mode

$$\sigma_{11} \geqslant 0 \ then \ e^2 = \left(\frac{\sigma_{11}}{X_t}\right)^2 + \beta \left(\frac{\sigma_{12}}{S_c},\right) - 1 \tag{5.14}$$

- compressive fiber mode

$$\sigma_{11} \leqslant 0 \ then \ e^2 = \left(\frac{\sigma_{11}}{X_c}\right)^2 - 1, \tag{5.15}$$

- tensile matrix mode

$$\sigma_{22} \geqslant 0 \ then \ e^2 = \left(\frac{\sigma_{22}}{Y_t}\right)^2 + \left(\frac{\sigma_{12}}{S_c}\right) - 1, \tag{5.16}$$

- and finally, compressive matrix mode

$$\sigma_{11} \leqslant 0 \ then \ e^2 = \left(\frac{\sigma_{11}}{X_t}\right)^2 + \left[\left(\frac{Y_c}{2S_c}\right)^2 - 1\right] \frac{\sigma_{22}}{Y_c} + \left(\frac{\sigma_{12}}{S_c}\right) - 1. \tag{5.17}$$

For $\beta = 1$ we get the original criterion of Hashin[30] in the tensile fiber mode. For $\beta = 0$ we get the maximum stress criterion which, according to the LS-DYNA Theory Manual, is found to compare better to experiments. The criteria described above are stress-related, whereas it is sometimes desirable to limit also

the strains. This is possible in material model 54 using parameters specified in the *LS-DYNA Keyword Manual*[29]. When these strain parameters are not activated the material will be described as elastic-brittle. This means it will show linearly elastic behavior up to ultimate stress. Then, with the load increasing, the stress level in the material will be reduced to zero, simulating ultimate failure. By activating the strain parameters the ultimate strain can be sett to a higher level that the equivalent strain level of the ultimate stress. In this case the stress level will rise with increasing load until ultimate stress is reached, the the material will continue to be strained without increasing the level of stress inn the affected part of the material. Thus by using the strain limiting parameters as failure criteria the material model is elasto-plastic up to failure[31].

This material model is only valid for shell elements. The composite lay up can be defined by the *Part - Composite* option, with one layer per integration point through the thickness. In every integration point the respectable layer material, orientation and layer thickness is defined. LS-DYNA uses classical lamination theory to properly model the transverse shear deformation. Lamination theory is applied to correct for the assumption of a uniform constant shear strain through the thickness of the shell.

5.5.3 Material 55 - Enhanced composite damage

Except for the failure criterion this material model has the same possibilities as material model 54. The failure criterion described in this model is based on the the Tsai-Wu failure model [19]. The model applies two fiber failure modes and one combined tensile and compressive matrix mode. The two fiber modes are treated as in the Chang-Chang criteria. The failure criterion is defined as follows[27]:

- tensile fiber mode

$$\sigma_{11} \geqslant 0 \ \textit{then} \ e^2 = \left(\frac{\sigma_{11}}{X_t}\right)^2 + \beta \left(\frac{\sigma_{12}}{S_c}\right) - 1 \tag{5.18}$$

- compressive fiber mode

$$\sigma_{11} \leqslant 0 \ \textit{then} \ e^2 = \left(\frac{\sigma_{11}}{X_c}\right)^2 - 1 \tag{5.19}$$

- tensile and compressive matrix mode

$$e^2 = \frac{\sigma_{22}^2}{Y_c Y_t} + \left(\frac{\sigma_{12}}{S_c}\right)^2 + \frac{(Y_c - Y_t)\,\sigma_{22}}{Y_c Y_t} - 1 \tag{5.20}$$

5.5.4 Material 47 - User defined material

This is the material model in which the Puck failure criterion is implemented. In addition to the failure criteria, a damage model is implemented as well. This enables the model to describe the nonlinearity found in experimental observations. This material model is thoroughly described in chapter 6.

Chapter 6

Case study 1: Puck failure model

The implemented Puck failure model in the LS-DYNA code builds on the work done by Wiegand et al. [22], who uses the full three dimensional version of the failure model. The damage behavior is described as suggested by Puck in [10], with an effective stiffness $E_{eff} = E\eta$. To verify the accuracy of the model, several trials have been carried out. The basic behavior and stability has been tested thoroughly, and the results have been compared to other material models in LS-DYNA and published numerical work. The material model has also been used to replicate material test results.

6.1 Basic behavior

The model should be able to describe elastic behavior within the prescribed elastic strengths of the material. When the applied load inflict the level of stress causing first ply failure, the stress-strain curve should show some softening before reaching ultimate failure (i.e. not go from linear elastic elongation to ultimate failure in an instance). It should also be possible to control the softening. The model should be able to replicate the softening shown in mechanical testing for the same material.

The material model continuously observes the failure parameters for interfiber failure and fiber failure in tension and compression. When one of the two fiber failure criteria reaches failure in an element, the element is deleted. When the interfiber failure criteria reach failure in an element, the element is not deleted, but the damage condition is activated, i.e. reducing the values of E_2, G_{12} and ν_{12} when further load is applied.

When the model is shown to behave realistically in simple loading conditions it can be tested in more complex loading. Most failure criteria realistically describe the point of failure for single loading in one of the material axis or in shear, but when the loading becomes more complex the different criteria do not agree. The Puck failure criterion has been ranked as one of the best in the WWFE[32] for

predicting combined loading conditions.

The model should realistically update the stiffness of the material after damage initiation, where the stress-strain behavior starts behaving nonlinear. The updated stiffness must also be stored so that repeated on and off loading behavior is realistic. Typical on and off loading curve for loading conditions after initial damage is illustrated in figure 6.1. [13] First the specimen is loaded with P_1, then unloaded. The second time it is loaded it follows the offloading curve up to P_1 linear elastic, then the damage condition continue degrading the specimen. The same is repeated when loading P_2 is reached. This illustrates that when damage first has degraded the material properties, the material will not regain its initial stiffness.

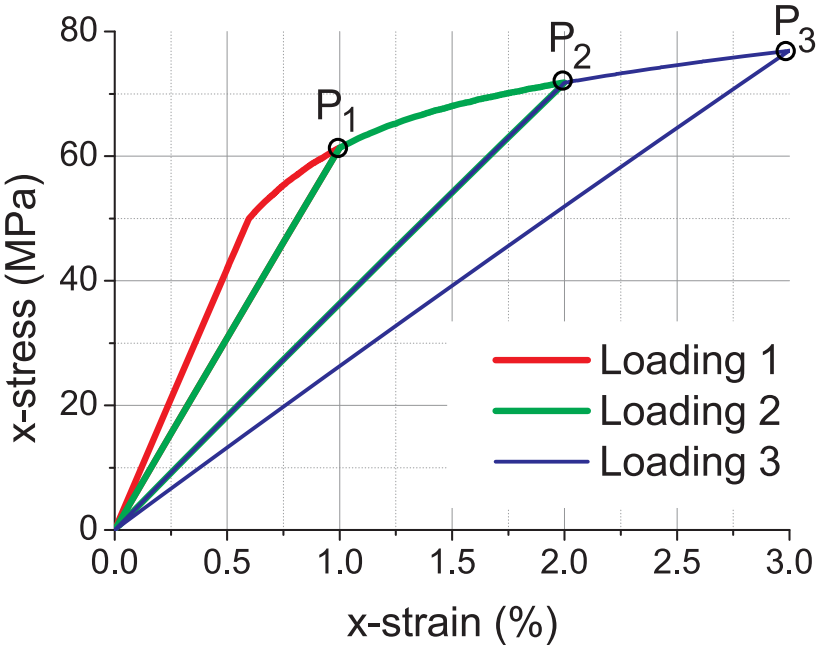

Figure 6.1: Repeated on and off loading

6.2 Material tests

The tested laminates are made up of stitched unidirectional (UD) glass fiber reinforced polymer matrix (DION 9102-683) composite plies. The laminates are stacked with ply-orientations $[0]_N$, $[90]_N$, $[\pm 45]_N$, $[0/90]_N$, $[\pm 45/90]_N$, $[\pm 45/90_6/\pm 45]$ and $[0/\pm 45/90]_N$, here N is the number of times the stacking sequence is repeated through the thickness of the laminate (typically $N = 6$). It can be seen that the lay ups of the latter five laminates are not symmetric with respect

to the mid-plane of the laminate. The reason for this is that it is faster and cheaper to produce laminates with a lay up stacked in a repeating fashion. When the lay up is made up of a multi repeating order of thin plies, the effects of the non-symmetric lay up decrease when the number of repetitions of the sequence increases. This effect can be illustrated by first calculating the coupling matrix for a single repetition of the non-symmetric lamina sequence $[90/\pm 45/0]$, using Equation (2.51), and (2.52) from Chapter 2.3. Then the **a**- and **B**-matrix is calculated in the same manner for ten repetitions of the same stacking sequence, $[90/\pm 45/0]_{10}$, only this time with thiner plies, so that the total laminate thickness is the same.

For the $[90/\pm 45/0]$-laminate the stiffness and coupling matrices are calculated as

$$\mathbf{A} = 1.0e+0.6 \begin{bmatrix} 1.8988 & 0.6090 & -0.0000 \\ 0.6090 & 1.8988 & 0.0000 \\ -0.0000 & 0.0000 & 0 \end{bmatrix}, \tag{6.1}$$

$$\mathbf{B} = 1.0e+07 \begin{bmatrix} 1.6310 & -0.0000 & -0.2718 \\ -0.0000 & -1.6310 & -0.2718 \\ 0.2718 & 0.2718 & 0.6449 \end{bmatrix}, \tag{6.2}$$

and for the $[90/\pm 45/0]_{10}$-laminate the stiffness and coupling matrices are calculated as

$$\mathbf{A} = 1.0e+0.6 \begin{bmatrix} 1.8988 & 0.6090 & -0.0000 \\ 0.6090 & 1.8988 & 0.0000 \\ -0.0000 & 0.0000 & 0 \end{bmatrix}, \tag{6.3}$$

$$\mathbf{B} = 1.0e+06 \begin{bmatrix} 1.6310 & -0.0000 & -0.2718 \\ -0.0000 & -1.6310 & -0.2718 \\ 0.2718 & 0.2718 & 0.6449 \end{bmatrix}. \tag{6.4}$$

In Equation (6.1) and (6.3) it is shown that the stacking sequence has no impact on the stiffness matrix **A**, only the total thickness of the plies in the various orientations affects these properties. In Equation (6.2) and (6.4) on the other hand, it is show that by reducing the thickness of each ply and increasing the repetitions of the stacking sequence the coupling effects defined by the **B**-matrix is reduced to a tenth. The material properties used are found in Table 6.1 in Chapter 6. The input file from the Matlab-calculations are found in the Appendix..

The tests conducted are standard coupon tests in tension and compression in addition to the *v-notched rail shear test*. Two types of experiments have been conducted in order to predict the shear stiffness; tension tests of $[\pm 45]_N$ coupons, and v-notched rail shear tests of cross-ply laminates. For tension tests of the $[\pm 45]_N$ coupons the shear stiffness is calculated by the formula

$$G_{12} = \frac{E_x}{2(1+\nu_{xy})}, \tag{6.5}$$

where E_x is the stiffness in the direction of the applied load and ν_{xy} is the in-plane Poisson's ratio.

When defining the reduction factor η there are three different damage effects that can be studied. Tensile test of UD-laminates loaded in the transverse direction, $[90]_N$-laminates, should show the actual reduction in the transverse stiffness E_2 and the reduction in the Poisson's ratio, ν_{12} can be evaluated by studying the minor Poisson's ratio, ν_{21}. By studying shear tests of cross-ply laminates, $[\pm 45]_N$, the actual reduction in shear stiffness G_{12} can be evaluated. It is shown that at least two of these propagate differently, and consequently they are both used to define the reduction factor η. The two η values are then evaluated against each other when implemented in the analysis predicting the damage propagations of the laminates: $[\pm 45/90]_N$, $[\pm 45/90_6/\pm 45]_N$ and $[0/\pm 45/90]_N$.

6.3 FE analysis

In the FEA, four node shell elements with a nonlinear material model, have been used. The elements are two-dimensional and describe the laminate lay up with integration points through the thickness. Each integration point represents a ply in the laminate, and the integration points are located at the center of the element and in the middle of each ply. The fiber orientations are defined independently in each integration point. A local coordinate system is attached to each element, and translates and rotates with the element as deformation proceeds. The global coordinate system remains fixed. Element deformation is decomposed into a rigid-body component, which is identical to rigid-body motion of the local system, and a straining component that can be described by degrees of freedom measured in the local system.

When using shell elements through the thickness shear is not allowed to variate from one layer to the next, only linearly variating overall shear is possible. In order to see how this effects the outcome, all the simulations have been conducted using solid elements as well. With solid elements defining each layer in the laminate, through the thickness shear is allowed to variate due to differences in Poisson's effects. Cross sections are not constrained to remain plane, as it is when using shell elements.

The degradation of the material properties after first ply failure is implemented by multiplying the three material parameters; E_2, G_{12} and ν_{12} with the reduction factor η, as suggested by Puck[10]. The optimal values of η have been found through inverse modeling using the LS-DYNA finite element code in combination with the optimization tool LS-OPT. One value of η is based on the tensile tests of $[90°]_N$-coupons describing a reduction in E_2 after failure initiation. The other is based on the tensile tests of $[\pm 45]_N$-coupons describing a reduction in G_{12}. One computational expensive operation, when using the Puck failure model in three dimensions, is the search for the most critical action plane. This is the

plane parallel to the fibers where the matrix failure criterion has its maximum value, and consequently where the failure will occur. As mentioned above the three stress components that are acting on the action surface, are the ones governing the IFF. The action plane is defined by the angle θ_{fp}, see Figure 3.4 in Chapter 3.2.3. The search for the most critical action plane should be carried out in the range $-90° \leqslant \theta \leqslant 90°$. One cost effective methodology is the Golden Section Search[22]. This procedure has been proven to be an effective tool when searching for the action plane using the Puck criterion by Wiegand et al. in [22]. In this implementation the search is conducted by starting with a coarse search picking the area of interest, and refining the search area for each search cycle.

6.4 Results

6.4.1 Material testing

As pointed out above, one aim of the present study has been to investigate the behavior of a set of laminates after first ply failure. The material parameters describing this behavior have been extracted from FRPC-laminates made up of unidirectional plies. The deduced η-curves are illustrated in Figure 6.4. The values have been deduced from the tensile tests of $[90]_N$-coupons and $[\pm 45]_N$-coupons. The two resulting reduction factors offer different results when implemented in the material model. This difference can be seen in Figures 6.5 and 6.7. In Figures 6.9 through 6.12, on the other hand, the difference appears to be less evident. The elastic properties are listed in Table 6.1, where E_1 is the longitudinal- and E_2 is the transverse Young's modulus respectively, G_{12} is the shear modulus, ν_{12} is the major Poisson's ratio and ν_{23} is the transverse Poisson's ratio. The strength parameters are Y_c, Y_t, X_c, X_t and S_{12}, where Y represents transverse, X longitudinal and S shear parameters. The subscripts c and t refer to *compressive* and *tensile* strengths, respectively. The strengths refer to first ply failure, i.e. damage initiation. Subscript u denotes ultimate failure. The pure transverse compression fracture angle is denoted as θ^0_{fp}. The influence this angle has on the failure envelope is illustrated in Figure 3.5. This angle is difficult to measure, therefore a realistic value for equivalent material found in literature[22] has been used.

6.4.2 Basic material properties

The Poisson's ratio, ν_{12}, and the longitudinal tensile parameters are deduced from the tensile tests of $[0]_N$-coupons, the compressive longitudinal parameters are deduced from compressive tests of $[0/90]_N$-coupons. The transverse parameters are deduced from tests on $[90]_N$-coupons. The shear properties are obtained by studying the tensile tests on $[\pm 45]_N$-coupons and the v-notched rail shear test for

test specimens with $[0/90]_N$ lay up.

Table 6.1: Material properties deduced from material testing.

E_1	40500	MPa
E_2	13900	MPa
G_{12}	4000	MPa
ν_{12}	0.25	
ν_{23}	0.30	
Y_c	200	MPa
Y_t	35	MPa
Y_{tu}	62.7	MPa
X_c	400	MPa
X_t	681	MPa
S_{12}	50	MPa
θ^0_{fp}	51°	

6.4.3 The Reduction factor η

Two approaches have been taken to define the reduction factor η. One by studying the tensile tests of $[90]_N$-coupons seen in Figure 6.2, and the other by studying the tensile tests of $[\pm 45]_N$-coupons seen in Figure 6.3. For the study on the tensile $[90]_N$-coupon test, splines were used to describe η as a function of the interfiber failure criterion. For the study on the tensile $[\pm 45]_N$-coupon test, a two term exponetial decay function were used to describe η as a function of the interfiber failure criterion. The splines and the exponetial decay functions where both optimized using LS-DYNA along with the optimization tool LS-OPT. The two resulting curves describing η can be seen in Figure 6.4

The red and blue color of the material test curves in Figure 6.2 and 6.3 can also be seen in Figure 6.4 on the two η-curves. This coloring will be continued in the following, blue referring to the η-value deduced from the tensile $[90]_N$-coupon tests, and red the tensile $[\pm 45]_N$-coupon tests.

When the two η-curves are used in an FEA, simulating the two input tests, the differences are quite evident. The η-value is proportional to the secant stiffness in the simulation seen in the Figures 6.6 and 6.8, and as seen in Figure 6.5 and 6.7. This *minor* difference results in larger differences in the stress-strain relations.

6.4.4 Validation of the model using shell elements

All material properties defined for the simulations above have been used in the following simulations using shell elements when predicting the behavior of

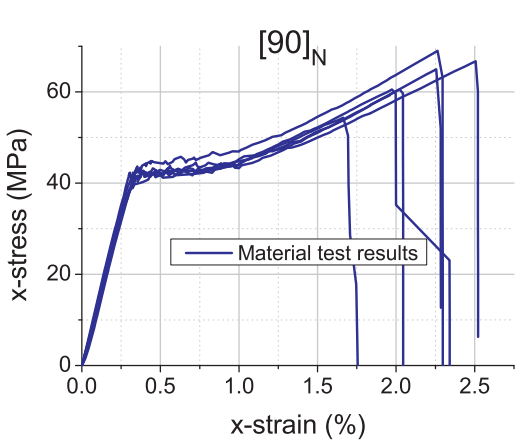

Figure 6.2: Experimental observations of the tensile $[90]_N$-coupon test.

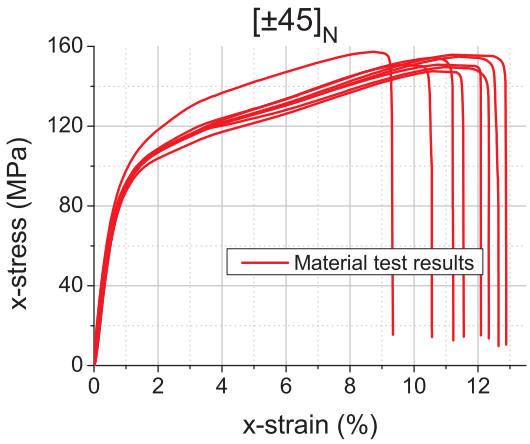

Figure 6.3: Experimental observations of the tensile $[\pm 45]_N$-coupon test.

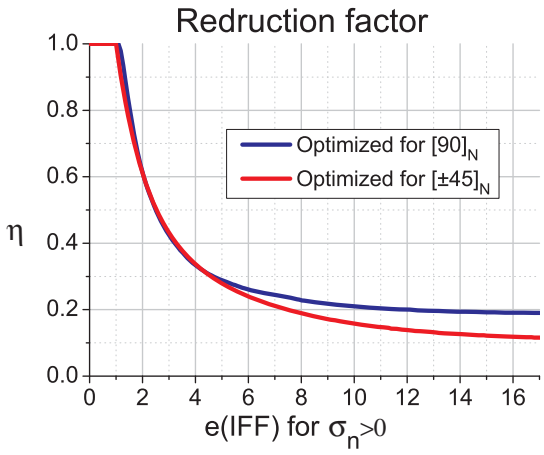

Figure 6.4: Reduction factor η as a function of the interfiber failure criterion for tensile failure.

$[\pm 45/90]_N$-coupons (Figure 6.9 and 6.10), $[\pm 45/0/90]_N$-coupons(Figure 6.11 and 6.12) and $[\pm 45/90_6/\pm 45]_N$-coupons(Figure 6.13 and 6.14), subjected to tensile loading. Once again, blue curves indicate reduction factor based on the tensile $[90]_N$-coupon tests, and red the tensile $[\pm 45]_N$-coupon tests.

6.4.5 Validation of the model using solid elements

All material properties defined for the simulations above have been used in the following simulations using solid elements when predicting the behavior of

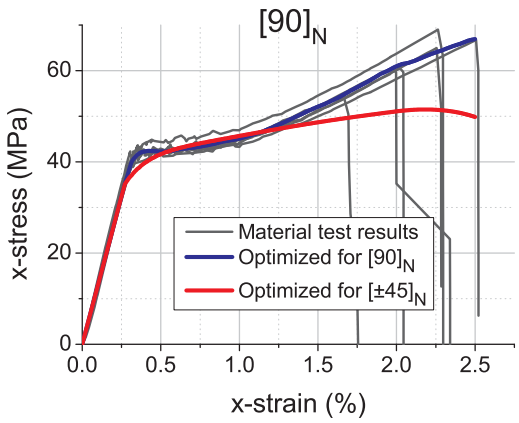

Figure 6.5: Comparing observed and predicted stress-strain curves for $[90]_N$-coupon test using shell elements.

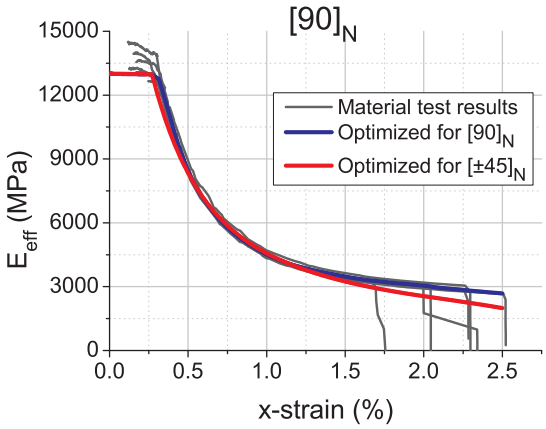

Figure 6.6: Comparing observed and predicted effective Young's modulus for $[90]_N$-coupon test using shell elements.

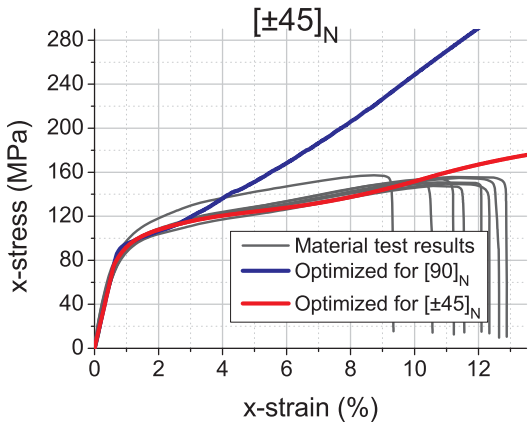

Figure 6.7: Comparing observed and predicted stress-strain curves for $[\pm 45]_N$-coupon test using shell elements.

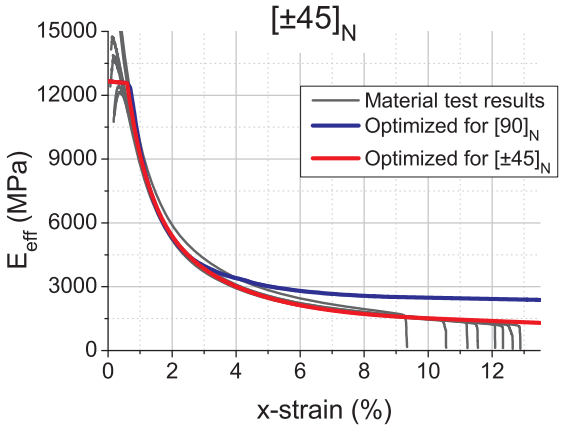

Figure 6.8: Comparing observed and predicted effective shear modulus for $[\pm 45]_N$-coupon test using shell elements.

$[\pm 45/90]_N$-coupons (Figure 6.9 and 6.10), $[\pm 45/0/90]_N$-coupons(Figure 6.11 and 6.12) and $[\pm 45/90_6/\pm 45]_N$-coupons(Figure 6.13 and 6.14), subjected to tensile loading. Once again, blue curves indicate reduction factor based on the tensile $[90]_N$-coupon tests, and red the tensile $[\pm 45]_N$-coupon tests. One should keep in mind that the η-curves are optimized for shell elements. No optimization has been conducted for solid elements, so simulations predicting the behavior of $[90]_N$- and $[\pm 45]_N$-coupons subjected to tensile loading are conducted as verification simu-

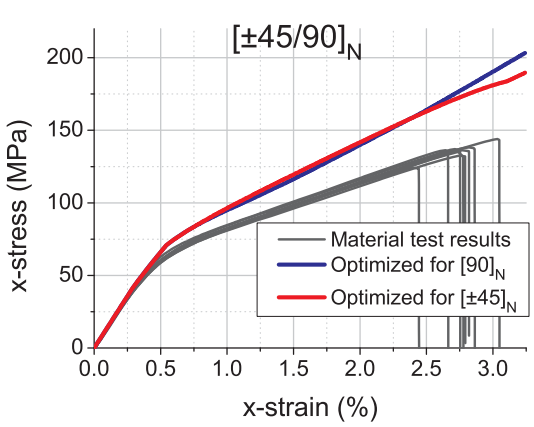

Figure 6.9: Comparing observed and predicted stress-strain curves for $[\pm 45/90]_N$-coupon test using shell elements.

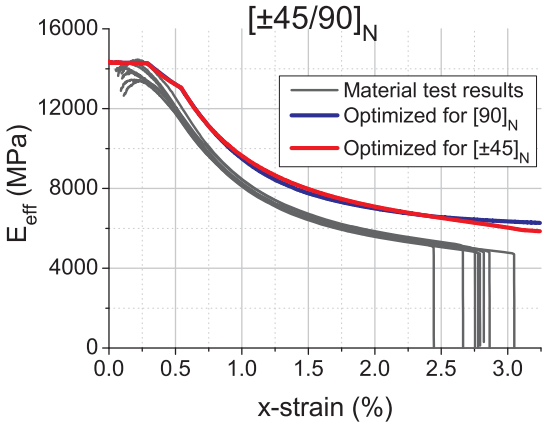

Figure 6.10: Comparing observed and predicted effective shear modulus for $[\pm 45/90]_N$-coupon test using shell elements.

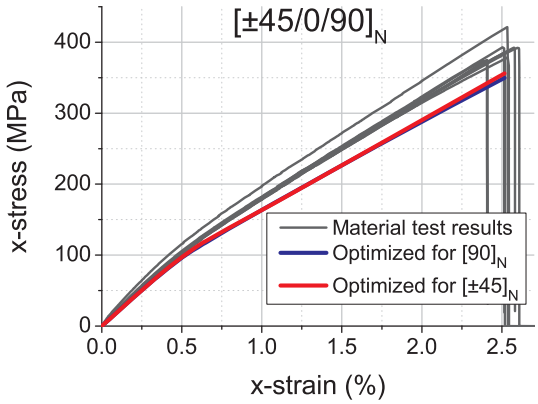

Figure 6.11: Comparing observed and predicted stress-strain curves for $[\pm 45/0/90]_N$-coupon test using shell elements.

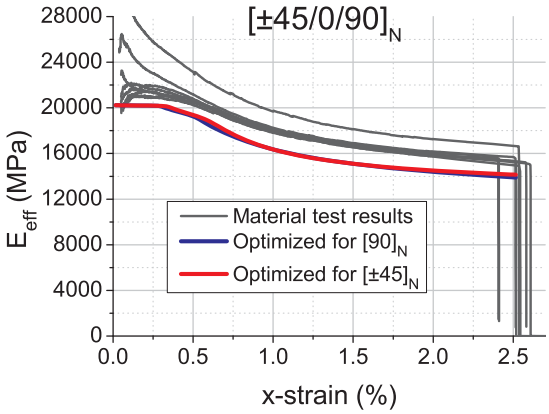

Figure 6.12: Comparing observed and predicted effective shear modulus for $[\pm 45/0/90]_N$-coupon test using shell elements.

lations as well. To model the complete test specimen would make the analysis too computational costly, so only a small section of the coupons are modeled. It is assumed symmetry about origo in the axial cross in Figure 6.15.

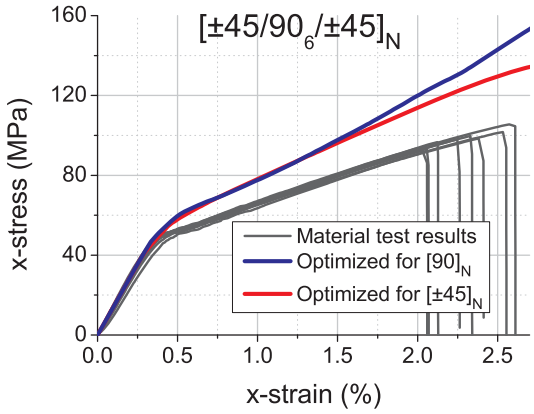

Figure 6.13: Comparing observed and predicted stress-strain curves for $[\pm 45/90_6/\pm 45]$-coupon test using shell elements.

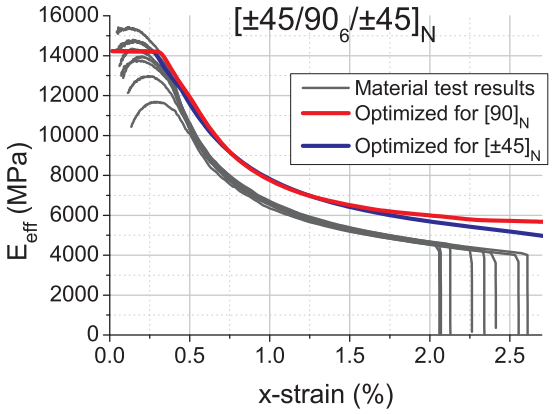

Figure 6.14: Comparing observed and predicted effective shear modulus for $[\pm 45/90_6/\pm 45]$-coupon test using shell elements.

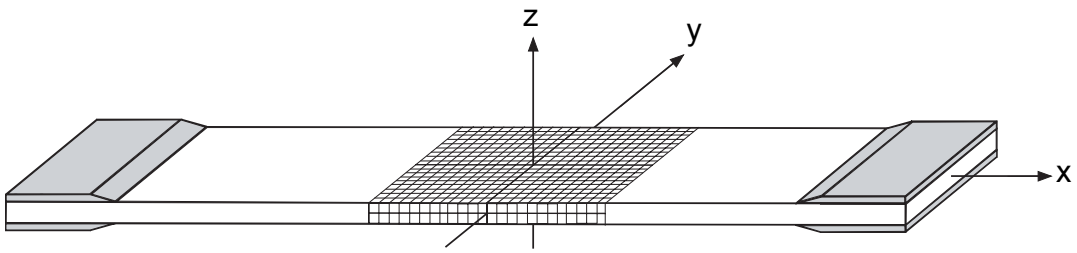

Figure 6.15: Illustration of the tested coupons with tabs.

6.4.6 Comparing results against other available material models

The results from the implemented material model based on the Puck failure criterion is shown to provide results in good agreement with experimental observations. The three material models presented in Section 5.5 are compared to the previous results using the implemented material model. These material models are only applicable to shell elements, so all of the following curves results from FEA based on shell elements. All other material parameters are the same. The reduction factors are only used for the implemented material model since no such damage description is applicable to the other material models. For material model 22, the stiffness of a ply after reaching any failure criterion after being subjected to an increasing load, is reduced to zero. The remaining plies continue to carry load as the load keeps increasing, until they also reach one of the failure criteria of the material model. Material model 54 and 55 allows a specimen to be

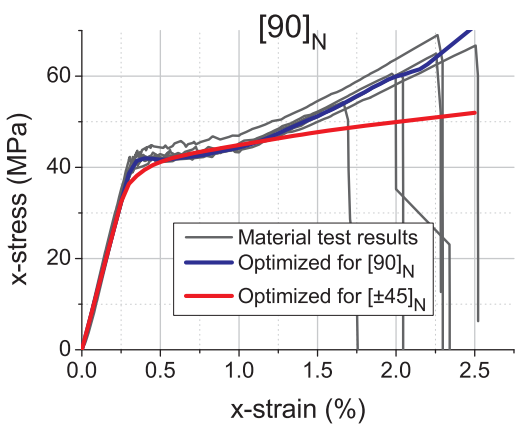

Figure 6.16: Comparing observed and predicted stress-strain curves for $[90]_N$-coupon test using solid elements.

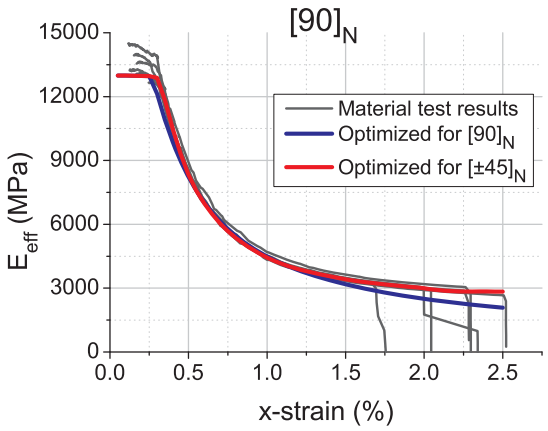

Figure 6.17: Comparing observed and predicted effective Young's modulus for $[90]_N$-coupon test using solid elements.

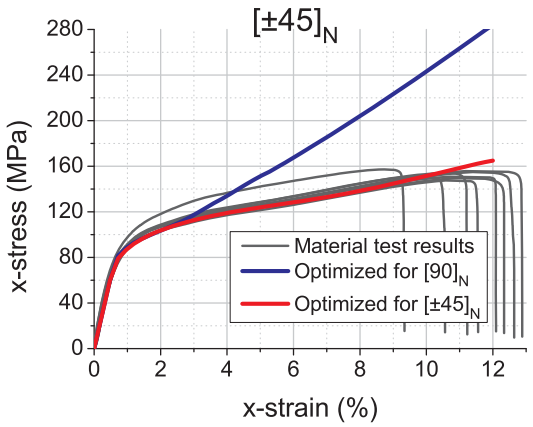

Figure 6.18: Comparing observed and predicted stress-strain curves for $[\pm 45]_N$-coupon test using solid elements.

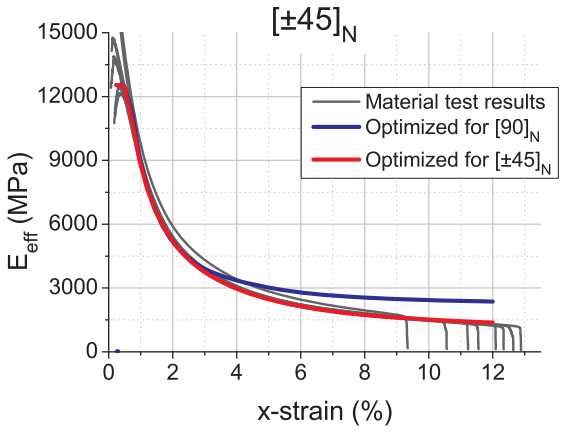

Figure 6.19: Comparing observed and predicted effective shear modulus for $[\pm 45]_N$-coupon test using solid elements.

strained after a failure criterion is reached, but the stresses that caused failure, in the element in question, are not allowed to increase. This behavior is evident in the $[90]_N$-coupons and $[\pm 45]_N$-coupons, seen in Figure 6.26 and 6.27, respectively.

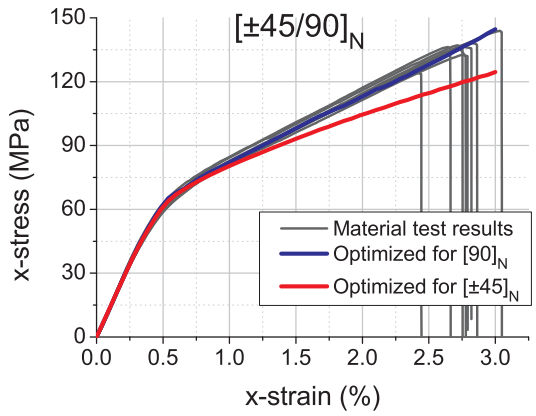

Figure 6.20: Comparing observed and predicted stress-strain curves for $[\pm 45/90]_N$-coupon test using solid elements.

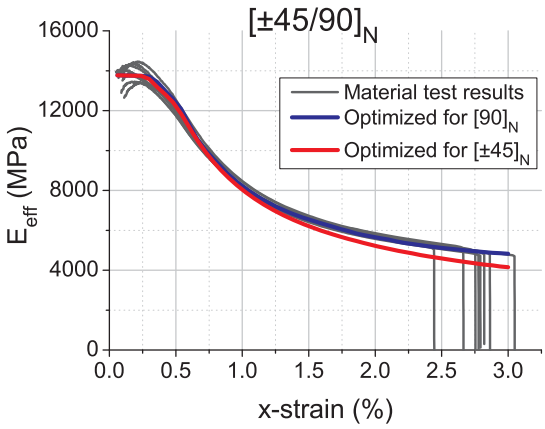

Figure 6.21: Comparing observed and predicted effective shear modulus for $[\pm 45/90]_N$-coupon test using solid elements.

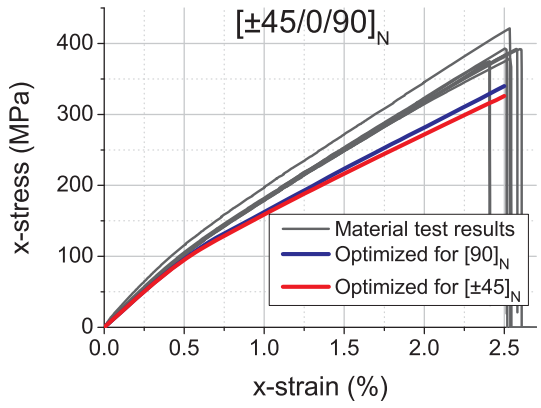

Figure 6.22: Comparing observed and predicted stress-strain curves for $[\pm 45/0/90]_N$-coupon test using solid elements.

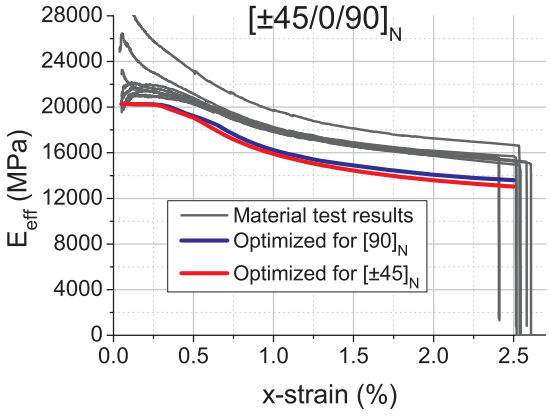

Figure 6.23: Comparing observed and predicted effective shear modulus for $[\pm 45/0/90]_N$-coupon test using solid elements.

6.5 Discussion

The tested materials are laminates made up of UD plies. The plies are constructed of vacuum infused non crimp fabric. The non crimp fabric is stitched in order to keep the fibers correctly aligned through the vacuum infusion. The stitching contributes with a stiffening factor to the transverse direction. The Puck failure criterion is developed for transversely isotropic materials where the matrix is the

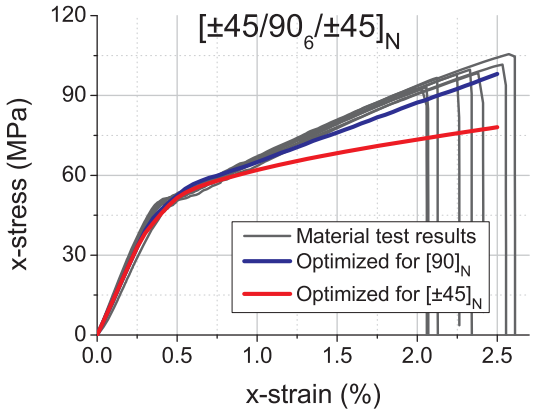

Figure 6.24: Comparing observed and predicted stress-strain curves for $[\pm 45/90_6/\pm 45]$-coupon test using solid elements.

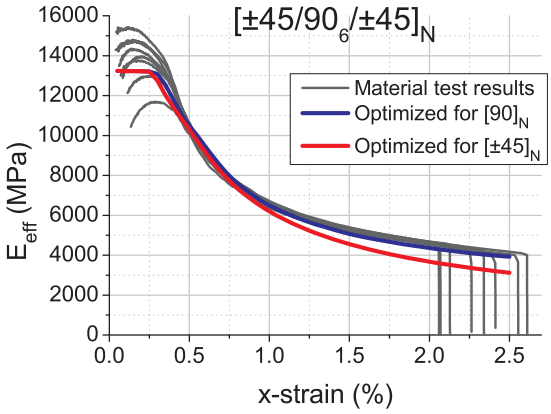

Figure 6.25: Comparing observed and predicted effective shear modulus for $[\pm 45/90_6/\pm 45]$-coupon test using solid elements.

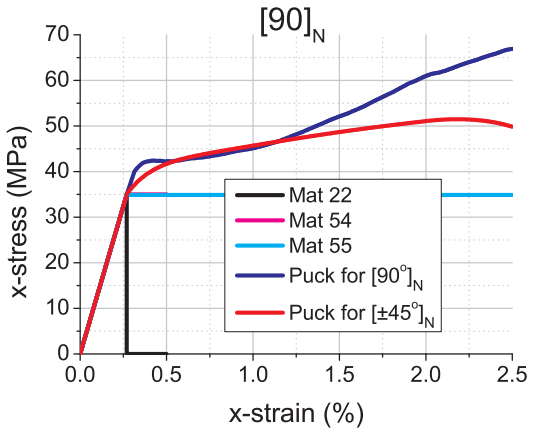

Figure 6.26: Comparing the material models for tensile tests on $[90]_N$-coupons using shell elements.

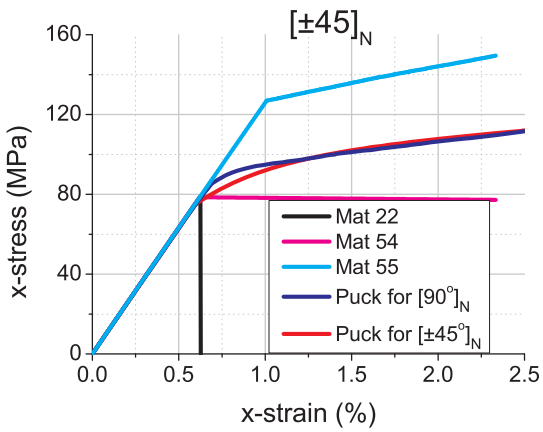

Figure 6.27: Comparing the material models for tensile tests on $[\pm 45]_N$-coupons using shell elements.

bearing constituent in all transverse directions to the fibers. The stitching provides stiffness and strength only in one transverse direction, the in-plane direction transverse to the fibers. Using these arguments the stiffness obtained from this transverse direction should be higher than for directions other than that of the stitching. This may explain why the predicted damage behavior of the $[\pm 45]_N$ coupon tests, based on the transverse stiffness degradation, did not correspond with the experimentally observed behavior. The stiffening effect of the stitching

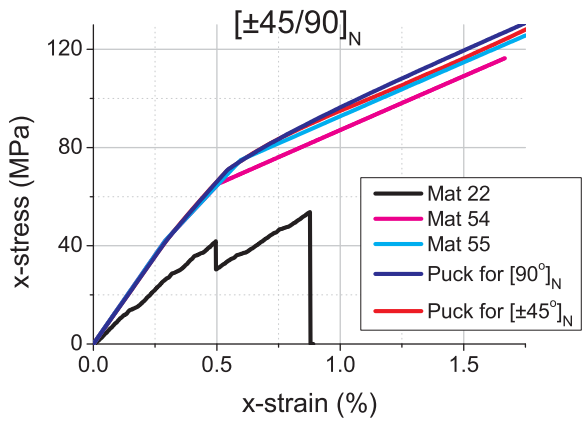

Figure 6.28: Comparing the material models for tensile tests on $[\pm 45/90]_N$-coupons using shell elements.

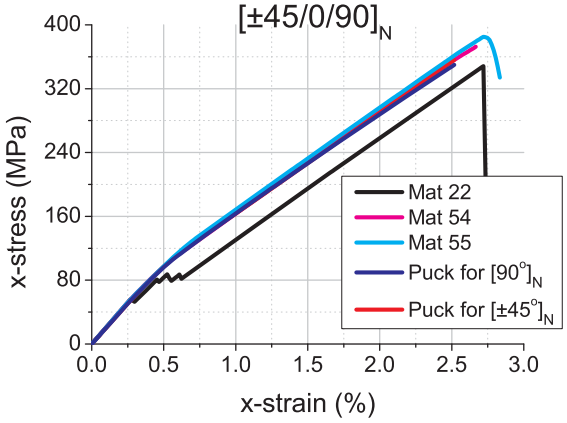

Figure 6.29: Comparing the material models for tensile tests on $[\pm 45/0/90]_N$-coupons using shell elements.

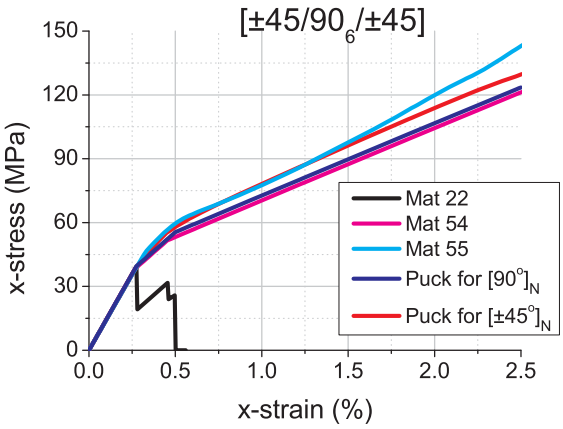

Figure 6.30: Comparing the material models for tensile tests on $[\pm 45/90/\pm 45]$-coupons using shell elements.

is evident in the transversely tensile loaded UD-coupon. It behaves as if there are some loosely fitted fibers embedded in the transverse direction that eventually, after being straightened out and strained, fracture. This behavior should be less evident in the 45°-direction which is off-axis for both fibers and stitching. As suggested by Puck[10] the damage-curve deduced from the $[90]_N$-coupon tests is used to degrade the E_2, G_{12} and ν_{12} parameters. This can explain the difference between the predicted and the experimentally observed behavior of the $[\pm 45]_N$ coupon tests. When analyzing the laminates presented in this study, it might be better to degrade E_2 and G_{12} separately.

The UD-lamina properties observed in the tensile $[0]_N$-coupon tests, show $X_{tu} = 681MPa$ at $\epsilon_{11} = 0.0177$, which supposedly is the ultimate strain in the $11-$direction. This contradicts the observations of the tensile $[\pm 45/0/90]_N$- and $[0/90]_N$-coupon tests where the laminates are strained past $\epsilon_x = 0.025$ which is equivalent to $\epsilon_{11} = 0.025$ for the plies oriented with fibers in the loading direction. If the plies, with fibers oriented in the loading direction, had failed at the predicted strain level, it would have significantly reduced the stiffness. When plies with fibers oriented in the loading direction fail, it usually results in instantaneous ultimate failure for the whole laminate[13]. These observations suggest that ϵ_{1u} should have a greater value than that observed in the tensile $[0]_N$-coupon tests (see Chapter 4.3). In laminates with various ply orientations these experimental observations indicate that $\epsilon_{1u} = 0.025$. Pure UD-laminates are seldom used in real life applications, but it should be noted that this ultimate strain value is not applicable to UD-laminates.

The analyses using shell elements seem to result in too stiff results for the verification laminates, except for the laminate containing plies with fibers orientations in the loading direction. As mentioned above, the material data gathered from UD laminate testing might not be suitable for describing ply behavior in laminates with multiple ply orientations. This is shown to be the case for the ultimate strength in the 11-direction, and further investigations should be made in order to see if this is an issue for the stiffness in the 11-direction as well. The shell elements have been restrained from translation in the z-direction(see Figure 6.15), not allowing for the out of plane deformation forced by the non symmetric lay up. This would also explain stiffer results from these simulations.

When the analyses are conducted using solid elements, the resulting stress-strain curves have somewhat the same shape as for the shell element simulations, but it seems the initial stiffness is slightly reduced. This is best seen in the plotting of the effective stiffness, E_{eff}, where the curves for the solid elements bears the same shape, but are lowered by the reduced initial stiffness. The same reduction factors that are optimized for shell elements have been used. The validity of this action is proved in Figure 6.16 and 6.18 where the respective curves fall nicely in with the experimental observations. The brick elements allow for different poisson effects in the various plies through the thickness of the laminate, i.e. cross sections do not need to be plane after deformation as they do for the shell elements. This constraint makes the laminates constructed using shell elements stiffer than the ones using solid elements. Only few repetitions of the stacking sequence have been modeled for the solid element simulations. As mentioned in Chapter 2.3, increasing the stacking sequence frequency result in reduced out of plane coupling, subsequently increasing the in-plane stiffness. Consequently these simulations using solid elements are expected to show lowered stiffnesses due to a reduced stacking sequence frequency.

In Figures 6.26 through 6.30 the results from 4 different material models are shown. Material model 22 and 54 use the Chang Chang composite failure model.

Material model 54 is a much more complex material model than 22, and it seems it is also more stable. During this study material model 22 often failed to find equilibrium when material model 54 showed no problems. It seems material model 54 is a more robust model, and the better choice if the Chang Chang criterion is to be used. If the post first ply failure behavior is to be investigated, material model 22 should not be used. It can give a good description of when a ply fails since the stress strain curve suddenly drops, but the stiffness after the first ply failure is far from correct. Post first ply failure is better described in material model 54 and 55(uses the Tsai-Wu failure criterion). In Figure 6.28,6.29 and 6.30 it can be seen that these two models coincide well with the results using the Puck failure criterion. In Figure 6.28 and 6.30 it can be seen that material model 54 predicts failure at an earlier point than material model 55 and the results from the Puck failure criterion. This is an unexpected observation since the Tsai-Wu is supposedly the more conservative criterion in tension(see Figure 3.6). This can be a consequence of the strange behavior material model 55 shows in Figure 6.27. The reason for this behavior has not been found. The input files for numerical analyses using material model 55 and 54 are identical. They even use the same material keyword card[29], the only difference is what failure criteria the material model calls. Not only is it strange that the model behave linear elastic beyond the ultimate shear strength, the amount of stress subjected to the model increases after failure. The model is meant to be able to be strained an additional amount after failure (must be specified how much in the input file) without being able to bear a higher level of stress.

On the basis of these experiences, material model 54 seems the best alternative to the implemented material model based on the Puck failure criterion. In the continuation of this study, experiments will be conducted on filament winded pipes. The pipes will be subjected to a combination of torsion and compression (τ_{12} and σ_{22}) providing experimental observations for the upper-left corner of the failure locus seen in Figure 3.5. The value of θ^0_{fp} can then be chosen so that the failure envelope suits the experimental observations as well as possible.

Chapter 7

Case study 2: Pinhole loaded FRPC plate

7.1 Problem description

The pinhole loaded FRPC plate problem is an exercise that shows the impact different laminate lay ups have on the failure mechanisms and load bearing capacity. The rigid pin is the only restriction on the plate, and the load P is applied as a distributed load to the far end of the plate. Chang et al.[33] performed a large experimental program on pin-loaded plates made of T300/1034C graphite/epoxy laminate material with different ply orientations. The test program included different geometries where, in addition to the material properties, the failure strength and failure models were reported. Three stacking sequences are considered in this study, $[0/90]_{NS}$, $[\pm 45]_{NS}$ and $[0/\pm 45/90]_{NS}$. The nominal failure strengths and failure modes were reported in Chang's work as 458-S (MPa), 550-T (MPa) and 641-B (MPa), respectively. The capital letters indicate S for shear, T for tension and B for bearing failure mode. The three failure modes are illustrated in Figure 7.2.

The geometry and the material properties of the plate are shown in Figure 7.1 and listed in Table 7.1.

7.2 FE analysis

The plate is modeled using the same four node shell elements with integration points through the thickness, used in Case study 1.

Only half the plate is modeled due to symmetry about the x-axis (see axis in Figure 7.1). All nodes along the symmetry line are restrained from translations in the y-direction (see model in Figure 7.3). The rigid pin preventing the plate form moving in the direction of the applied load is modeled using eight node solid elements with a rigid body material model. The pin is con-

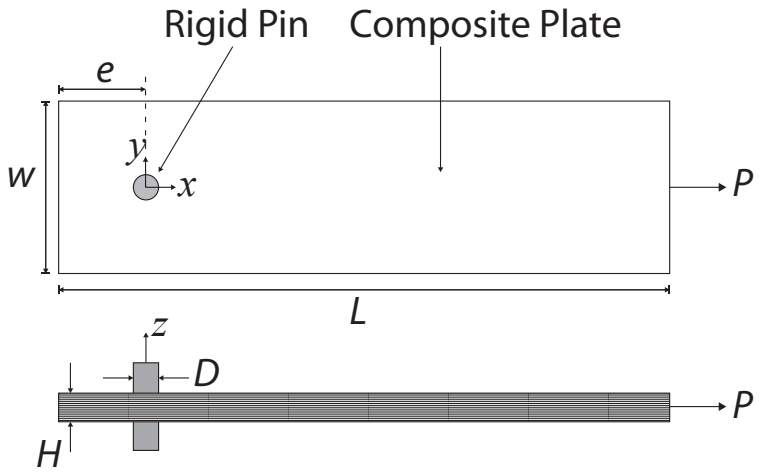

Figure 7.1: Schematic description of the pinhole loaded plate problem.

Table 7.1: Material properties used in Case study 2: Pinhole loaded plate.

L	178	mm
H	3	mm
D	12.7	mm
w/D	5	
e/D	3	
E_1	147	GPa
E_2	11.7	GPa
G_{12}	6.2	GPa
ν_{12}	0.3	
Y_c	204	MPa
Y_t	43	MPa
X_c	1380	MPa
X_t	1730	MPa
S_{12}	133	MPa

strained from all translations and rotations. The contact formulation called *CONTACT_NODES_TO_SURFACE*, is thoroughly described in the LS-DYNA Keyword User's Manual[29]. The surface of the pin and the edge nodes of the plate are basically known throughout the analysis allowing for a simple contact description. To avoid problems with the contact simulation, the location of the nodes on the plate (slave nodes) matches the location of the nodes on the rigid pin (master surface). To ensure that non of the slave nodes has passed over the element boundary of the master surface, the hole has a slightly larger radius than the pin. The meshing of the model has been generated manually. The mesh is

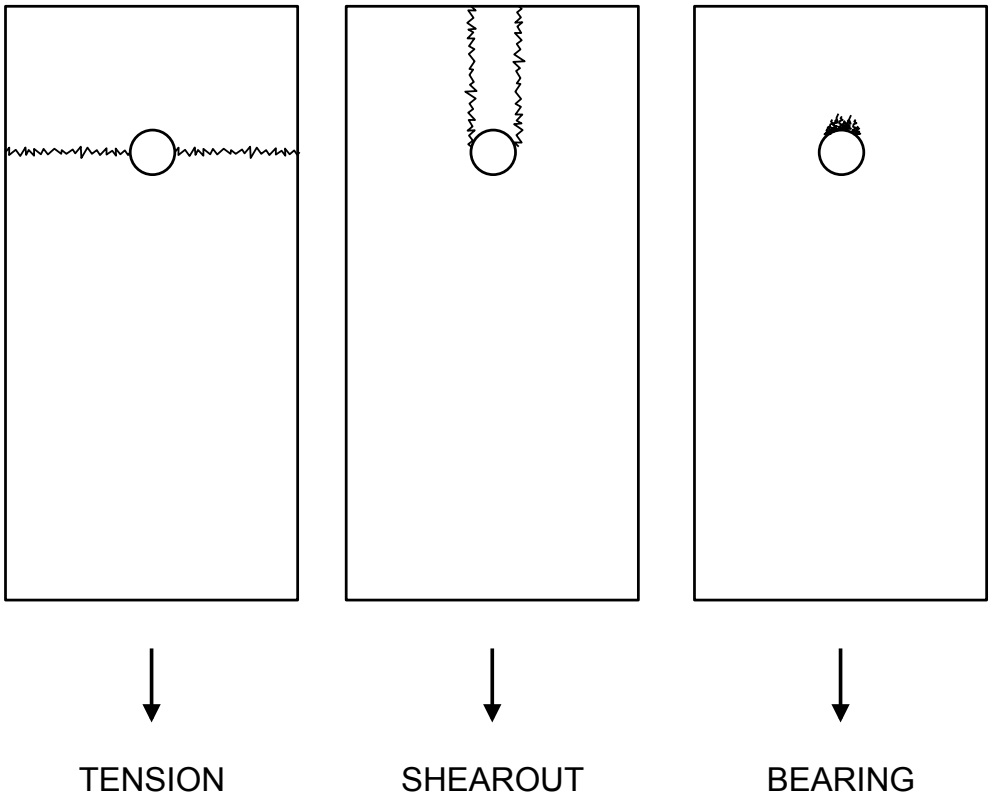

Figure 7.2: Illustration of the three basic failure modes.

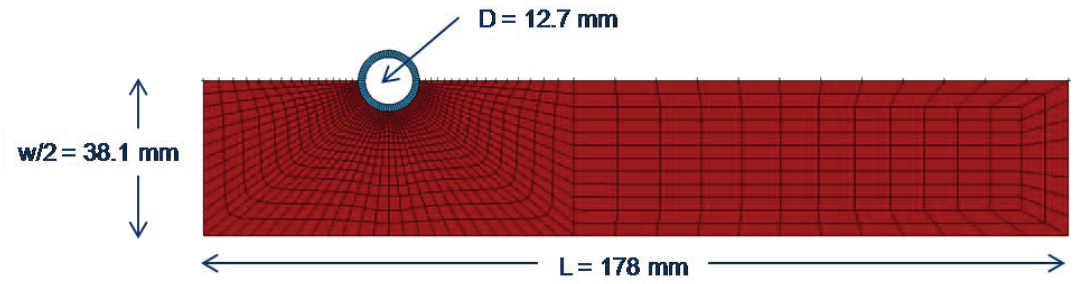

Figure 7.3: In the FEA only half the plate is modeled due to symmetry along the x-axis.

fine with many small elements in the area of interest around the pin, and courser with large elements in the rest of the model. It is around the pin, failure is most likely to start, and it is desirable to be able to differ between the different failure modes. It is also important that the mesh does not dictate the direction or mode of failure. To minimize the mesh sensitivity of the failure condition, the elements should be made of equal size and shape in all directions from the pin's point of view. There are two competing objectives when meshing a model, the mesh

in the area of interest should be as fine as possible, and the computational cost should be kept down. More elements result in more integration points demanding increasing computational cost, but on the other hand, more elements also result in finer strain distribution. The size of the elements also has an impact on the time step when using an explicit time integration. The time step cannot be larger than the time a sound wave takes to pass through the shortest crossing of the element. This is not a consideration one needs to take into account when using implicit time integration, static or dynamic. When simulating failure by deletion of elements, the abrupt changes in stiffness may cause implicit time integration to fail. The static implicit solver usually fails to find equilibrium, but a dynamic implicit solver may add sufficient inertia to the model so that the solver succeeds in finding equilibrium. The time step size for explicit time integration may be increased by adding non physical mass to the model. This technique is called mass-scaling. By adding non physical mass to increase the time step in a dynamic analysis, the result is affected ($F = ma$). The amount of added mass must be limited in order to keep the analysis from generating dynamic effects due to the added inertia. These dynamic effects may cause stress concentrations that lead to non physical failure.

In this analysis, the time step demanded by explicit time integration was shown to be too computational costly without adding an amount of mass scaling causing undesirable dynamic effects. Static implicit time integration, showed to be unstable when approaching failure. Dynamic time integration was for these reasons chosen for this analysis.

The load is applied as a forced displacement at the far right end of the plate. The displacement is forced on all the nodes along this edge.

7.3 Results

The stress-displacement curves shown in Figure 7.4 show the relationship between the applied load and the displacement of the edge of the plate where the load is applied in the direction of the load (see Figure 7.1). The stress plotted in the stress-strain curve is collected from the calculated boundary force in the displacement nodes. The force is divided by the cross section area of the plate at the displacement edge in order to derive stress values plotted in Figure 7.4.

The contour plots shown in Figure 7.5, 7.6 and 7.7 are saved from the moment right before the model failed, i.e. when the respective stress-strain curves have their maximum in Figure 7.4. In Figre 7.5, 7.6 and 7.7 the value of the Puck fiber failure in compression is illustrated. Failure initiates when the criterion reaches unity.

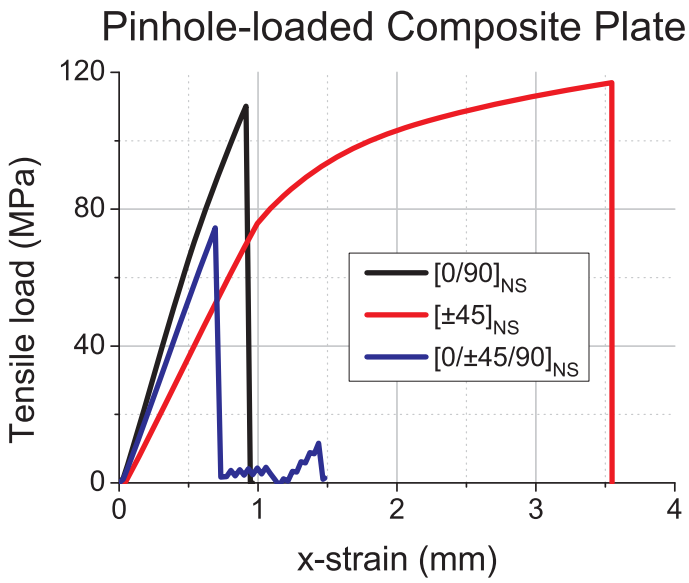

Figure 7.4: Stress-strain curves for the three different laminates that are investigated.

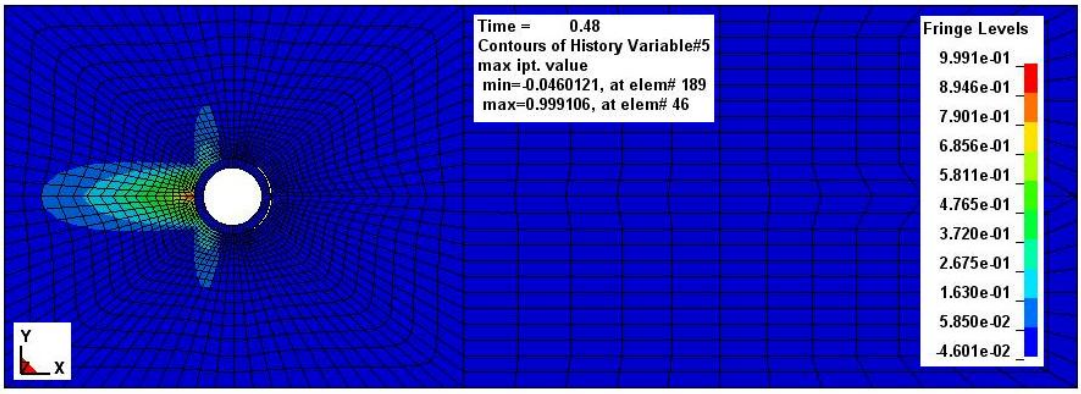

Figure 7.5: Contour plot showing the variations Puck fiber failure criterion in compression over the $[(0/90)_6]_S$-laminate. Failure initiates when value reaches unity

7.4 Discussion

When comparing the analysis using the Puck failure criterion to those of Chang et al.[33], the differences are evident. The load bearing capacity is drastically lower in the Puck simulations. Also, in the results found by Chang et al. the $[(0/\pm 45/90)_3]_S$-laminate shows the best load bearing capacity, while in the Puck simulations the $[(\pm 45)_6]_S$-laminate has the greatest load bearing capacity. One

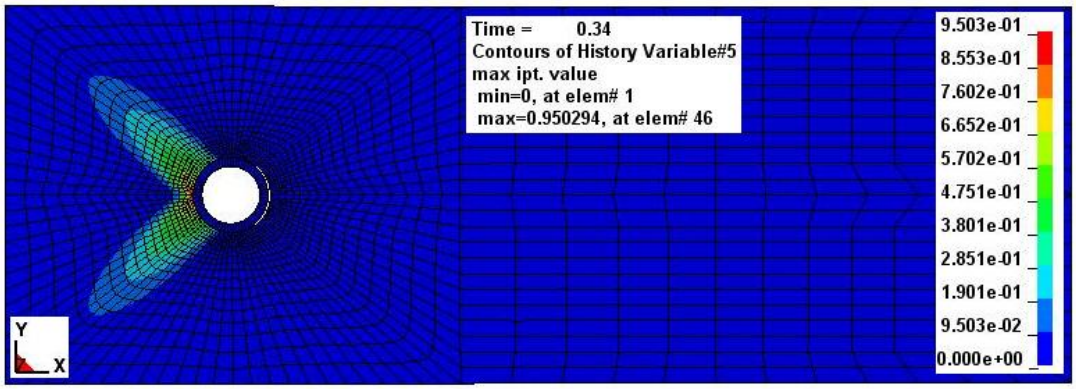

Figure 7.6: Contour plot showing the variations Puck fiber failure criterion in compression over the $[(\pm 45)_6]_S$-laminate. Failure initiates when value reaches unity

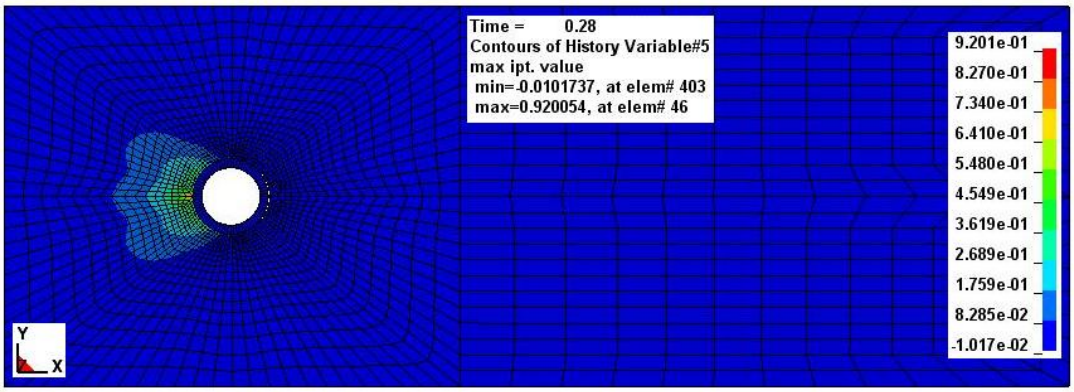

Figure 7.7: Contour plot showing the variations Puck fiber failure criterion in compression over the $[(0/\pm 45/90)_3]_S$-laminate. Failure initiates when value reaches unity

should notice that this capacity is reached after first ply failure and that the post first ply failure behavior has not been evaluated for the material in question. In the Puck simulations an arbitrary reduction factor shown to describe post failure behavior for glass fiber reinforced laminates well. Figure 6.28, 6.29 and 6.30 in Chapter 6, showed the results using different reduction factors (Note that the curve for Mat 22 shows results when a reduction factor is not applied). Both results predict the same failure modes for the three different laminates. In Figure 7.5 one can see the concentration of the failure criterion prompting a *tension*-failure mode, in Figure 7.6 the concentration of the failure criterion prompts a *shearout*-failure mode, and finally Figure 7.7 shows the build up of *bearing*-failure. These laminates failed in the same modes as predicted in the literature examples described in Section 7.1.

Fracture analysis is a difficult problem for numerical solution methods because the singularity at the crack tip is not adequately described by traditional formulations unless the meshes are extremely fine. Beltyschko and some of his students have developed the extended finite element method (X-FEM) [34] to address these types of problems.

Chapter 8

Case study 3: Shear Test Geometry

8.1 Problem description

FiReCo is a company located in Fredrikstad, Norway working with composite materials. They handle a variety of projects, from detailed product development to full scale production. They have in cooperation with SINETF come up with some findings within the v-noched rail shear test standard (ASTM d7078). They wanted to analyze and optimize the shear test by investigating various specimen geometries and laminate lay ups. The shear properties of quad-axial laminates (laminates with fiber direction in 4 directions) were investigated, even though the standard does not recommend using plies with orientations other than 0° and 90°. Apparently the quad-axial laminates were too stiff for the test fixture, and the specimen rotated when loaded in shear. When increasing the torque of the bolts holding the specimen in place, the specimen suffered crushing damage by the fixture before adequate torque level was reached. The tests were then repeated with fewer plies, the distance between the notches were reduced, and the notch radius was increased from 3 to 5 mm. When this new specimen geometry was tested, it fractured at the compression side of the notch (as seen in Figure 8.2), and DIC-measurements(see section 4.5) showed a strain concentration in the fracture area before fracture initiated. This strain concentration was not shown in test specimens with the standard notch radius. It seemed to be located in the area where the fibers in the $-45°$-direction changed from being continuous to being chopped off by the radius at the bottom of the notch.

The test configuration showing the described results, was shown to be replicable using the Puck failure criterion. It was carried out in an attempt to understand what caused this strain concentration, what ply was the first to fail and in what failure mode it failed. The material properties were the same as for the materials tested in *Case study 1: Puck failure criterion* in Chapter 6, and they are listed in Table 8.1.

Table 8.1: Material properties used in Case study 3: Shear test

E_1	40500	MPa
E_2	13900	MPa
G_{12}	4000	MPa
ν_{12}	0.25	
ν_{23}	0.30	
Y_c	200	MPa
Y_t	35	MPa
Y_{tu}	62.7	MPa
X_c	400	MPa
X_t	681	MPa
S_{12}	50	MPa
θ^0_{fp}	51°	

8.2 FE analysis

The analysis was conducted using the same four node shell elements, with centered integration points through the thickness, as described in Chapter 6 and 7. In Figure 8.3 the geometry of the specimen, and the test fixture is illustrated. All nodes within the shaded rectangle denoted *Clamped* is restrained from all translations and rotations, and all nodes within the shaded rectangle denote *Forced displacement* is restrained from translations in x- and z-direction, and all rotations. The load is applied as a forced displacement in the positive y-direction. The total height of the specimen in the y-direction is 56 mm, and the total width in the x-direction is 76 mm. These measurements are valid for all the tested specimens. The different geometries are defined by the values for H and R shown in figure 8.3. For the specimen analyzed here, the value of H is 20 mm, and notch radius R is 5 mm.

The meshing of the model has been carried out manually. The objective of the meshing is to have elements of equal size and shape in the area of interest, which is the area around the notch. The mesh is symmetric about the horizontal and vertical centerline.

8.3 Results

A contour plot from the FEA is shown in Figure 8.4. The contour plot shows the distribution of the Puck compressive fiber failure criterion over the specimen. The other failure criteria are not plotted here, but the matrix failure criterion has already passed unity on the tensile side of the notch, at the moment this

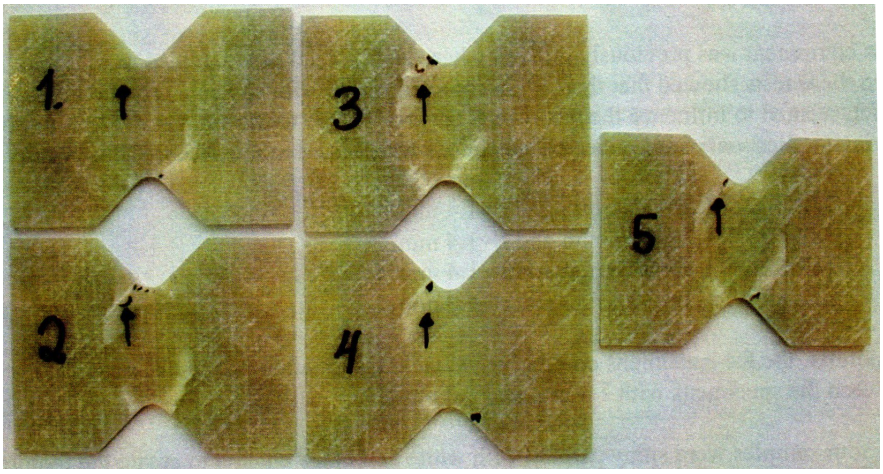

Figure 8.1: Shear test specimen $[0/\pm 45/90]_3$

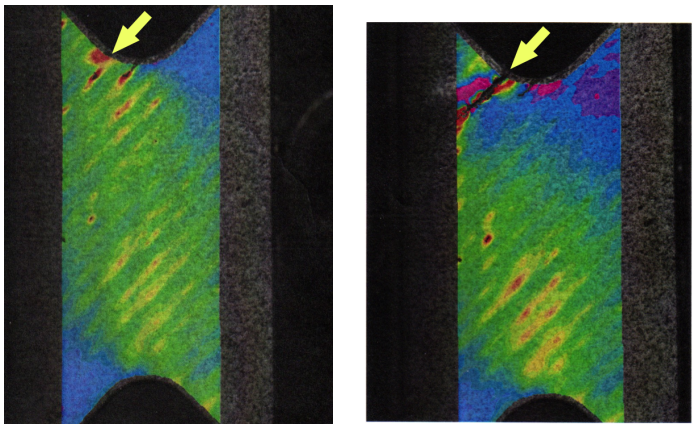

Figure 8.2: DIC showing y-strain in compression, and the same test after failure

contour plot was plotted. The tensile fiber failure criterion was far from unity when the plot was plotted. The plot shows the maximum value of the criterion through the thickness of the laminate. The contour plot shown in Figure 8.4 is taken right after failure. In Figure 8.6 the nominal shear stress between the two notches are plotted as the forced displacement, δ_{22} is applied in the y-direction. The two contour plots illustrated in Figure 8.4 saved at simulation time: 1.1, and 8.5 saved at simulation time 1.2 are indicated in the stress plot.

8.4 Discussion

The location of the global failure seen in Figure 8.1 is most likely made visible in this manner after fiber failure (see Chapter 3.1.1). The presence of matrix damage does not necessarily lead to global failure. The levels of matrix failure observed

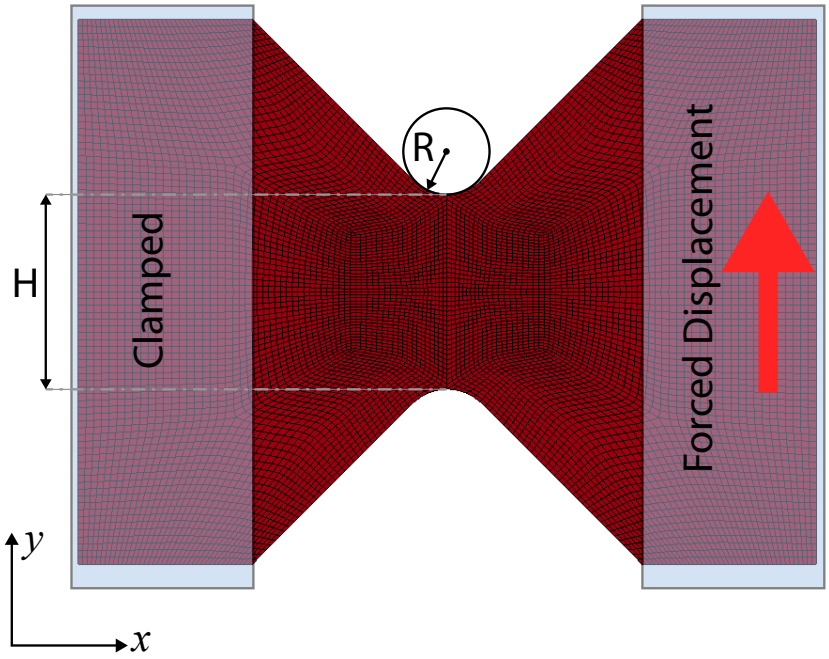

Figure 8.3: FE model of test specimen

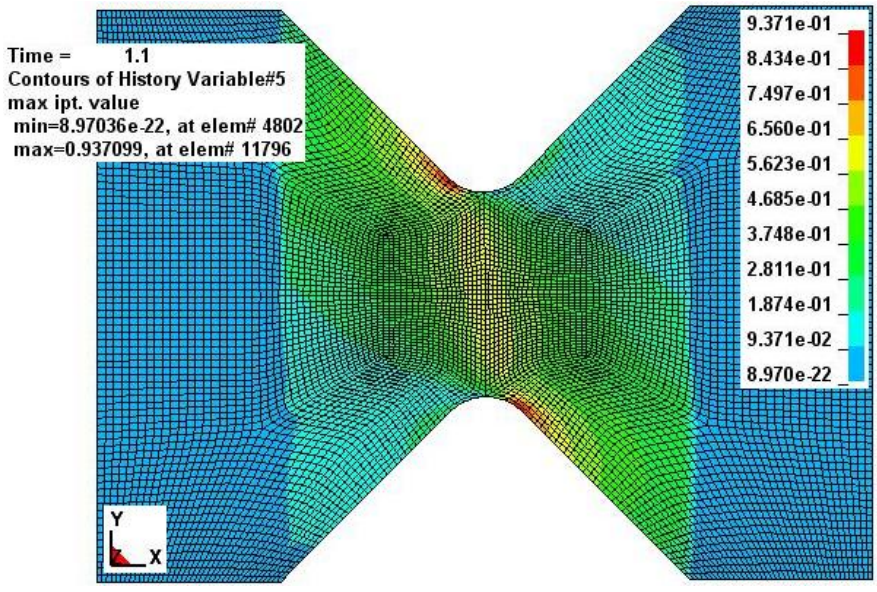

Figure 8.4: Shear test model showing contour plot of Puck's Fiber Failure criteria. Failure initiate when criterion reaches unity.

on the tensile side of the notch is relatively small compared to the equivalent matrix damage observed in the UD laminates loaded in the transverse direction

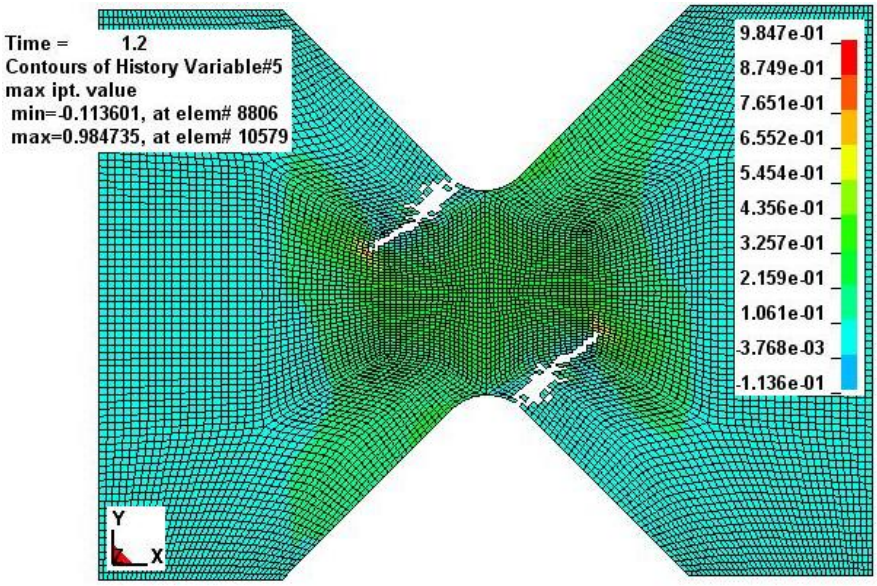

Figure 8.5: Shear test model showing contour plot of Puck's Fiber Failure criteria after failure. Failure illustrated with element erosion.

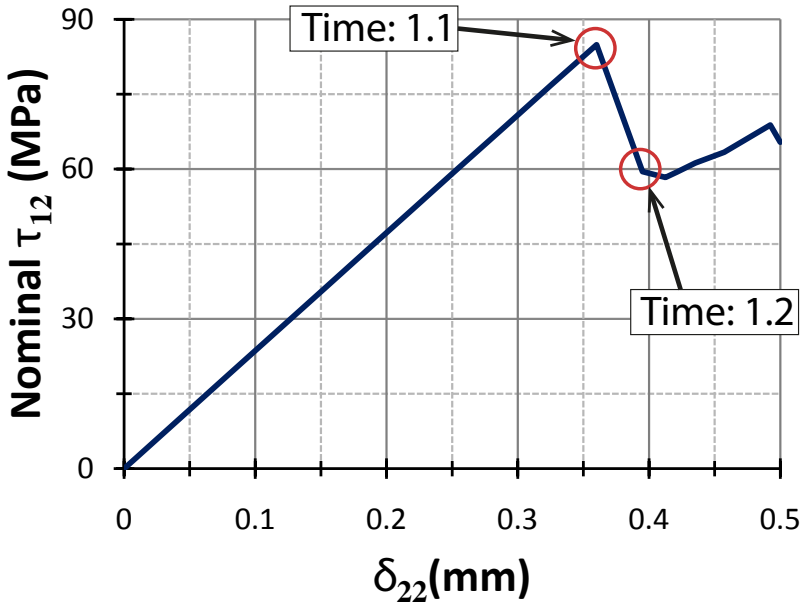

Figure 8.6: Plot showing nominal shear stress between the notches as the forced displacement δ_{22} in the y-direction is applied as illustrated in Figure 8.3.

in *Case study 1*, described in Chapter 6. In these experimental observations no violent damage could be measured at this level of matrix damage. The interfiber failure criterion on the tensile side of the notch had a value of approximately 3.5

when the compressive fiber failure reached unity, on the compressive side of the notch. In Case study 1, the inter fiber failure criterion of the transversely tensile loaded UD laminate had a value of above 10 at the strain level at which the first test specimen failed in the materiel test (see Figure 6.5)

The maximum value of the compressive fiber failure criterion is held by the plies with fiber oriented from the upper left to the lower right. These plies experience a compressive loading in the fiber direction, and the fibers in the plies are therefore subjects of a buckling problem. The most critical fibers are obviously those with the highest stress and lowest support. The fibers with the lowest support, are the ones found in the plies oriented in the $\pm 45°$. These plies have fibers following the edge of the notches, and the fibers that are located along the free edge, are the ones with the lowest support against buckling. There will always be stress concentrations around corners and notches in structures under loading, as is the case in this experiment. The location of the stress concentration in this experiment happens to be located in the area where the fibers in the mentioned plies go from being continuous to being chopped off by the notch radius, as illustrated in Figure 8.7.

The maximum through the thickness value was plotted in the contour plot seen in Figure 8.4, rather than the distribution of the value in the most critical layer. The purpose of the ongoing investigation is not to find the most effective lay up, but rather the most desirable geometry of the specimen. The most desirable geometry gives the lowest shear stress peaks between the notches compared to the average shear. This test is also one of the few measuring shear strength. If the geometry forces some other type of failure before the specimen is allowed to fail in shear, the measured shear strength will be lower than it should. Failure in the FEA initiated in one of the layers that was subjected to compressive stress in the fiber direction, and the compressive fiber failure criterion was the mode that initiated the failure. It seams that when adding the plies with $\pm 45°$-orientation in the laminate lay up, failure is not caused by shear directly. The shear loading of the specimen, subjects these plies to a compressive loading in the fiber direction that eventually causes failure. Consequently, increasing the ply shear strength may not cause this specimen to sustain higher shear loading

Finally it should be noted that the direction of the initial crack is in the direction of one of the lamina orientations. This largely agrees with the theory presented in Chapter 3.1 on crack propagation, that crack development usually propagates in a direction parallel to fibers.

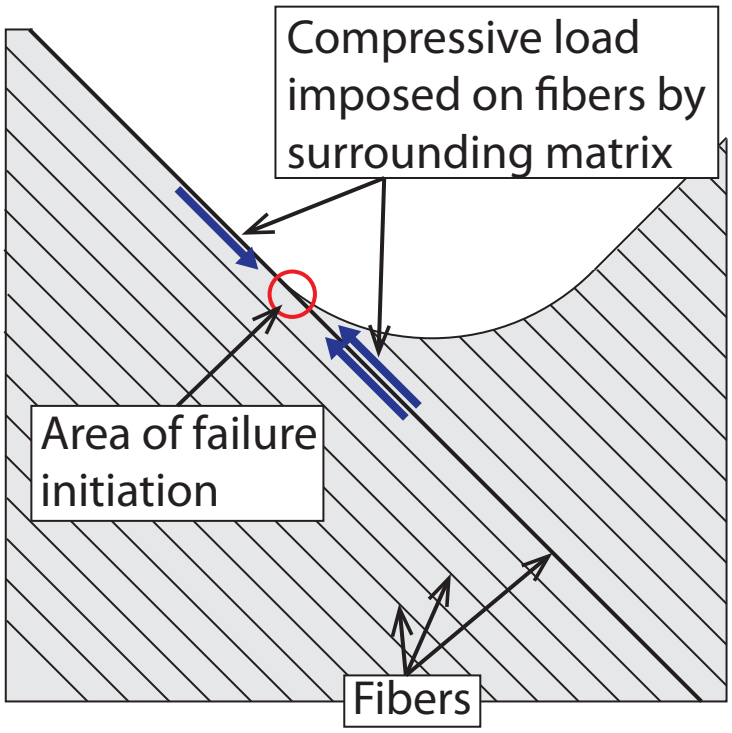

Figure 8.7: Illustration of the notch area in the ply that suffered compressive fiber failure.

Chapter 9

Conclusion

This Thesis for the degree of Master of Science is based on work carried out in the COMPCT project at SINTEF Materials and Chemistry, Department of Synthesis and Properties.

The basic theory presented in Chapter 2.1 seems to be quite inadequate for exact behavioral description of fiber reinforced polymer composite laminates. Even with a large database with the data from extensive material testing, it seemed difficult to find the right lamina properties. The rule of mixtures is a nice theoretical introduction to build an understanding for the basics of composite material. It presents the complexity of fiber reinforced composites in an easy-to-follow manner, but it is unable to scope all the different parameters affecting the behavior of composite material. If the properties of the constituents are to be used to predict the material properties of the composite, micro mechanical modeling might be effective. Otherwise, it seems as if the material properties for a composite laminate needs to be thoroughly tested in tension, compression and shear with various laminate lay ups, in order to back calculate the material properties for a single ply.

All the analyses presented in this thesis are made using implicit time integration. In Case study 2 and 3, the presentation of results would have benefitted from explicit time integration. In these studies the aim was to investigate the failure propagation, by evaluating the fracture mode and the propagation of crack formations. In the simulations in question, failure would present itself by deleted elements, also called element erosion (as long as no nodes are deleted, the mass would be preserved - see Chapter 5.3 for lumped mass). When using the implicit time integration, the model failed to find equilibrium in the time step the first elements were deleted. The deletion of elements caused convergence failure. The reason these models were not simulated using explicit time integration was that the time steps were too small, and the elements too many for the computational capacity available during the work on this thesis. The amount of mass scaling necessary to reduce the computational cost to a reasonable level for the available capacity, caused undesirable dynamic effects. In an attempt to stabilize the

models using implicit dynamic time integration, both numerical- (changing the γ value in the Newmark β Method) and physical damping (viscous) were evaluated.

The materials that were to be delivered and tested in the COPACT project during this thesis are still not available for material testing at SINTEF. For this reason, material test results from another project were used. These are the material test results presented and used in *Case study 1* described in Chapter 6. A thorough literature study of the various material testing methods for composite laminates were then undertaken. Also material tests on pure epoxy specimens were conducted. The tests were conducted on v-notched test specimen using the Iosipescu shear test (ASTM D 5379). A Digital image correlation (DIC) setup were used to measure the strains. A photograph taken of the test setup is presented in Figure 4.6. These tests were similar to the once discussed in *Case study 3* in Chapter 8, even though these were conducted with another test fixture on composite laminates, DIC were used as strain measurement.

Defining the material properties is not straight forward even with a large database of material test results available. The results from test conducted on unidirectional laminates is not always suited to describe the behavior of unidirectional plies, when they are part of a laminate with multiple ply orientations. One example is that the unidirectional laminates loaded in the fiber direction evaluated in *Case study 1* in Chapter 6, failed at a strain level equivalent to 680 MPa, but plies loaded in the fiber direction sustained strain levels equivalent to over 1000 MPa when situated in a laminate with plies oriented in multiple directions. It also became clear that some material properties was difficult to obtain directly, and these properties had to be found indirectly by back calculation of laminate test results using classical laminate theory. One effective method is using an optimization tool, e.g. LS-OPT, together with LS-DYNA. This scheme was used when defining the reduction factors in *Case study 1* described in Chapter 6. By assuming approximate values and defining an appropriate range for each of the unknown material properties, it is possible to simulate loading on a laminate lay up for which experimental observations exists. LS-OPT then variate the unknown material properties until the simulation fit the experimental observations.

When sufficient material properties were obtained in *Case study 1*, the numerical model was verified by modeling laminates that had not been used to obtain the material properties. Both shell elements and solid elements were used in the validation. The results showed that the simplifications made by describing the laminates using shell elements made the laminates to stiff. The behavior of the modeled laminates after first ply failure, were in good agreement with the results seen in experimental observations. Both with respect to the strain level at which failure occurred and the non linear stress-strain relationship after failure initiation. The shell elements produced results that where stiffer, and the solid elements produced results that were somewhat softer than the material test results displayed. The results for solid elements being to soft can be explained by the fact that the complete laminate lay up was not modeled. Only a few

repetitions of the stacking sequence were modeled in order to make the model less computational costly. The reduced repetition of stacking sequence may have lowered the out of plain effects, thus reducing the through the thickness shear variations caused by the clamped ends of the specimens. The out of plane effect is shown in the calculated example with the **A**- and **B**-matrix for a given laminate in the Equations (6.1) through (6.4).

The results using the implemented Puck failure model was compared with results using three other models based on Chang-Chang and Tsai-Wu failure models. The implemented material model based on Puck was shown to produce results, using shell elements, that were as good or better than the other models. In addition the implemented model is applicable to solid elements in contrast to the other models describing composite laminates. In the failure locus describing failure in the domain of in-plane transverse and shear loading seen in Figure 3.6 in Chapter 3.2.4 it can be seen that it is in the area of combines shear and transverse compressive loading the failure models differ the most. As a final remark, it should also be mentioned that the implemented material model may become even more accurate when the fracture angle for pure transverse compressive load can be defined by combined loading on filament winded tubes, which is scheduled in the continuation of the COMPACT project.

The effects of the reduction factor was seen to be quite significant when applied to unidirectional laminates strained in the transverse direction or cross ply laminates strained in a direction in 45° to the fibers. Small differences in the factor produced large divergence in the propagation of the stress-strain curves for these laminates(see Figure 6.5 and 6.7 in Chapter 6). The difference in reduction factor had less effect on the outcome in the laminates with a more complex laminate lay up. It seem evident that a mean curve of the two reduction factors can be used in the continuation of the COMPACT project. The straining level at which the two curves displayed different results were at approximate 2% strain. These levels of deformation is usually not interesting in structural applications of composite material. In other words, the two reduction factors produced results with little divergence within the deformation levels of interest.

The material model, based on the Puck failure criterion, and findings describing the post first play failure for in-plane loading will be used in the continuation of this project. The COMPACT project is to be terminated by the end of 2013. In the following year, de-lamination is to be investigated, and a series of material trials are currently being planned. The material trials include: combined loading (compression and shear) of filament winded pipes and out of plane impact loading on FRPC-laminates. The filament winded pipe test will provide results for the upper left corner of the failure locus seen in Figure 3.5 in Chapter 3.2.3. These results will allow for indirect measurement of the fracture angle θ^0_{fp}, also described in Chapter 3.2.3.

The results found in *Case study 2: Pinhole loaded FRPC plate*, should be further investigated. The reason for the divergence between literature results

and the results found in this study needs to be identified. The work presented in *Case study 3: Shear Test Geometry*, should be compared to results of the other specimen geometries. Both Case study 2 and 3 should be analyzed using explicit time integration, so that the propagation of the cracks initiated can be studied. It would be interesting to analyze these cases using the Extended Finite Element Method (X-FEM) [35][34] described briefly in Chapter 7.4. A generalized element formulation [36] has recently been implemented in the LS-DYNA finite element code. The element formulation combines X-FEM and isogeometric (using the same basis functions as CAD) analysis in LS-DYNA without the need for additional programing. It is not clear if these elements currently are able to model the anisotropy necessary for correct description of fiber reinforced composite materials. These methods should definitely be evaluated in the continuation of the COMPACT project.

An article based on the results found using shell elements in *Case study 1: Puck failure criterion* have been submitted and accepted by peer review as a conference article, and was presented at the MekIT'11 conference in Trondheim May 2011.

Bibliography

[1] "Bmw sauber f1 team," *http://www.sauber-motorsport.com/Carbon-fibre-145.*

[2] "Ragasco."

[3] "Bmw oracle," *http://bmworacleracing.com/en/yacht/index.html.*

[4] "Lockheed martin - joint strike fighter f35," *http://www.lockheedmartin.com /news/press_releases/2005/LOCKHEEDMARTINF35TEAMONTRACKFO RFINA.html.*

[5] "Umoe mandal - skjold class fpb," *http://www.um.no/WEB/um200.nsf/pages /A80E0562C2.*

[6] "Cornell uneversity," *http://www.cheme.cornell.edu/cheme/graduate/Energy.cfm.*

[7] "gamesa," *http://www.compositesworld.com/articles/carbon-fiber-in-the-wind.*

[8] W. Marsden and D. J. Irving, "How to analyse composites," *NAFEMS Ltd*, 2002.

[9] D. H. F. L. Matthews, G. A. O. Davies and C. Soutis, "Finite element modelling of composite material and structures," *Woodhead publishing limited*, vol. ISBN: 978-1-85573-422-7 (book), 2009.

[10] A. Puck and H. Shürmann, "Failure analysis of frp laminates by means of physically based phenomenological odels.," *Composites Science and Technology*, vol. 58, no. 7, pp. 1045–1067, 1998.

[11] M. A. Sutton, J. Orteu, and H. W. Schneier, *Image Correlation for Shape, Motion and Deformation Measurements.* Springer, 2009.

[12] M. E. Bechly and P. D. Clausen, "Structural design of a composite wind turbine blade using finite element analysis," *Journal of Computers & Structures*, vol. 63, no. 3, pp. 639–646, 1997.

[13] B. D. Agarwal, L. J. Broutman, and K. Chandrashekhara, *Analysis and Performance of Fiber Composites*, vol. 3rd ed. John Wiley & Sons, Inc., 2006.

[14] J. C. Halpin and S. W. Tsai, "Effects of environmental factors on composite materials," *AFML-TR 67-423, Dayton, OH*, June 1969.

[15] R. C. Novak and M. A. DeCrescente, "Impact behavior of unidirectional resin matrix composites tested in fiber direction," vol. Second Conference, pp. 311–323, 1972.

[16] P. W. R. Beaumont, "A fracture mechanics approach to failure in fibrous composites," *J. Adhes.*, no. 6, pp. 107–137, 1974.

[17] A. Kelly, "Strong solids," *Clarendon Press*, 1973.

[18] G. A. Cooper and A. Kelly, "Strong solids," *Journal of Mech. Phys. Solids*, vol. 279, no. 15, 1967.

[19] S. W. Tsai and E. M. Wu, "A general theory of strength for anisotropic materials," *Journal of Composite Materials*, vol. 5, pp. 58–81, January 1971.

[20] K. S. Liu and S. W. Tsai, "A progressive quadratic failure criterion for a laminate," *Composites Science and Technology*, vol. 58, no. 7, pp. 1023–1032, 1998.

[21] F. Chang and K. Y. Chang, "Post-failure analysis of bolted composite joints in tension or shear-out mode failure," *Journal of Composite Materials*, vol. 21, pp. 809–833, September 1987.

[22] J. Wiegand, N. Petrinic, and B. Elliott, "An algorithm for detection of the fracture angle for the three-dimentional puck matrix failure criterion for ud composites," *Composites Science and Technology*, vol. 68, pp. 2511–2517, 2008.

[23] A.Puck, J.Kopp, and M.Knops, "Guidelines for the determination of the parameters in puck's action plane strength criterion," *Composites Science and Technology*, vol. 62, no. 3, pp. 371–378, 2002.

[24] D. E. W. D. F. Adams, "Further development of the iosipescu shear test method," *Exp. Mech*, vol. 27, no. 1, pp. 113–119, 1987.

[25] "Correlatied solutions," *http://www.correlatedsolutions.com/index.php/products/vic-3d-2010/vic3d*.

[26] R. D. Cook, D. S. Malkus, M. E. Plesha, and R. J. Witt, *Concept and Application of Finite Element Analysis*. John Wiley & Sons, Inc., 4 ed., 2002.

[27] livermore, *LS-DYNA Theory Manual*. Livermore, 2007.

[28] A. K. Chopra, *Dynamics of Structures, Theory and Applications to Earthquake Engineering*. Pearson Prentice Hall, 3 ed., 2007.

[29] *LS-DYNA Keyword User's Manual*. Livermore Software Technology Corporation (LSTC), version 971 ed., 2007.

[30] Z. Hashin, "Failure criteria for unidirectional fiber composites," *J. Appl. Mech.*, vol. 47, no. 2, pp. 329–334, 1980.

[31] K. Schwizerhof, K. Weimar, T. Münz, and T. Rottner, "Crashworthiness analysis with enhanced composite material models in ls-dyna - merits and limits," *LS-DYNA World Conference, Detroit, Michigan, USA*, 1998.

[32] M. Hinton, A. Kaddour, and P. Soden, *Failure criteria in fiber reinforced plymer composites: The World-Wide Failure Exercise*. Elisvier, 2003.

[33] F.K.Chang, R.A.Scott, and G.S.Springer, "Failure of composite laminates containing pin loaded holes-method of solution," *Journal of Composite Materials*, vol. 18, pp. 255–278, 1984.

[34] N. Moes, J. Dolbow, and T. Belytschko, "A finite element method for crack growth without remeshing," *International Journal for Numerical Methods in Engineering*, vol. 46, no. 1, pp. 131–150, 1999.

[35] F. Grytten and M. Polanco-Loria, "Modelling of fibre reinforced polymer composites subjected to impact loading – state of the art," *SINTEF rapport*, vol. ISBN: 978-82-1405011-0, 2010.

[36] D. J. Benson, Y. Bazilevs, E. D. Luycker, M. C. Hsu, M. Scott, T. J. R. Hughes, and T. Belytschko, "A generalized finite element formulation for arbitrary basis functions: from isogeometric analysis to xfem.," *International Journal for Numerical Methods in Engineering*, vol. 83, no. 6, pp. 765–785, 2010.

Appendix A

Conference article

Progressive Failure Analysis of Fiber Reinforced Polymer Composites

R. K. Joki*
Mechanics Division
Department of Mathematics
University of Oslo
e–mail: reidakj@math.uio.no

F. Grytten
Department of Synthesis and Properties
SINTEF Materials and Chemistry

H. Osnes
Mechanics Division
Department of Mathematics
University of Oslo

Summary The present study addresses the use of progressive failure analysis to predict the failure mechanisms of fiber reinforced polymer composites (FRPC) subjected to in-plane loading. The first ply failure is calculated using the Puck failure criterion [1]. The material properties and damage characteristics for unidirectional (UD) laminates are extracted from extensive material testing. The properties of non-UD laminates are then calculated using classical laminate theory. Accurate description of the failure parameters is crucial for reliable prediction of the failure propagation. Exponential decay and spline functions have been used to describe the material degradation. This progressive failure analysis is shown to be a promising way of predicting the the non-linear stress-strain relations of FRPC-laminates after failure initiation.

Introduction

The search for a model that realistically describes failure and degradation of FRPC-laminates has been the subject of many papers in recent years, see, e.g., [2]. The strength analysis of laminates is still underdeveloped compared to the analysis of stresses and strains, and the relations between them. Especially, there is a lack of degradation models that agree well with material testing and are simple to implement in design. The *continuum damage mechanics* community is developing analytical tools to describe the initiation and evolution of damage, so that the complete failure process can be represented. In the world wide failure exercise (WWFE) [3], the Puck failure criterion [1] was ranked very high. This attracted attention to the model, and further development was undertaken by several contributors [2, 4–6].

In the present study, load-displacement curves from a large number of tests performed on a specific type of FRPC-laminates have been investigated. The test results provide a large body of data suitable for estimation of the parameters for stiffness and strength as well as the behavior after initial failure leading up to ultimate failure of the laminates tested. This has made it possible to develop a material model based on tested material data that gives accurate predictions of the material's damage behavior.

Progressive Failure Analysis

Failure in an FRPC-laminate is usually not a unique event, but rather a gradual progressive sequence of microcracking and delamination leading to structural collapse. Failure often initiates with a tiny crack in the matrix of the plies with fibers oriented transversely to the tensile loading. These cracks usually propagate perpendicular to the loading direction. When increasing

the load, more cracks will initiate and develop, which in turn serve to reduce the stiffness of the laminate. The cracks usually propagate through the entire thickness of the ply, but are unable to propagate into the adjacent plies, particularly if the adjacent plies have fibers oriented in the direction of the loading. Thus these cracks terminate at the interface of two plies. This will produce a stress concentration at the crack tip that may initiate the formation of cracks between the plies causing delamination. (Delamination will not be discussed in this paper.) Finally, with the loading still increasing, the load carrying fibers will also start to fracture, further reducing the stiffness until the last fibers fracture leading to ultimate failure of the laminate [7].

In this study the Puck failure criterion [1] has been implemented into the LS-DYNA finite element code. The Puck failure criterion has a large number of parameters that need to be determined. This has made the model less attractive compared with other failure criteria, even though it was one of the better criteria tested in the WWFE. In order to simplify the application of the failure model, Puck proposed pragmatic solutions for some of the parameters [8].

The Puck failure criterion has separate expressions for fiber failure (FF) and inter fiber failure (IFF). IFF is assumed to be caused by the normal and shear stresses (σ_n, τ_{nt} and τ_{n1}) that are acting on the fracture plane. From Figure 1, in which these stresses are illustrated, it can be seen that these are the only stress components that are contributing to IFF. Positive normal stress on this plane will promote fracture, and negative normal stress will increase the material's shear strength, thus counteract fracture, as seen in Figure 2. The function e, introduced in Equation (2), is controlled by the stress state in the specimen, and initiate failure when $e = 1$. Fracture will occur in the plane where $e(\sigma)$ first reaches unity. The angle of the fracture plane is called θ_{fp}, as seen in Figure 1. The stresses acting on the fracture plane are obtained by transformation of

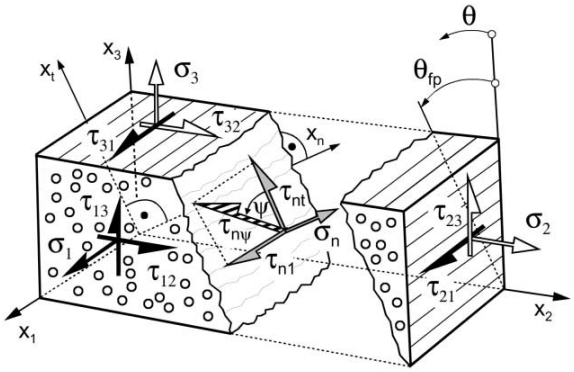

Figure 1: The stress components σ_n, τ_{nt} and τ_{n1} acting on the fracture plane which is defined by θ_{fp}. [8]

the three-dimensional stress tensor from material coordinates to the fracture plane. The fracture plane tractions are given by [2]

$$\begin{aligned} \sigma_n &= \sigma_{22}cos^2\theta_{fp} + \sigma_{33}sin^2\theta_{fp} + 2\sigma_{23}cos\theta_{fp}sin\theta_{fp}, \\ \tau_{n1} &= \sigma_{12}cos\theta_{fp} + \sigma_{13}sin^2\theta_{fp}, \\ \tau_{nt} &= -\sigma_{22}sin\theta_{fp}cos\theta_{fp} + \sigma_{33}sin\theta_{fp}cos\theta_{fp} + \sigma_{23}(cos^2\theta_{fp} - sin^2\theta_{fp}). \end{aligned} \tag{1}$$

The failure locus is defined by the following criteria

$$
\begin{aligned}
e^2 &= \left(\frac{\sigma_n}{R_n}\right)^2 + \left(\frac{\tau_{n1}}{R_{n1} - p_{n1}\sigma_n}\right)^2 + \left(\frac{\tau_{nt}}{R_{nt} - p_{nt}\sigma_n}\right)^2 = 1 \text{ for } \sigma_n \geq 0, \\
e^2 &= \left(\frac{\tau_{n1}}{R_{n1} - p_{n1}\sigma_n}\right)^2 + \left(\frac{\tau_{nt}}{R_{nt} - p_{nt}\sigma_n}\right)^2 = 1 \text{ for } \sigma_n < 0,
\end{aligned}
\tag{2}
$$

where R_n is the resistance of the fracture plane against normal failure induced by σ_n. The parameters R_{n1} and R_{nt} are the resistance of the fracture plane against shear, and finally, p_{n1} and p_{nt} are the slope parameters representing internal friction effects (Mohr-Coulomb type of failure) [2]. In [8], Puck suggests the following values for these parameters

$$
\begin{aligned}
R_n &= Y_t, \\
R_{n1} &= S_{12}, \\
R_{nt} &= \frac{Y_c}{2tan(\theta^0_{fp})}, \\
p_{nt} &= -\frac{1}{tan(2\theta^0_{fp})}, \\
p_{n1} &= p_{nt}\frac{R_{n1}}{R_{nt}}.
\end{aligned}
\tag{3}
$$

Here Y_t and Y_c are the transverse strength values in tension and compression, respectively, and S_{12} is the shear strength. The angle θ^0_{fp} is the angle at which a specimen loaded in uniaxial compression in the transverse fiber direction fracture due to shear failure. When subjected to in-plane loading, IFF is provoked by σ_{22} and τ_{12}. The shape of the failure envelope depends strongly on θ^0_{fp}, which is illustrated in Figure 2. This angle can be viewed upon as a material property and has a constant value for a given material. It should not be confused with the fracture angle defining the action plane of an arbitrary loading condition θ_{fp} as shown in Figure 1.

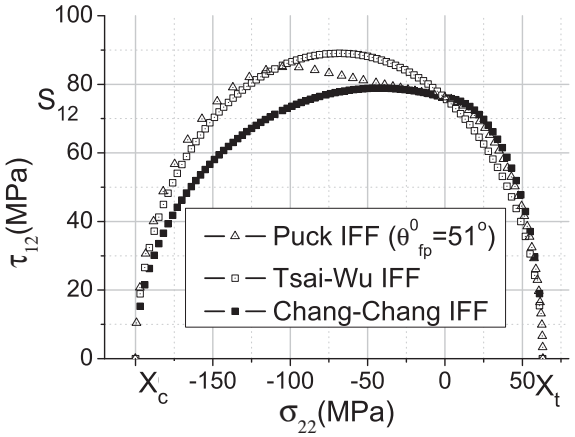

Figure 2: Failure envelope for the Puck IFF criterion for different values of θ^0_{fp}.

When the stress and strain conditions leading to first local failure are determined, one needs to describe the global post failure behavior. It is well known that the stiffness of the area of

the laminate that is subjected to local failure is reduced. Experimental data suggest that such degradation of stiffness is continuous, and not sudden [1].

Puck [1] argues that opening cracks should be regarded as *smeared*, and that the transverse modulus E_2, the shear modulus G_{12} and the Poisson's ratio ν_{12}, all should be diminished by the same reduction factor η after the initial IFF condition is reached. The degradation is to be done by continuously updating the effective value of the three parameters, e.g., $E_{2eff} = E_2 \times \eta$. When defining η, it is necessary to evaluate compressive- and tensile loading separately. In contrast to tensile stress, compressive stress does not allow cracks to open, thus only a small reduction factor should be designated in such cases. The Puck IFF criterion allows for this by having separate IFF-expressions for compression and tension. According to Puck the described degradation procedure should build on experimentally deduced curves of η. In the present study E_2, G_{12} and ν_{12} are degraded using this reduction factor.

From the material tests investigated, it seems evident that while IFF propagates in a gradual progressive manner, FF evolves more as a single event when the state of stress in the fiber direction reaches the criterion $e = 1$. Therefore no reduction factor has been applied in connection with to the FF criterion, the finite elements in question are deleted when the criterion reaches unity. For FF e is defined as

$$e = \frac{1}{\epsilon_{1T}} \left(\epsilon_1 + \frac{\nu_{f12}}{E_{f1}} m_{\sigma f} \sigma_2 \right) \quad for \;\; \sigma_1 > 0, \tag{4}$$

$$e = \frac{1}{\epsilon_{1C}} \left| \left(\epsilon_1 + \frac{\nu_{f12}}{E_{f1}} m_{\sigma f} \sigma_2 \right) \right| + (10\gamma_{21})^2 \;\; for \;\; \sigma_1 < 0, \tag{5}$$

where the compressive fracture strain ϵ_{1C} is given as a positive value and $(10\gamma_{21})^2$ is a purely empirical value suggested by Puck [1] in order to include the effects of shear when predicting fiber failure in compression. The factor $m_{\sigma f}$ accounts for a *stress magnification effect* caused by the different moduli of fibers and matrix. Typical values are 1.3 for glass fiber and 1.1 for carbon fiber [1]. No variation of this factor is suggested for different types of matrix material.

Material Testing

The tested laminates are made up of stitched unidirectional (UD) glass fiber reinforced polymer matrix (DION 9102-683) composite plies. The plies are made up of vacuum infused UD-fiber mats. The fibers are stitched together in order to stay in place during the vacuum infusion. The laminates are stacked with ply-orientations $[0]_N$, $[90]_N$, $[\pm 45]_N$, $[0/90]_N$, $[\pm 45/90]_N$, $[\pm 45/90_6/\pm 45]_N$ and $[0/\pm 45/90]_N$, where N is the number of times the stacking sequence is repeated through the thickness of the laminate. It can be seen that the lay-up of the latter five laminates are not symmetric with respect to the mid-plane of the laminate. The reason for this is that it is faster and cheaper to produce laminates with a lay-up stacked in a repeating fashion. A non-symmetric lay-up may lead to coupling between in- and out of plane effects, i.e., subjecting a composite laminate to plane tensile loading may cause it to bend and/or twist if the lay-up is non-symmetric. When the laminate is made up of a multi repeating order of thin plies, the effects of the non symmetric lay-up decreases when the number of repetitions of the sequence increases. The experiments conducted are standard coupon tests loaded in tension and compression in addition to the *v-notched rail shear test*. All the coupon tests are conducted using extensometer with a gage length of 80 mm. In the tensile tests there where no indications of necking, and the normal stresses measured where steadily increasing until failure.

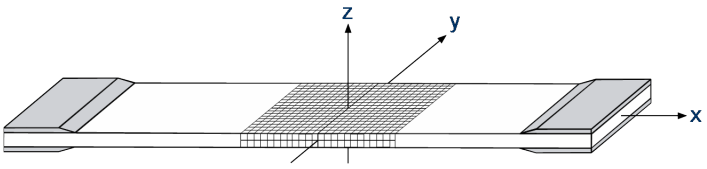

Figure 3: An illustration of the test specimen. The load is applied in the x-direction.

Two types of experiments have been conducted in order to predict the shear stiffness; tension tests of $[\pm 45]_N$ coupons, and v-notched rail shear tests of cross-ply laminates. The latter is the only of these two that is suitable for prediction of shear strength. The $[\pm 45]_N$ coupons can be used to calculated the shear stiffness by evaluating the formula

$$G_{12} = \frac{E_x}{2(1+\nu_{xy})}, \tag{6}$$

where E_x is the measured stiffness in the direction of the applied load and ν_{xy} is the in-plane Poisson's ratio.

Finite Element Analysis

The procedure for predicting the response of an FRPC structure involves a number of parameters. The optimal set of parameters for the progressive failure model has been found through inverse modeling using the LS-DYNA finite element code in combination with the optimization tool LS-OPT. In the simulations, four node shell elements with a nonlinear material model have been used. The elements are two-dimensional and describe the laminate lay-up with several integration points through the thickness. Each integration point represents a ply in the laminate, and the integration points are located at the center of the element and in the middle of each ply. The fiber orientations are defined independently in each integration point. A local coordinate system is attached to each element, and translates and rotates with the element as deformation proceeds. The global coordinate system remains fixed. Element deformation is decomposed into a rigid-body component, which is identical to rigid-body motion of the local system, and a straining component that can be described by degrees of freedom measured in the local system. Hencky strain is used as strain measure.

The degradation of the material properties after first ply failure is implemented by multiplying the three material parameters E_2, G_{12} and ν_{12} with the reduction factor η, as suggested by Puck [1]. One of the most expensive operations, with respect to computational costs, when using the Puck failure criterion in three dimensions, is the search for the critical action plane. The action plane is the plane parallel to the fibers where the stress components σ_n, τ_{nt} and τ_{n1} have their maximum, and consequently where the fracture will occur. As mentioned above, these three stress components are the only ones affecting IFF. The action plane is defined by the angle θ_{fp}, see Figure 1. The search for the critical action plane should be done in the range $-90^\circ \leq \theta \leq 90^\circ$. A cost effective methodology is the Golden Section Search [2]. This procedure has been proven to be an effective tool when searching for the action plane using the Puck criterion, see Wiegand et al. [2].

Results

Material testing

As pointed out above, one aim of the present study has been to investigate the behavior of a set of laminates after first ply failure. The material parameters describing this behavior have been extracted from FRPC-laminates made up of unidirectional plies. The deduced η-curves are illustrated in Figure 4. The values have been deduced from the tensile tests of $[90]_N$-coupons and $[\pm 45]_N$-coupons. The two resulting reduction factors offer different results when implemented in the material model. This difference can be seen in Figures 5 and 7. In Figures 9 through 14, on the other hand, the difference appears to be less evident. The elastic properties are listed in Table 2, where E_1 is the longitudinal- and E_2 is the transverse Young's modulus respectively, G_{12} is the shear modulus, ν_{12} is the major Poisson's ratio and ν_{23} is the transverse Poisson's ratio. The strength parameters are Y_c, Y_t, X_c, X_t and S_{12}, where Y represents transverse, X longitudinal and S shear parameters. The subscripts c and t refer to $compressive$ and $tensile$ strengths, respectively. The strengths refer to first ply failure, i.e. damage initiation. Subscript u denotes ultimate failure. The pure transverse compression fracture angle is denoted as θ^0_{fp}. The influence this angle has on the failure envelope is illustrated in Figure 2. This angle is difficult to measure, therefore a realistic value for equivalent material found in literature [2] has been used.

Deduced material properties

The Poisson's ratio, ν_{12}, and the longitudinal tensile parameters are deduced from the tensile tests of $[0]_N$-coupons, while the compressive longitudinal parameters are determined from compression tests of $[0/90]_N$-coupons. The transverse parameters are calculated from tests on $[90]_N$-coupons. The shear properties are obtained by studying the tensile tests on $[\pm 45]_N$-coupons and the v-notched rail shear test for test specimens with $[0/90]_N$-lay-up.

Table 2: Material properties deduced from material testing.

E_1	38600	MPa
E_2	13900	MPa
G_{12}	4000	MPa
ν_{12}	0.25	
ν_{23}	0.30	
Y_c	200	MPa
Y_t	20.1	MPa
Y_{tu}	62.7	MPa
X_{cu}	400	MPa
X_{tu}	681	MPa
S_{12}	50	MPa
S_{12u}	76.3	MPa
θ^0_{fp}	51°	

Finite element analysis

The reduction factor η was adjusted in order to replicate the stress-strain curve from the tensile $[90]_N$-coupon test. This was performed through inverse modeling using the LS-DYNA fi-

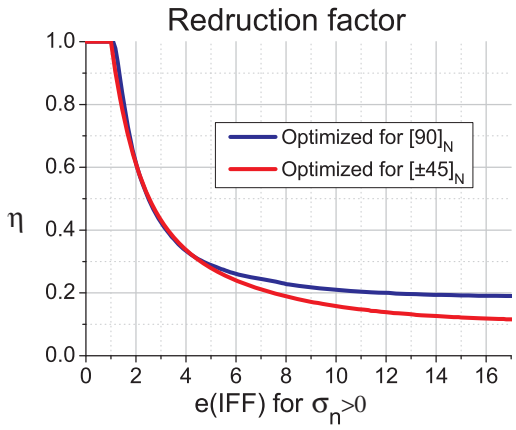

Figure 4: The reduction factor as a function of the IFF criterion for $\sigma_{22} > 0$.

nite element code in combination with the optimization tool LS-OPT. The final damage curve was described by spline functions. The material parameters for a single ply made up of UD-fibers, along with the optimized damage curve were then used to simulate the $[\pm 45]_N$ and the $[\pm 45/90]_N$-laminates, both loaded in tension in the $0°$-direction. The results from the simulations using the damage curve detained from the tensile $[90]_N$-coupon test, can be observed in Figures 5 trough 14 denoted *Optimized for* $[90]_N$. The same procedure was repeated with a damage curve obtained from the $[\pm 45]_N$-coupon test, resulting in a damage curve described by a two-term exponential decay expression. The analysis made using this damage curve can also be observed in Figures 5 trough 14. These analyses are denoted *Optimized for* $[\pm 45]_N$. The two reduction factors are plotted in Figure 4.

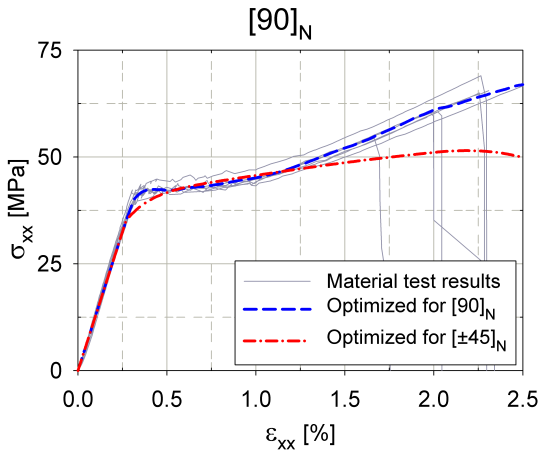

Figure 5: Comparing observed and predicted stress-strain curve for $[90]_N$-coupon test.

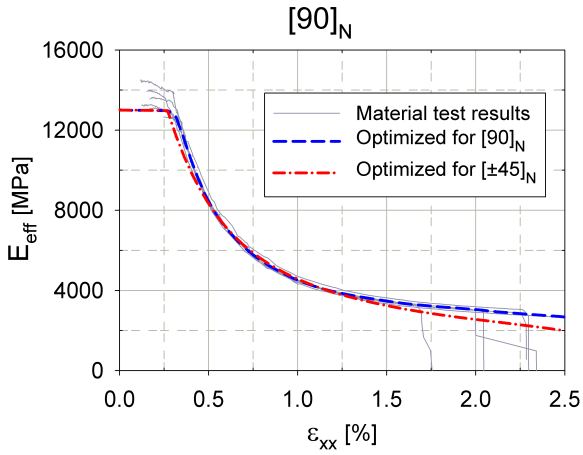

Figure 6: Comparing observed and predicted effective Young's modulus for $[90]_N$-coupon test.

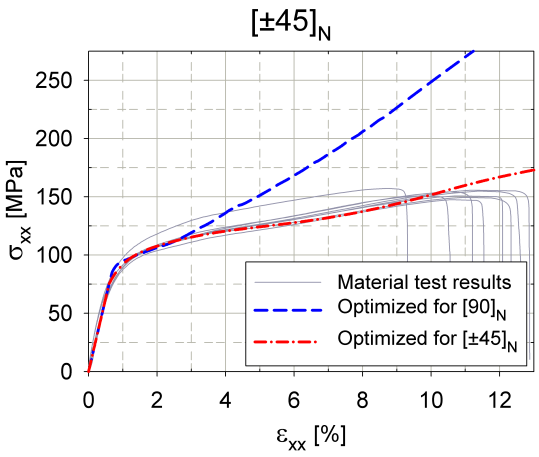

Figure 7: Comparing observed and predicted stress-strain curve for $[\pm 45]_N$-coupon test.

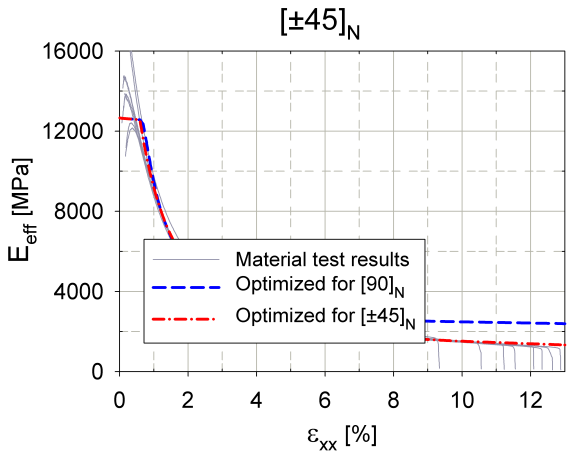

Figure 8: Comparing observed and predicted effective shear modulus for $[\pm 45]_N$-coupon test.

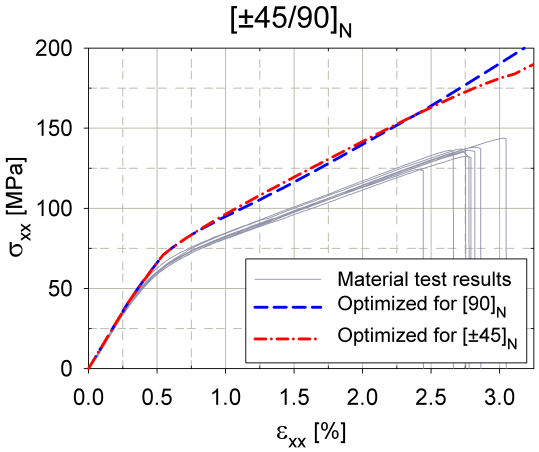

Figure 9: Comparing observed and predicted stress-strain curve for $[\pm 45/90]_N$-coupon test.

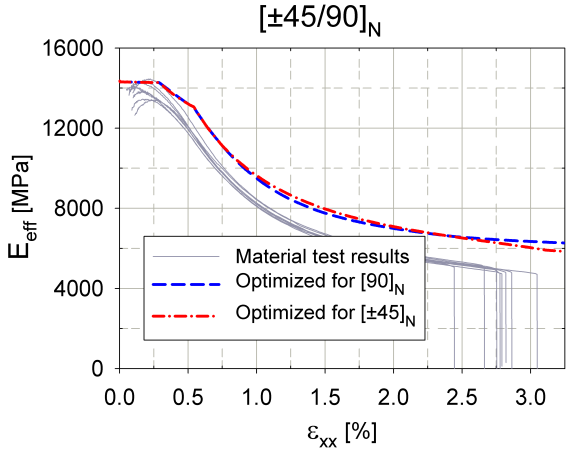

Figure 10: Comparing observed and predicted effective shear modulus for $[\pm 45/90]_N$-coupon test.

Discussion and Conclusion

The tested materials are made up of vacuum infused UD-fiber mats. The fibers are stitched together in order to stay in place during the vacuum infusion. Even dough the stitching is only there for processing reasons it may contribute with some stiffening factor to the transverse direction. The Puck failure criterion is developed for transversely isotropic materials where the matrix is the bearing constituent in all transverse directions to the fibers. The stitching can only provide stiffness and strength in one transverse direction, the in-plane direction transverse to the fibers. By these arguments the stiffness obtained from this transverse direction should be higher than for directions other than that of the stitching. This may explain why the predicted damage behavior of the $[\pm 45]_N$ coupon tests, based on the transverse stiffness degradation, did not correspond with the experimentally observed behavior. The stiffening effect of the stitching

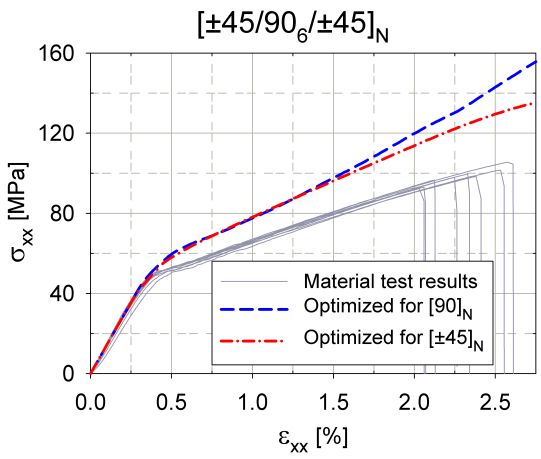

Figure 11: Comparing observed and predicted stress-strain curve for $[\pm 45/90_6/\pm 45]_N$-coupon test.

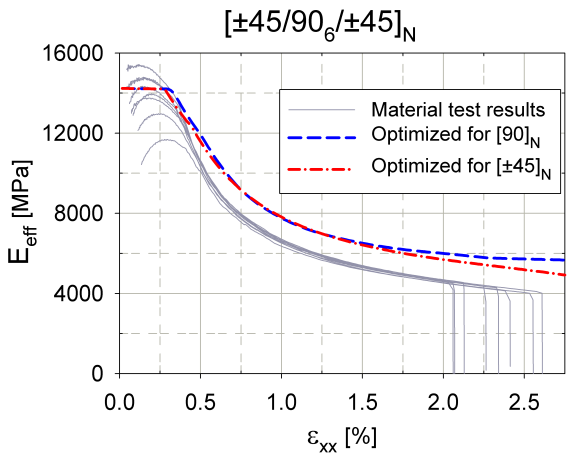

Figure 12: Comparing observed and predicted effective shear modulus for $[\pm 45/90_6/\pm 45]_N$-coupon test.

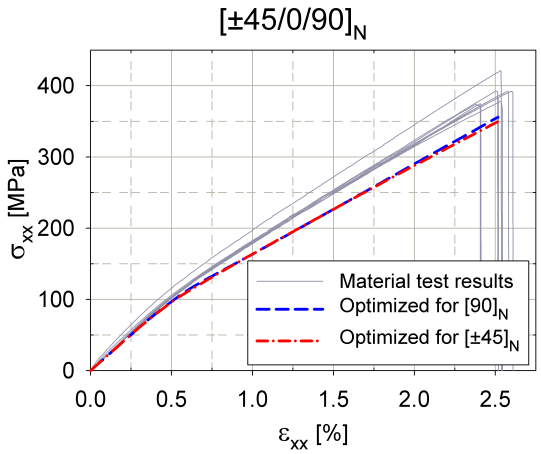

Figure 13: Comparing observed and predicted stress-strain curve for $[\pm 45/0/90]_N$-coupon test.

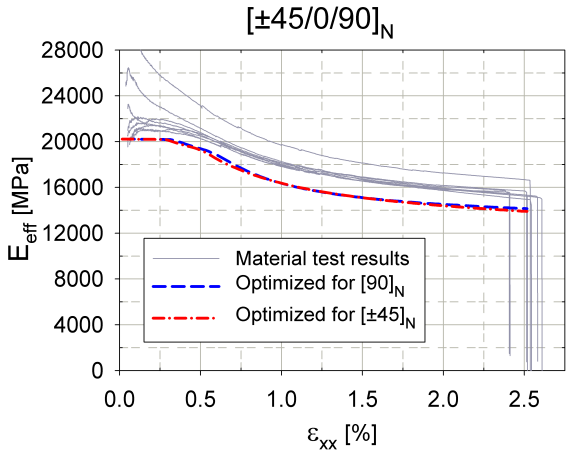

Figure 14: Comparing observed and predicted effective shear modulus for $[\pm 45/0/90]_N$-coupon test.

is evident in the transversely tensile loaded UD-coupon. It behaves as if there are some loosely fitted fibers embedded in the transverse direction that eventually, after being straightened out and strained, fracture. This behavior should be less evident in the $45°$-direction which is off-axis for both fibers and stitching. As suggested by Puck [1] the damage-curve deduced from the $[90]_N$-coupon tests is used to degrade the E_2, G_{12} and ν_{12} parameters. This can explain the difference between the predicted and the experimentally observed behavior of the $[\pm 45]_N$ coupon tests. When analyzing the laminates presented in this study, it might be better to degrade E_2 and G_{12} separately.

The tensile $[\pm 45/90]_N$-coupon tests came out stiffer in the FEA predictions than experimentally observed, but the shape of the damage behavior was similar. This can be explained by the fact

that the damage model describes a matrix that is stiffer than it really is. The laminates are not symmetric, but are constrained from out of plane translations. This also promotes a stiffer result.

The UD-lamina properties observed in the tensile $[0]_N$-coupon tests, shows $X_{tu} = 681MPa$ at $\epsilon_{11} = 0.0177$, which supposedly is the ultimate strain in the $11-$direction. This contradicts to the observations of the tensile $[\pm 45/0/90]_N$- and $[0/90]_N$-coupon tests where the laminates are strained past $\epsilon_x = 0.025$ which is equivalent to $\epsilon_{11} = 0.025$ for the plies oriented with fibers in the loading direction. If the plies, with fibers oriented in the loading direction, had failed at the predicted strain level, it would have significantly reduced the stiffness. When plies with fibers oriented in the loading direction fail, it usually result in instantaneous ultimate failure for the whole laminate [7]. These observations suggest that ϵ_{1u} should have a greater value than that observed in the tensile $[0]_N$-coupon tests. In laminates with various ply orientations these experimental observations indicate that $\epsilon_{1u} = 0.025$. Pure UD-laminates are seldom used in real life applications, but it should be noted that this ultimate strain value is not applicable to UD-laminates.

When a UD-laminate fracture due to a pure transverse compression, the angle of the resulting fracture plane, θ^0_{fp}, is difficult to measure. In the continuation of this study, there will be conducted experiments on filament winded pipes. The pipes will be subjected to a combination of torsion and compression (τ_{12} and σ_{22}) providing experimental observations for the upper-left corner of the failure envelope seen in Figure 2. The value of θ^0_{fp} can then be chosen so that the failure locus suits the experimental observations as good as possible.

References

[1] A. Puck and H. Schürmann, "Failure analysis of frp laminates by means of physically based phenomenological models," *Composites Science and Technology*, vol. 58, no. 7, pp. 1045–1067, 1998.

[2] J. Wiegand, N. Petrinic, and B. Elliott, "An algorithm for detection of the fracture angle for the three-dimentional puck matrix failure criterion for ud composites," *Composites Science and Technology*, vol. 68, pp. 2511–2517, 2008.

[3] M. Hinton, A. Kaddour, and P. Soden, eds., *Failure Criteria In Fiber Reinforced Polymer Composites: The World-Wide Failure Exercise*. Elsevier, 1. ed., 2004.

[4] G. C. Davila and P. P. Camanho, "Failure criteria for frp lamaminates in plane stress," tech. rep., NASA/TM-2003-212663, 2003.

[5] S. T. Pinho, L. Iannucci, and P. Robinson, "Physically-based failure models and criteria for laminated fiber-reinforced composites with emphasis on fiber kinking. part i: Development. compos part a-appl sci manufactart i: Development," *Compos Part A-Appl Sci Manufact*, vol. 37, no. 1, pp. 63–73, 2006.

[6] L. Greve and A. K. Pickett, "Modelling damage and failure in carbon/epoxy non-crimp fabric composites including effects of fabric pre-shear," *Compos Part A-Appl Sci Manufact*, vol. 37, no. 11, pp. 1983–2001, 2006.

[7] B. D. Agarwal, L. J. Broutman, and K. Chandrashekhara, *Analysis and Performance of Fiber Composites*. John Wiley & Sons, Inc., 3. ed., 2006.

[8] A. Puck, J. Kopp, and M. Knops, "Guidelines for the determination of the parameters in puck's action plane strength criterion," *Composites Science and Technology*, vol. 62, no. 3, pp. 371–378, 2002.

Appendix B

Input files

B.1 Matlab input-files

Here follows the two input-files used to calculate the effects of repeating the stacking sequence i Chapter 2.3, and the files used to generate the plots displayed in Figure 3.5 and 3.6.

```
% Lay-up effect on B-matrix
%
% Rediar Kvale Joki


clear all;

% Material data in N, mm units (including MPa = N/mm^2)
EL=40500;
ET=13900;
vLT=0.25;
GLT=4000;
t=1;

% Lay-up(s)
R=[90 45 -45 0 90 45 -45 0 90 45 -45 0 90 45 -45 0 90 45
-45 0 90 45 -45 0 90 45 -45 0 90 45 -45 0 90 45 -45 0]*3.14159/180;
%R=[90 45 -45 0]*3.14159/180;

% z-coordinates for top and bottom surfaces of plies as defined in AB&C
% Fig. 6-5
h=[-40*t -38*t -36*t -34*t -32*t -30*t -28*t -26*t -24*t -22*t -20*t
-18*t -16*t -14*t -12*t -10*t -8*t -6*t -4*t -2*t 0 2*t 4*t 6*t 8*t
10*t 12*t 14*t 16*t 18*t 20*t 22*t 24*t 26*t 28*t 30*t 32*t 34*t 36*t
38*t 40*t];
%h=[-40*t -20*t 0 20*t 40*t];

% Compliance (S-matrix)
S(1,1)=1/EL;
S(2,2)=1/ET;
S(1,2)=-vLT/EL;
S(3,3)=1/GLT;
S(2,1)=S(1,2);

% Stiffness (Q-matrix)
Q=inv(S);

Q(3,3)=2*Q(3,3);        % convert from engineering to tensor shear
strains

% Initialise A,B,D
A(1:3,1:3)=0;
B(1:3,1:3)=0;
D(1:3,1:3)=0;

% Calculate T and Q for each ply 'k'. Assemble A, B and D
for i=1:length(R)

% Transformation matrix (T-matrix)
    T(1,1)=cos(R(i))^2;
    T(2,2)=cos(R(i))^2;
    T(1,2)=sin(R(i))^2;
    T(2,1)=sin(R(i))^2;
    T(3,1)=-sin(R(i))*cos(R(i));
    T(3,2)=sin(R(i))*cos(R(i));
    T(1,3)=2*sin(R(i))*cos(R(i));
    T(2,3)=-2*sin(R(i))*cos(R(i));
    T(3,3)=cos(R(i))^2-sin(R(i))^2;

    Qk(:,:,i)=inv(T)*Q*T;             % Stiffness matrix for tensor
strains, following rotation
    Qk(:,3,i)=Qk(:,3,i)/2;            % Convert back to engineering
shear strains
    A=A+Qk(:,:,i)*(h(i+1)-h(i));                % Calculate A-matrix
    B=B+.5*Qk(:,:,i)*(h(i+1)^2-h(i)^2);         % Calculate B-matrix
    D=D+1/3*Qk(:,:,i)*(h(i+1)^3-h(i)^3);        % Calculate D-matrix
end

%Print A,B
A
B
```

```
%-------------------------------------------------------------
%Puck IFF with different values for theta
%-------------------------------------------------------------
clear
close
clc

Yt=62.7;
Yc=200;
S12=76.3;
%-------------------------------------------------------------
%45
%-------------------------------------------------------------
theta_fr=45/180*pi;
Rn=Yt;
Rn1=S12;
Rnt=Yc/2/tan(theta_fr);
pnt=-1/tan(2*theta_fr);
pn1=pnt*Rn1/Rnt;

sigma_11=0.0;
sigma_22=0.0;
sigma_33=0.0;
sigma_12=0.0;
sigma_23=0.0;
sigma_31=0.0;

r=Yt;
for i=0:180
e1=0;
while(abs(e1-1)>0.001)
sigma_22=r*cos(i/180*pi);
sigma_12=r*sin(i/180*pi);
teller=0;
for theta=-90:90
    sn=sigma_22*cos(theta/180*pi)^2+sigma_33*sin(theta/180*pi)
^2+2*sigma_23*cos(theta/180*pi)*sin(theta/180*pi);
    tn1=sigma_12*cos(theta/180*pi)+sigma_31*sin(theta/180*pi);
    tnt=-sigma_22*sin(theta/180*pi)*cos(theta/180*pi)+sigma_33*sin(theta/
180*pi)*cos(theta/180*pi)+sigma_23*(cos(theta/180*pi)^2-sin(theta/180*pi)
^2);
    if(sn<0)
        e=(tn1/(Rn1-pn1*sn))^2+(tnt/(Rnt-pnt*sn))^2;
    else
        e=(sn/Rn)^2+(tn1/(Rn1-pn1*sn))^2+(tnt/(Rnt-pnt*sn))^2;
    end
    teller=teller+1;
    THETA(teller)=theta;
    IFF(teller)=e;
end
e1=max(IFF);
dr=0.2;
sigma_22=(r+dr)*cos(i/180*pi);
sigma_12=(r+dr)*sin(i/180*pi);
teller=0;
for theta=-90:90
    sn=sigma_22*cos(theta/180*pi)^2+sigma_33*sin(theta/180*pi)
^2+2*sigma_23*cos(theta/180*pi)*sin(theta/180*pi);
    tn1=sigma_12*cos(theta/180*pi)+sigma_31*sin(theta/180*pi);
    tnt=-sigma_22*sin(theta/180*pi)*cos(theta/180*pi)+sigma_33*sin(theta/
180*pi)*cos(theta/180*pi)+sigma_23*(cos(theta/180*pi)^2-sin(theta/180*pi)
^2);
    if(sn<0)
        e=(tn1/(Rn1-pn1*sn))^2+(tnt/(Rnt-pnt*sn))^2;
    else
        e=(sn/Rn)^2+(tn1/(Rn1-pn1*sn))^2+(tnt/(Rnt-pnt*sn))^2;
    end
    teller=teller+1;
    THETA(teller)=theta;
    IFF2(teller)=e;
end
e2=max(IFF2);
de=e2-e1;
dedr=de/dr;
r=r+0.8*(1-e1)/dedr;
end
s(i+1)=sigma_22;
t(i+1)=sigma_12;
end
csvwrite('iff45s.csv',s);
csvwrite('iff45t.csv',t);
plot(s,t,':r');

hold on

%-------------------------------------------------------------
%50
%-------------------------------------------------------------
theta_fr=50/180*pi;
Rn=Yt;
Rn1=S12;
Rnt=Yc/2/tan(theta_fr);
pnt=-1/tan(2*theta_fr);
pn1=pnt*Rn1/Rnt;

sigma_11=0.0;
sigma_22=0.0;
sigma_33=0.0;
sigma_12=0.0;
sigma_23=0.0;
```

```
sigma_31=0.0;

r=Yt;
for i=0:180
e1=0;
while(abs(e1-1)>0.001)
sigma_22=r*cos(i/180*pi);
sigma_12=r*sin(i/180*pi);
teller=0;
for theta=-90:90
    sn=sigma_22*cos(theta/180*pi)^2+sigma_33*sin(theta/180*pi)
^2+2*sigma_23*cos(theta/180*pi)*sin(theta/180*pi);
    tn1=sigma_12*cos(theta/180*pi)+sigma_31*sin(theta/180*pi);
    tnt=-sigma_22*sin(theta/180*pi)*cos(theta/180*pi)+sigma_33*sin(theta/
180*pi)*cos(theta/180*pi)+sigma_23*(cos(theta/180*pi)^2-sin(theta/180*pi)
^2);
    if(sn<0)
        e=(tn1/(Rn1-pn1*sn))^2+(tnt/(Rnt-pnt*sn))^2;
    else
        e=(sn/Rn)^2+(tn1/(Rn1-pn1*sn))^2+(tnt/(Rnt-pnt*sn))^2;
    end
    teller=teller+1;
    THETA(teller)=theta;
    IFF(teller)=e;
end
e1=max(IFF);
dr=0.2;
sigma_22=(r+dr)*cos(i/180*pi);
sigma_12=(r+dr)*sin(i/180*pi);
teller=0;
for theta=-90:90
    sn=sigma_22*cos(theta/180*pi)^2+sigma_33*sin(theta/180*pi)
^2+2*sigma_23*cos(theta/180*pi)*sin(theta/180*pi);
    tn1=sigma_12*cos(theta/180*pi)+sigma_31*sin(theta/180*pi);
    tnt=-sigma_22*sin(theta/180*pi)*cos(theta/180*pi)+sigma_33*sin(theta/
180*pi)*cos(theta/180*pi)+sigma_23*(cos(theta/180*pi)^2-sin(theta/180*pi)
^2);
    if(sn<0)
        e=(tn1/(Rn1-pn1*sn))^2+(tnt/(Rnt-pnt*sn))^2;
    else
        e=(sn/Rn)^2+(tn1/(Rn1-pn1*sn))^2+(tnt/(Rnt-pnt*sn))^2;
    end
    teller=teller+1;
    THETA(teller)=theta;
    IFF2(teller)=e;
end
e2=max(IFF2);
de=e2-e1;
dedr=de/dr;
r=r+0.8*(1-e1)/dedr;
end
s(i+1)=sigma_22;
t(i+1)=sigma_12;
end
csvwrite('iff50s.csv',s);
csvwrite('iff50t.csv',t);
plot(s,t,'--b');

hold on

%-------------------------------------------------------------
%55
%-------------------------------------------------------------
theta_fr=55/180*pi;
Rn=Yt;
Rn1=S12;
Rnt=Yc/2/tan(theta_fr);
pnt=-1/tan(2*theta_fr);
pn1=pnt*Rn1/Rnt;

sigma_11=0.0;
sigma_22=0.0;
sigma_33=0.0;
sigma_12=0.0;
sigma_23=0.0;
sigma_31=0.0;

r=Yt;
for i=0:180
e1=0;
while(abs(e1-1)>0.001)
sigma_22=r*cos(i/180*pi);
sigma_12=r*sin(i/180*pi);
teller=0;
for theta=-90:90
    sn=sigma_22*cos(theta/180*pi)^2+sigma_33*sin(theta/180*pi)
^2+2*sigma_23*cos(theta/180*pi)*sin(theta/180*pi);
    tn1=sigma_12*cos(theta/180*pi)+sigma_31*sin(theta/180*pi);
    tnt=-sigma_22*sin(theta/180*pi)*cos(theta/180*pi)+sigma_33*sin(theta/
180*pi)*cos(theta/180*pi)+sigma_23*(cos(theta/180*pi)^2-sin(theta/180*pi)
^2);
    if(sn<0)
        e=(tn1/(Rn1-pn1*sn))^2+(tnt/(Rnt-pnt*sn))^2;
    else
        e=(sn/Rn)^2+(tn1/(Rn1-pn1*sn))^2+(tnt/(Rnt-pnt*sn))^2;
    end
    teller=teller+1;
    THETA(teller)=theta;
    IFF(teller)=e;
end
```

```
e1=max(IFF);
dr=0.2;
sigma_22=(r+dr)*cos(i/180*pi);
sigma_12=(r+dr)*sin(i/180*pi);
teller=0;
for theta=-90:90
    sn=sigma_22*cos(theta/180*pi)^2+sigma_33*sin(theta/180*pi)
^2+2*sigma_23*cos(theta/180*pi)*sin(theta/180*pi);
    tn1=sigma_12*cos(theta/180*pi)+sigma_31*sin(theta/180*pi);
    tnt=-sigma_22*sin(theta/180*pi)*cos(theta/180*pi)+sigma_33*sin(theta/
180*pi)*cos(theta/180*pi)+sigma_23*(cos(theta/180*pi)^2-sin(theta/180*pi)
^2);
    if(sn<0)
        e=(tn1/(Rn1-pn1*sn))^2+(tnt/(Rnt-pnt*sn))^2;
    else
        e=(sn/Rn)^2+(tn1/(Rn1-pn1*sn))^2+(tnt/(Rnt-pnt*sn))^2;
    end
    teller=teller+1;
    THETA(teller)=theta;
    IFF2(teller)=e;
end
e2=max(IFF2);
de=e2-e1;
dedr=de/dr;
r=r+0.8*(1-e1)/dedr;
end
s(i+1)=sigma_22;
t(i+1)=sigma_12;
end
csvwrite('iff55s.csv',s);
csvwrite('iff55t.csv',t);
plot(s,t,'g');

legend('\theta^0_{fp} =45^{\circ}','\theta^0_{fp} =50^{\circ}','\theta^0_
{fp} =55^{\circ}')
```

```
%-------------------------------------------------
%Failure envelopes for different failure criteria
%-------------------------------------------------
close all
clc


Yt=63;
Yc=200;
S12=76;
YS=((Yc/(2*S12))^2-1);

%-------------------------------------------------
%Chang-Chang IFF (sigma_22<0)
%-------------------------------------------------
sigma_22=(-Yc:0);
sigma_12=S12*sqrt(1-(sigma_22/(2*S12)).^2-YS*sigma_22/Yc);
s=sigma_22;
t=sigma_12;
%csvwrite('chch_s.csv',s');
csvwrite('chch_t.csv',t');
plot(s,t,'b:');
xlabel('\sigma_2_2','FontSize',19)
ylabel('\tau_1_2','FontSize',19)
title('Comparing failure criteria','FontSize',20)
grid on
hold on
%-------------------------------------------------
%Tsai-Wu IFF
%-------------------------------------------------
sigma_22=0;
sigma_12=0;
sigma_22=(-Yc:Yt);
sigma_12=S12*sqrt(1-(sigma_22.^2)/(Yc*Yt)-(Yc-Yt)*sigma_22/(Yc*Yt));
s=sigma_22;
t=sigma_12;
csvwrite('tsai_s.csv',s');
csvwrite('tsai_t.csv',t');
plot(s,t,'r--');
hold on


%-------------------------------------------------
%Puck IFF
%-------------------------------------------------
s=0;
t=0;
theta_fr=48.2/180*pi;
Rn=Yt;
Rn1=S12;
Rnt=Yc/2/tan(theta_fr);
pnt=-1/tan(2*theta_fr);
pn1=pnt*Rn1/Rnt;

sigma_11=0.0;
sigma_22=0.0;
sigma_33=0.0;
sigma_12=0.0;
sigma_23=0.0;
sigma_31=0.0;

r=Yt;
for i=0:180
e1=0;
while(abs(e1-1)>0.001)
sigma_22=r*cos(i/180*pi);
sigma_12=r*sin(i/180*pi);
teller=0;
for theta=-90:90
    sn=sigma_22*cos(theta/180*pi)^2+sigma_33*sin(theta/180*pi)
^2+2*sigma_23*cos(theta/180*pi)*sin(theta/180*pi);
    tn1=sigma_12*cos(theta/180*pi)+sigma_31*sin(theta/180*pi);
    tnt=-sigma_22*sin(theta/180*pi)*cos(theta/180*pi)+sigma_33*sin(theta/
180*pi)*cos(theta/180*pi)+sigma_23*(cos(theta/180*pi)^2-sin(theta/180*pi)
^2);
    if(sn<0)
        e=(tn1/(Rn1-pn1*sn))^2+(tnt/(Rnt-pnt*sn))^2;
    else
        e=(sn/Rn)^2+(tn1/(Rn1-pn1*sn))^2+(tnt/(Rnt-pnt*sn))^2;
    end
    teller=teller+1;
    THETA(teller)=theta;
    IFF(teller)=e;
end
e1=max(IFF);
dr=0.2;
sigma_22=(r+dr)*cos(i/180*pi);
sigma_12=(r+dr)*sin(i/180*pi);
teller=0;
for theta=-90:90
    sn=sigma_22*cos(theta/180*pi)^2+sigma_33*sin(theta/180*pi)
^2+2*sigma_23*cos(theta/180*pi)*sin(theta/180*pi);
    tn1=sigma_12*cos(theta/180*pi)+sigma_31*sin(theta/180*pi);
    tnt=-sigma_22*sin(theta/180*pi)*cos(theta/180*pi)+sigma_33*sin(theta/
180*pi)*cos(theta/180*pi)+sigma_23*(cos(theta/180*pi)^2-sin(theta/180*pi)
^2);
    if(sn<0)
        e=(tn1/(Rn1-pn1*sn))^2+(tnt/(Rnt-pnt*sn))^2;
    else
        e=(sn/Rn)^2+(tn1/(Rn1-pn1*sn))^2+(tnt/(Rnt-pnt*sn))^2;
```

```
    end
    teller=teller+1;
    THETA(teller)=theta;
    IFF2(teller)=e;
end
e2=max(IFF2);
de=e2-e1;
dedr=de/dr;
r=r+0.8*(1-e1)/dedr;
end
s(i+1)=sigma_22;
t(i+1)=sigma_12;
end
plot(s,t,'k-');
csvwrite('puck_s.csv',s');
csvwrite('puck_t.csv',t');
hold on

legend('Chang-Chang','Tsai-wu','Puck','FontSize',14,-1)


%-------------------------------------------------
%Chang-Chang IFF (sigma_22>0)
%-------------------------------------------------
sigma_22=0;
sigma_12=0;
sigma_22=(0:Yt);
sigma_12=S12*sqrt(1-(sigma_22/Yt).^2);
u=sigma_22;
v=sigma_12;
plot(u,v,'b:');
csvwrite('chch_u.csv',u');
csvwrite('chch_v.csv',v');
hold on
```

B.2 LS-DYNA input-file for Case study 1

From this study only two of the 15 k-files are presented, one describing the use of shell elements and one using solid elements. The first input-file uses shell elements to model a [±45/0/90]-laminate layup, and the second uses solid elements to model a [±45/90_6/ ± 45]-laminate layup. The node- and element-numbering lists and some other lists are omitted from the displayed text. Omitted text is indicated with: "...".

```
$# LS-DYNA Keyword file created by LS-PREPOST 3.1 (Beta) - 19Aug2010(08:33)
$# Created on Mar-28-2011 (10:28:43)
*KEYWORD
*TITLE
$# title
DBLT_0
*CONTROL_IMPLICIT_DYNAMICS
$#   imass     gamma      beta    tdybir    tdydth    tdybur     irate
         0  0.500000  0.250000     0.0001.0000E+281.0000E+28         0
*CONTROL_IMPLICIT_GENERAL
$#  imflag       dt0    imform      nsbs       igs     cnstn      form
zero_v
         1  0.010000         2         1         2         0         0
1
*CONTROL_SHELL
$#  wrpang     esort     irnxx    istupd    theory       bwc     miter
proj
 20.000000         0        -1         0         2         2         1
0
$# rotascl    intgrd    lamsht    cstyp6    tshell    nfail1    nfail4
psnfail
  1.000000         0         1         1         0         0         0
0
$# psstupd    irquad     cntco
         0         0         0
*CONTROL_SOLUTION
$#    soln       nlq     isnan     lcint
         0         0         0      1000
*CONTROL_TERMINATION
$#  endtim    endcyc     dtmin    endeng    endmas
  2.000000         0     0.000     0.000     0.000
*DATABASE_BNDOUT
$#      dt    binary      lcur     ioopt
  0.001000         0         0         1
*DATABASE_ELOUT
$#      dt    binary      lcur     ioopt
  0.001000         0         0         1
*DATABASE_GLSTAT
$#      dt    binary      lcur     ioopt
  0.001000         0         0         1
*DATABASE_MATSUM
$#      dt    binary      lcur     ioopt
  0.001000         0         0         1
*DATABASE_NODOUT
$#      dt    binary      lcur     ioopt      dthf     binhf
  0.001000         0         0         1     0.000         0
*DATABASE_BINARY_D3PLOT
$#      dt      lcdt      beam     npltc    psetid
  0.001000         0         0         0         0
$#   ioopt
         0
*DATABASE_EXTENT_BINARY
$#   neiph     neips    maxint    strflg    sigflg    epsflg    rltflg
engflg
        13        17         4         0         1         1         1
1
$#  cmpflg    ieverp    beamip     dcomp      shge     stssz    n3thdt
ialemat
         0         0         0         1         1         1         2
1
$# nintsld   pkp_sen      sclp    unused     msscl     therm    intout
nodout
         0         0  1.000000         0         0         0STRESS
STRESS
*BOUNDARY_PRESCRIBED_MOTION_SET
$#    nsid       dof       vad      lcid        sf       vid     death
birth
         4         1         2         4  1.000000         01.0000E+28
0.000
*BOUNDARY_SPC_SET
$#    nsid       cid      dofx      dofy      dofz     dofrx     dofry
dofrz
         1         0         1         0         0         0         0
0
*SET_NODE_LIST_TITLE
NODESET(SPC) 1
$#     sid       da1       da2       da3       da4    solver
         1     0.000     0.000     0.000     0.000MECH
$#    nid1      nid2      nid3      nid4      nid5      nid6      nid7
nid8
       171       172         0         0         0         0         0
0
*BOUNDARY_SPC_SET
$#    nsid       cid      dofx      dofy      dofz     dofrx     dofry
dofrz
         2         0         0         1         0         0         0
0
*SET_NODE_LIST
$#     sid       da1       da2       da3       da4    solver
         2     0.000     0.000     0.000     0.000MECH
$#    nid1      nid2      nid3      nid4      nid5      nid6      nid7
nid8
       171       173         0         0         0         0         0
0
*BOUNDARY_SPC_SET
$#    nsid       cid      dofx      dofy      dofz     dofrx     dofry
dofrz
         3         0         0         0         1         0         1
0
*SET_NODE_LIST
```

```
$#     sid       da1       da2       da3       da4    solver
         3     0.000     0.000     0.000     0.000MECH
$#    nid1      nid2      nid3      nid4      nid5      nid6      nid7
nid8
       171       172       173       174         0         0         0
0
*PART_COMPOSITE
$# title
Composite
$#     pid    elform      shrf      nloc     marea      hgid    adpopt
ithelfrm
         1         2     0.000     0.000     0.000         0         0
0
$#    mid1    thick1        b1    ithid1      mid2    thick2        b2
ithid2
         1  0.125000     0.000         0         1  0.125000 90.000000
0
         1  0.125000-45.000000         0         1  0.125000 45.000000
0
         1  0.125000     0.000         0         1  0.125000 90.000000
0
         1  0.125000-45.000000         0         1  0.125000 45.000000
0
*MAT_USER_DEFINED_MATERIAL_MODELS
$      MID        RO        MT       LMC       NHV    IORTHO     IBULK
IG
$#     mid        ro        mt       lmc       nhv    iortho     ibulk
ig
         1 1.8000E-9        47        17        17         1         6
3
$    IVECT     IFAIL   ITERMAL
$#   ivect     ifail    itherm    ihyper      ieos
         1         1         0         0         0
$     AOPT      MAXC        XP        YP        ZP        A1        A2
A3
$#    aopt      mafc        xp        yp        zp        a1        a2
a3
  2.000000  1.000000     0.000     0.000     0.000  1.000000     0.000
0.000
$       V1        V2        V3        D1        D2        D3      BETA
$#      v1        v2        v3        d1        d2        d3      beta
     0.000     0.000     0.000     0.000  1.000000     0.000     0.000
$       E1       v12       G12        E2       v23         K       Ef1
vf12
$#      p1        p2        p3        p4        p5        p6        p7
p8
 40500.000  0.280000 4000.0000 13000.000  0.300000 58846.148 4.0000E+5
0.200000
$    eps1T     eps1C     mSigf        Yt        Yc       S12     theta
crv1
$#      p1        p2        p3        p4        p5        p6        p7
p8
  0.028000  0.021000  1.100000 35.000000 200.00000 50.000000 51.000000
1.000000
$     crv2
$#      p1        p2        p3        p4        p5        p6        p7
p8
  2.000000     0.000     0.000     0.000     0.000     0.000     0.000
0.000
*DEFINE_CURVE_TITLE
Compression
$#    lcid      sidr       sfa       sfo      offa      offo    dattyp
         1         0  1.000000  1.000000     0.000     0.000         0
$#                a1                  o1
           1.0000000               0.000
...

*DEFINE_CURVE_TITLE
Tension
$#    lcid      sidr       sfa       sfo      offa      offo    dattyp
         2         0  1.000000  1.000000     0.000     0.000         0
$#                a1                  o1
           1.0000000               0.000


 ...

*DEFINE_CURVE_TITLE
Loading
$#    lcid      sidr       sfa       sfo      offa      offo    dattyp
         4         0  1.000000  1.000000     0.000     0.000         0
$#                a1                  o1
                0.000               0.000
             2.0000000           0.1000000
*SET_NODE_LIST_TITLE
nodeforskyvning
$#     sid       da1       da2       da3       da4    solver
         4     0.000     0.000     0.000     0.000MECH
$#    nid1      nid2      nid3      nid4      nid5      nid6      nid7
nid8
       174       173         0         0         0         0         0
0
*ELEMENT_SHELL
$#   eid     pid      n1      n2      n3      n4      n5      n6      n7
n8
       1       1     171     173     174     172       0       0       0
0
*NODE
$#   nid               x               y               z      tc      rc
     171           0.000           0.000           0.000       0       0
     172           0.000       2.0000000           0.000       0       0
```

```
     173       3.0000000           0.000           0.000       0       0
     174       3.0000000       2.0000000           0.000       0       0
*END
*COMPONENT
$#    clid    color1    color2    color3    color4
         1  0.769000  0.004000  0.110000     0.000         0         0
0
$# name
Part 1
*COMPONENT_PART
$#     pid      clid
         1         1
*COMPONENT_END
```

```
$# LS-DYNA Keyword file created by LS-PREPOST 3.1 (Beta) - 19Aug2010(08:33)
$# Created on Apr-12-2011 (13:13:33)
*KEYWORD
*TITLE
$# title
LS-DYNA keyword deck by LS-PrePost
*CONTROL_IMPLICIT_GENERAL
$#  imflag       dt0    imform      nsbs       igs     cnstn      form
zero_v
         1  0.020000         2         1         2         0         0
1
*CONTROL_TERMINATION
$#  endtim    endcyc     dtmin    endeng    endmas
  1.000000         0     0.000     0.000     0.000
*DATABASE_BNDOUT
$#      dt    binary      lcur     ioopt
  0.010000         0         0         1
*DATABASE_GLSTAT
$#      dt    binary      lcur     ioopt
  0.010000         0         0         1
*DATABASE_MATSUM
$#      dt    binary      lcur     ioopt
  0.010000         0         0         1
*DATABASE_NODFOR
$#      dt    binary      lcur     ioopt
  0.010000         0         0         1
*DATABASE_NODOUT
$#      dt    binary      lcur     ioopt      dthf     binhf
  0.010000         0         0         1     0.000         0
*DATABASE_BINARY_D3PLOT
$#      dt      lcdt      beam     npltc    psetid
  0.010000         0         0         0         0
$#   ioopt
         0
*BOUNDARY_PRESCRIBED_MOTION_SET
$#    nsid       dof       vad      lcid        sf       vid     death
birth
         6         1         2         3  1.000000         01.0000E+28
0.000
*BOUNDARY_SPC_SET
$#    nsid       cid      dofx      dofy      dofz     dofrx     dofry
dofrz
         1         0         1         0         0         0         0
0
*SET_NODE_LIST_TITLE
NODESET(SPC) 1
$#     sid       da1       da2       da3       da4    solver
         1     0.000     0.000     0.000     0.000MECH
$#    nid1      nid2      nid3      nid4      nid5      nid6      nid7
nid8
         1         2         3         4         5         6         7
8

...

*BOUNDARY_SPC_SET
$#    nsid       cid      dofx      dofy      dofz     dofrx     dofry
dofrz
         2         0         0         0         1         0         0
0
*SET_NODE_LIST_TITLE
NODESET(SPC) 2
$#     sid       da1       da2       da3       da4    solver
         2     0.000     0.000     0.000     0.000MECH
$#    nid1      nid2      nid3      nid4      nid5      nid6      nid7
nid8
       127       138       149       160       171       182       193
204

...

*BOUNDARY_SPC_SET
$#    nsid       cid      dofx      dofy      dofz     dofrx     dofry
dofrz
         3         0         0         1         0         0         0
0
*SET_NODE_LIST_TITLE
NODESET(SPC) 3
$#     sid       da1       da2       da3       da4    solver
         3     0.000     0.000     0.000     0.000MECH
$#    nid1      nid2      nid3      nid4      nid5      nid6      nid7
nid8
       177       178       179       180       181       182       183
184

...

*BOUNDARY_SPC_SET
$#    nsid       cid      dofx      dofy      dofz     dofrx     dofry
dofrz
         4         0         1         1         1         0         0
0
*SET_NODE_LIST_TITLE
NODESET(SPC) 4
$#     sid       da1       da2       da3       da4    solver
         4     0.000     0.000     0.000     0.000MECH
$#    nid1      nid2      nid3      nid4      nid5      nid6      nid7
nid8
        61         0         0         0         0         0         0
0
```

```
*BOUNDARY_SPC_SET
$#    nsid       cid      dofx      dofy      dofz     dofrx     dofry
dofrz
         5         0         1         0         1         0         0
0
*SET_NODE_LIST_TITLE
NODESET(SPC) 5
$#     sid       da1       da2       da3       da4    solver
         5     0.000     0.000     0.000     0.000MECH
$#    nid1      nid2      nid3      nid4      nid5      nid6      nid7
nid8
        50        39        28        17        72        83        94
105
         6       116         0         0         0         0         0
0
*PART
$# title

$#     pid     secid       mid     eosid      hgid      grav    adpopt
tmid
         1         1         3         0         1         0         0
0
*SECTION_SOLID_TITLE
Brick
$#   secid    elform       aet
         1         1         0
*MAT_USER_DEFINED_MATERIAL_MODELS
$      MID        RO        MT       LMC       NHV    IORTHO     IBULK
IG
$#     mid        ro        mt       lmc       nhv    iortho     ibulk
ig
         3 1.8000E-5        47        17        17         1         6
3
$    IVECT     IFAIL   ITERMAL
$#   ivect     ifail    itherm    ihyper      ieos
         1         1         0         0         0
$     AOPT      MAXC        XP        YP        ZP        A1        A2
A3
$#    aopt      mafc        xp        yp        zp        a1        a2
a3
  2.000000  1.000000     0.000     0.000     0.000  1.000000  1.000000
0.000
$       V1        V2        V3        D1        D2        D3      BETA
$#      v1        v2        v3        d1        d2        d3      beta
     0.000     0.000     0.000 -1.000000  1.000000     0.000     0.000
$       E1       v12       G12        E2       v23         K       Ef1
vf12
$#      p1        p2        p3        p4        p5        p6        p7
p8
 40500.000  0.280000 4000.0000 13000.000  0.400000 58846.148 4.0000E+5
0.200000
$    eps1T     eps1C     mSigf        Yt        Yc       S12     theta
crv1
$#      p1        p2        p3        p4        p5        p6        p7
p8
  0.027200  0.021000  1.100000 35.000000 200.00000 50.000000 47.000000
1.000000
$     crv2
$#      p1        p2        p3        p4        p5        p6        p7
p8
  2.000000     0.000     0.000     0.000     0.000     0.000     0.000
0.000
*HOURGLASS
$#    hgid       ihq        qm       ibq        q1        q2    qb/vdc
qw
         1         4  0.100000         0  1.500000  0.060000  0.100000
0.100000
*PART
$# title

$#     pid     secid       mid     eosid      hgid      grav    adpopt
tmid
         2         1         4         0         1         0         0
0
*MAT_USER_DEFINED_MATERIAL_MODELS
$      MID        RO        MT       LMC       NHV    IORTHO     IBULK
IG
$#     mid        ro        mt       lmc       nhv    iortho     ibulk
ig
         4 1.8000E-5        47        17        17         1         6
3
$    IVECT     IFAIL   ITERMAL
$#   ivect     ifail    itherm    ihyper      ieos
         1         1         0         0         0
$     AOPT      MAXC        XP        YP        ZP        A1        A2
A3
$#    aopt      mafc        xp        yp        zp        a1        a2
a3
  2.000000  1.000000     0.000     0.000     0.000  1.000000 -1.000000
0.000
$       V1        V2        V3        D1        D2        D3      BETA
$#      v1        v2        v3        d1        d2        d3      beta
     0.000     0.000     0.000  1.000000  1.000000     0.000     0.000
$       E1       v12       G12        E2       v23         K       Ef1
vf12
$#      p1        p2        p3        p4        p5        p6        p7
p8
 40500.000  0.280000 4000.0000 13000.000  0.400000 58846.148 4.0000E+5
0.200000
$    eps1T     eps1C     mSigf        Yt        Yc       S12     theta
```

```
crv1
$#      p1        p2        p3        p4        p5        p6        p7
p8
  0.027200  0.021000  1.100000 35.000000 200.00000 50.000000 47.000000
1.000000
$     crv2
$#      p1        p2        p3        p4        p5        p6        p7
p8
  2.000000     0.000     0.000     0.000     0.000     0.000     0.000
0.000
*PART
$# title

$#     pid     secid       mid     eosid      hgid      grav    adpopt
tmid
         3         1         1         0         1         0         0
0
*MAT_USER_DEFINED_MATERIAL_MODELS
$      MID        RO        MT       LMC       NHV    IORTHO     IBULK
IG
$#     mid        ro        mt       lmc       nhv    iortho     ibulk
ig
         1 1.8000E-5        47        17        17         1         6
3
$    IVECT     IFAIL   ITERMAL
$#   ivect     ifail    itherm    ihyper      ieos
         1         1         0         0         0
$     AOPT      MAXC        XP        YP        ZP        A1        A2
A3
$#    aopt      mafc        xp        yp        zp        a1        a2
a3
  2.000000  1.000000     0.000     0.000     0.000     0.000  1.000000
0.000
$       V1        V2        V3        D1        D2        D3      BETA
$#      v1        v2        v3        d1        d2        d3      beta
     0.000     0.000     0.000 -1.000000     0.000     0.000     0.000
$       E1       v12       G12        E2       v23         K       Ef1
vf12
$#      p1        p2        p3        p4        p5        p6        p7
p8
 40500.000  0.280000 4000.0000 13000.000  0.400000 58846.148 4.0000E+5
0.200000
$    eps1T     eps1C     mSigf        Yt        Yc       S12     theta
crv1
$#      p1        p2        p3        p4        p5        p6        p7
p8
  0.027200  0.021000  1.100000 35.000000 200.00000 50.000000 47.000000
1.000000
$     crv2
$#      p1        p2        p3        p4        p5        p6        p7
p8
  2.000000     0.000     0.000     0.000     0.000     0.000     0.000
0.000
*MAT_USER_DEFINED_MATERIAL_MODELS
$      MID        RO        MT       LMC       NHV    IORTHO     IBULK
IG
$#     mid        ro        mt       lmc       nhv    iortho     ibulk
ig
         2 1.8000E-5        47        17        17         1         6
3
$    IVECT     IFAIL   ITERMAL
$#   ivect     ifail    itherm    ihyper      ieos
         1         1         0         0         0
$     AOPT      MAXC        XP        YP        ZP        A1        A2
A3
$#    aopt      mafc        xp        yp        zp        a1        a2
a3
  2.000000  1.000000     0.000     0.000     0.000  1.000000     0.000
0.000
$       V1        V2        V3        D1        D2        D3      BETA
$#      v1        v2        v3        d1        d2        d3      beta
     0.000     0.000     0.000     0.000  1.000000     0.000     0.000
$       E1       v12       G12        E2       v23         K       Ef1
vf12
$#      p1        p2        p3        p4        p5        p6        p7
p8
 40500.000  0.280000 4000.0000 13000.000  0.400000 58846.148 4.0000E+5
0.200000
$    eps1T     eps1C     mSigf        Yt        Yc       S12     theta
crv1
$#      p1        p2        p3        p4        p5        p6        p7
p8
  0.027200  0.021000  1.100000 35.000000 200.00000 50.000000 47.000000
1.000000
$     crv2
$#      p1        p2        p3        p4        p5        p6        p7
p8
  2.000000     0.000     0.000     0.000     0.000     0.000     0.000
0.000
*DEFINE_CURVE_TITLE
Compression
$#    lcid      sidr       sfa       sfo      offa      offo    dattyp
         1         0  1.000000  1.000000     0.000     0.000         0
$#                a1                  o1
           1.0000000             0.000

...

*DEFINE_CURVE_TITLE
Tension
```

```
$#    lcid      sidr       sfa       sfo      offa      offo    dattyp
         2         0  1.000000  1.000000     0.000     0.000         0
$#              a1                  o1
           1.0000000               0.000

...

*DEFINE_CURVE_TITLE
loading
$#    lcid      sidr       sfa       sfo      offa      offo    dattyp
         3         0  1.000000  1.000000     0.000     0.000         0
$#              a1                  o1
             0.000               0.000
           1.0000000           0.0625000
           2.0000000           0.0625000
*SET_NODE_LIST_TITLE
Node forskyvning
$#     sid       da1       da2       da3       da4    solver
         6     0.000     0.000     0.000     0.000MECH
$#    nid1      nid2      nid3      nid4      nid5      nid6      nid7
nid8
      1211      1212      1213      1214      1215      1216      1217
1218

...

*ELEMENT_SOLID
$#   eid     pid      n1      n2      n3      n4      n5      n6      n7
n8
    2497       1       1     122     133      12       2     123     134
13

...

*NODE
$#   nid               x               y               z      tc      rc
       1           0.000           0.000           0.000       0       0

...

*END
*COMPONENT
$#    clid    color1    color2    color3    color4
         1  0.769000  0.004000  0.110000     0.000         0         0
0
$     AOPT      MAXC        XP        YP        ZP        A1        A2
A3
$# name
Part 1
*COMPONENT_PART
$     AOPT      MAXC        XP        YP        ZP        A1        A2
A3
$#     pid      clid
         1         1
$     AOPT      MAXC        XP        YP        ZP        A1        A2
A3
$#     pid      clid
         2         1
$#     pid      clid
         3         1
*COMPONENT_END
```

B.3 LS-DYNA input-file for Case study 2

From this study only one of the tree input-files are presented. The node- and element-numbering lists and some other lists are omitted from the displayed text. Omitted text is indicated with: "...".

```
$# LS-DYNA Keyword file created by LS-PREPOST 3.1 (Beta) - 19Aug2010(08:33)
$# Created on Apr-19-2011 (08:30:25)
*KEYWORD
*TITLE
$# title
Pin Holed Plate -mario-frode- (90/0)6s
*CONTROL_IMPLICIT_AUTO
$#   iauto    iteopt    itewin     dtmin     dtmax     dtexp
         1        11         5 3.0000E-4  0.020000  0.100000
*CONTROL_IMPLICIT_DYNAMICS
$#   imass     gamma      beta    tdybir    tdydth    tdybur     irate
         1  0.500000  0.250000     0.0001.0000E+281.0000E+28         0
*CONTROL_IMPLICIT_GENERAL
$#  imflag       dt0    imform      nsbs       igs     cnstn      form
zero_v
         1  0.020000         2         1         2         0         0
0
*CONTROL_SHELL
$#  wrpang     esort     irnxx    istupd    theory       bwc     miter
proj
 20.000000         0        -1         0         2         2         1
0
$# rotascl    intgrd    lamsht    cstyp6    tshell    nfail1    nfail4
psnfail
  1.000000         0         1         1         0         0         0
0
$# psstupd    irquad     cntco
         0         0         0
*CONTROL_TERMINATION
$#  endtim    endcyc     dtmin    endeng    endmas
  1.000000         0     0.000     0.000     0.000
*CONTROL_TIMESTEP
$#  dtinit    tssfac      isdo    tslimt     dt2ms      lctm     erode
ms1st
  0.100000  0.900000         3     0.000 1.0000E-5         0         0
0
$#  dt2msf   dt2mslc     imscl
     0.000         0        -1
*DATABASE_BNDOUT
$#      dt    binary      lcur     ioopt
  0.020000         0         0         1
*DATABASE_GLSTAT
$#      dt    binary      lcur     ioopt
  0.020000         0         0         1
*DATABASE_MATSUM
$#      dt    binary      lcur     ioopt
  0.020000         0         0         1
*DATABASE_NODOUT
$#      dt    binary      lcur     ioopt      dthf     binhf
  0.020000         0         0         1     0.000         0
*DATABASE_BINARY_D3PLOT
$#      dt      lcdt      beam     npltc    psetid
  0.020000         0         0         0         0
$#   ioopt
         0
*DATABASE_EXTENT_BINARY
$#   neiph     neips    maxint    strflg    sigflg    epsflg    rltflg
engflg
         0         5         8         0         1         1         1
1
$#  cmpflg    ieverp    beamip     dcomp      shge     stssz    n3thdt
ialemat
         0         0         0         1         1         1         2
1
$# nintsld   pkp_sen      sclp    unused     msscl     therm    intout
nodout
         0         0  1.000000         0         0         0STRESS
STRESS
*BOUNDARY_PRESCRIBED_MOTION_SET_ID
$#      id
heading
         0Nodeforskyvning
$#    nsid       dof       vad      lcid        sf       vid     death
birth
         2         1         2         2  1.000000         01.0000E+28
0.000
*BOUNDARY_SPC_SET
$#    nsid       cid      dofx      dofy      dofz     dofrx     dofry
dofrz
         1         0         0         0         1         0         0
0
*SET_NODE_LIST_TITLE
NODESET(SPC) 1
$#     sid       da1       da2       da3       da4    solver
         1     0.000     0.000     0.000     0.000MECH
$#    nid1      nid2      nid3      nid4      nid5      nid6      nid7
nid8
         1         2         3         4         5         6         7
8

...

*BOUNDARY_SPC_SET
$#    nsid       cid      dofx      dofy      dofz     dofrx     dofry
dofrz
         3         0         0         1         0         0         0
0
*SET_NODE_LIST_TITLE
NODESET(SPC) 3
$#     sid       da1       da2       da3       da4    solver
```

```
         3     0.000     0.000     0.000     0.000MECH
$#    nid1      nid2      nid3      nid4      nid5      nid6      nid7
nid8
         1         5         9        13        17        21        25
29
...

*CONTACT_NODES_TO_SURFACE_ID
$#     cid
title
         1Rigid Pin constraint
$#    ssid      msid     sstyp     mstyp    sboxid    mboxid       spr
mpr
         1         2         3         3         0         0         0
0
$#      fs        fd        dc        vc       vdc    penchk        bt
dt
     0.000     0.000     0.000     0.000     0.000         0
0.0001.0000E+20
$#     sfs       sfm       sst       mst      sfst      sfmt       fsf
vsf
  1.000000  1.000000     0.000     0.000  1.000000  1.000000  1.000000
1.000000
*PART_COMPOSITE
$# title
Pin holed plate
$#     pid    elform      shrf      nloc     marea      hgid    adpopt
ithelfrm
         1         2     0.000     0.000     0.000         0         0
0
$#    mid1    thick1        b1    ithid1      mid2    thick2        b2
ithid2
         1  0.010000 90.000000         0         1  0.010000     0.000
0
         1  0.010000 90.000000         0         1  0.010000     0.000
0
         1  0.010000 90.000000         0         1  0.010000     0.000
0
         1  0.010000 90.000000         0         1  0.010000     0.000
0
         1  0.010000 90.000000         0         1  0.010000     0.000
0
         1  0.010000 90.000000         0         1  0.010000     0.000
0
         1  0.010000     0.000         0         1  0.010000 90.000000
0
         1  0.010000     0.000         0         1  0.010000 90.000000
0
         1  0.010000     0.000         0         1  0.010000 90.000000
0
         1  0.010000     0.000         0         1  0.010000 90.000000
0
         1  0.010000     0.000         0         1  0.010000 90.000000
0
*PART
$# title
BlockMesh2
$#     pid     secid       mid     eosid      hgid      grav    adpopt
tmid
         2         1         2         0         0         0         0
0
*SECTION_SOLID_TITLE
Rigid pin
$#   secid    elform       aet
         1         1         0
*MAT_RIGID_TITLE
Rigid Pin
$#     mid        ro         e        pr         n    couple         m
alias
         2 7.8000E-9 2.1000E+5  0.300000     0.000     0.000     0.000
$#     cmo      con1      con2
  1.000000         7         7
$# lco or a1      a2        a3        v1        v2        v3
     0.000     0.000     0.000     0.000     0.000     0.000
*MAT_USER_DEFINED_MATERIAL_MODELS
$      MID        RO        MT       LMC       NHV    IORTHO     IBULK
IG
$#     mid        ro        mt       lmc       nhv    iortho     ibulk
ig
         1 1.8000E-9        47        17        17         1         6
3
$    IVECT     IFAIL   ITERMAL
$#   ivect     ifail    itherm    ihyper      ieos
         1         1         0         0         0
$     AOPT      MAXC        XP        YP        ZP        A1        A2
A3
$#    aopt      mafc        xp        yp        zp        a1        a2
a3
  2.000000  1.000000     0.000     0.000     0.000  1.000000     0.000
0.000
$       V1        V2        V3        D1        D2        D3      BETA
$#      v1        v2        v3        d1        d2        d3      beta
     0.000     0.000     0.000     0.000  1.000000     0.000     0.000
$       E1       v12       G12        E2       v23         K       Ef1
vf12
$#      p1        p2        p3        p4        p5        p6        p7
p8
147000.000  0.300000 6200.0000 11700.000  0.300000 58846.148 4.0000E+5
```

```
0.200000
$    eps1T     eps1C     mSigf        Yt        Yc       S12     theta
crv1
$#      p1        p2        p3        p4        p5        p6        p7
p8
  0.011769  0.009388  1.100000 43.000000 204.00000 133.00000 51.000000
11.000000
$     crv2
$#      p1        p2        p3        p4        p5        p6        p7
p8
 12.000000     0.000     0.000     0.000     0.000     0.000     0.000
0.000
*DEFINE_CURVE_SMOOTH_TITLE
displacement
$#    lcid      sidr      dist    tstart      tend     trise        v0
         1         0  3.000000     0.000  2.000000  0.100000     0.000
*DEFINE_CURVE_TITLE
Forskyvning steg for steg
$#    lcid      sidr       sfa       sfo      offa      offo    dattyp
         2         0  1.000000  1.000000     0.000     0.000         0
$#                a1                o1
                0.000             0.000
            0.0500000         0.0100000
            0.4000000         0.5000000
            1.0000000         0.7500000
            2.0000000         0.7500000
*DEFINE_CURVE_TITLE
Damage compression
$#    lcid      sidr       sfa       sfo      offa      offo    dattyp
        11         0  1.000000  1.000000     0.000     0.000         0
$#                a1                o1
            1.0000000             0.000

...

*DEFINE_CURVE_TITLE
Damage tensile
$#    lcid      sidr       sfa       sfo      offa      offo    dattyp
        12         0  1.000000  1.000000     0.000     0.000         0
$#                a1                o1
            1.0000000             0.000

...

*SET_NODE_LIST_TITLE
Node forskyvning
$#     sid       da1       da2       da3       da4    solver
         2     0.000     0.000     0.000     0.000MECH
$#    nid1      nid2      nid3      nid4      nid5      nid6      nid7
nid8
```

```
      1481      1484      1493      1502      1511      1520      1529
1538
      1547         0         0         0         0         0         0
0
*SET_NODE_LIST_TITLE
Rigid contact
$#     sid       da1       da2       da3       da4    solver
         5     0.000     0.000     0.000     0.000MECH
$#    nid1      nid2      nid3      nid4      nid5      nid6      nid7
nid8
        65        73        77        81        85        89        93
97
       101       105       283       287       291       295       299
303
       307       311       315      1046      1050      1054      1058
1062
      1066      1070      1074      1237      1241      1245      1249
1253
      1257      1261      1265      1034      1042         0         0
0
*ELEMENT_SOLID
$#   eid     pid      n1      n2      n3      n4      n5      n6      n7
n8
       1       2    1704    1706    1668    1630    1705    1667    1669
1631

 ...

*ELEMENT_SHELL
$#   eid     pid      n1      n2      n3      n4      n5      n6      n7
n8
       1       1       1       5       6       2       0       0       0
0

...

*NODE
$#   nid               x               y               z      tc      rc
       1     -38.0999985           0.000           0.000       0       0

...

*END
*COMPONENT
$#    clid    color1    color2    color3    color4
         1  0.769000  0.004000  0.110000     0.000         0         0
0
$# name
Part 1
*COMPONENT_PART
```

```
$#     pid      clid
         1         1
$#     pid      clid
         2         1
*COMPONENT_END
```

B.4 LS-DYNA input-file for Case study 3

From this study, the only LS-DYNA input-files used is presented. The node- and element-numbering lists and some other lists are omitted from the displayed text. Omitted text is indicated with: "...".

```
$# LS-DYNA Keyword file created by LS-PREPOST 3.1 (Beta) - 19Aug2010(08:33)
$# Created on Feb-14-2011 (12:40:55)
*KEYWORD
*TITLE
$# title
200_50_DBLTs
*CONTROL_HOURGLASS
$#     ihq        qh
         2  0.100000
*CONTROL_IMPLICIT_AUTO
$#   iauto    iteopt    itewin     dtmin     dtmax     dtexp
         0        11         5  0.001000  0.300000  0.100000
*CONTROL_IMPLICIT_DYNAMICS
$#   imass     gamma      beta    tdybir    tdydth    tdybur     irate
         1  0.500000  0.250000     0.0001.0000E+281.0000E+28         0
*CONTROL_IMPLICIT_GENERAL
$#  imflag       dt0    imform      nsbs       igs     cnstn      form
zero_v
         0  0.100000         2         1         2         0         0
0
*CONTROL_SHELL
$#  wrpang     esort     irnxx    istupd    theory       bwc     miter
proj
 20.000000         0        -1         0         2         2         1
0
$# rotascl    intgrd    lamsht    cstyp6    tshell    nfail1    nfail4
psnfail
  1.000000         0         1         1         0         0         0
0
$# psstupd    irquad     cntco
         0         0         0
*CONTROL_TERMINATION
$#  endtim    endcyc     dtmin    endeng    endmas
  1.500000         0     0.000     0.000     0.000
*CONTROL_TIMESTEP
$#  dtinit    tssfac      isdo    tslimt     dt2ms      lctm     erode
ms1st
  0.100000  0.700000         0     0.000     0.000         0         0
0
$#  dt2msf   dt2mslc     imscl
     0.000         0         0
*DATABASE_BNDOUT
$#      dt    binary      lcur     ioopt
  0.001000         0         0         1
*DATABASE_GLSTAT
$#      dt    binary      lcur     ioopt
  0.001000         0         0         1
*DATABASE_MATSUM
$#      dt    binary      lcur     ioopt
  0.001000         0         0         1
*DATABASE_NODOUT
$#      dt    binary      lcur     ioopt      dthf     binhf
  0.001000         0         0         1     0.000         0
*DATABASE_BINARY_D3PLOT
$#      dt      lcdt      beam     npltc    psetid
  0.001000         0         0         0         0
$#   ioopt
         0
*DATABASE_EXTENT_BINARY
$#   neiph     neips    maxint    strflg    sigflg    epsflg    rltflg
engflg
         0         5         8         0         1         1         1
1
$#  cmpflg    ieverp    beamip     dcomp      shge     stssz    n3thdt
ialemat
         0         0         0         1         1         1         2
1
$# nintsld   pkp_sen      sclp    unused     msscl     therm    intout
nodout
         0         0  1.000000         0         0         0STRESS
STRESS
*BOUNDARY_PRESCRIBED_MOTION_SET
$#    nsid       dof       vad      lcid        sf       vid     death
birth
         4         2         2         2  1.000000         01.0000E+28
0.000
*BOUNDARY_SPC_SET
$#    nsid       cid      dofx      dofy      dofz     dofrx     dofry
dofrz
         1         0         1         1         1         0         0
1
*SET_NODE_LIST
$#     sid       da1       da2       da3       da4    solver
         1     0.000     0.000     0.000     0.000MECH
$#    nid1      nid2      nid3      nid4      nid5      nid6      nid7
nid8
     10009     10010     10011     10012     10013     10014     10015
10016

  ...

*BOUNDARY_SPC_SET
$#    nsid       cid      dofx      dofy      dofz     dofrx     dofry
dofrz
         2         0         0         0         1         0         0
0
*SET_NODE_LIST_TITLE
NODESET(SPC) 2
$#     sid       da1       da2       da3       da4    solver
         2     0.000     0.000     0.000     0.000MECH
```

```
$#    nid1      nid2      nid3      nid4      nid5      nid6      nid7
nid8
      5005      5006      5007      5008      5009      5010      5011
5012

   ...

*BOUNDARY_SPC_SET
$#    nsid       cid      dofx      dofy      dofz     dofrx     dofry
dofrz
         4         0         1         0         1         0         0
1
*SET_NODE_LIST
$#     sid       da1       da2       da3       da4    solver
         4     0.000     0.000     0.000     0.000MECH
$#    nid1      nid2      nid3      nid4      nid5      nid6      nid7
nid8
      5006      5007      5008      5009      5010      5011      5012
5013

      ...

$#     pid    elform      shrf      nloc     marea      hgid    adpopt
ithelfrm
         1         2     0.000     0.000     0.000         1         0
0
$#    mid1    thick1        b1    ithid1      mid2    thick2        b2
ithid2
         1  0.250000 90.000000         0         1  0.250000 45.000000
0
         1  0.250000-45.000000         0         1  0.250000     0.000
0
         1  0.250000     0.000         0         1  0.250000-45.000000
0
         1  0.250000 45.000000         0         1  0.250000 90.000000
0
*HOURGLASS
$#    hgid       ihq        qm       ibq        q1        q2    qb/vdc
qw
         1         4  0.100000         0  1.500000  0.060000  0.100000
0.100000
*MAT_USER_DEFINED_MATERIAL_MODELS
$      MID        RO        MT       LMC       NHV    IORTHO     IBULK
IG
$#     mid        ro        mt       lmc       nhv    iortho     ibulk
ig
         1 1.0000E-5        47        17        17         1         6
3
$    IVECT     IFAIL   ITERMAL
$#   ivect     ifail    itherm    ihyper      ieos
         1         1         0         0         0
$     AOPT      MAXC        XP        YP        ZP        A1        A2
A3
$#    aopt      mafc        xp        yp        zp        a1        a2
a3
  2.000000  1.000000     0.000     0.000     0.000     0.000  1.000000
0.000
$       V1        V2        V3        D1        D2        D3      BETA
$#      v1        v2        v3        d1        d2        d3      beta
     0.000     0.000     0.000 -1.000000     0.000     0.000     0.000
$       E1       v12       G12        E2       v23         K       Ef1
vf12
$#      p1        p2        p3        p4        p5        p6        p7
p8
 38600.000  0.280000 4000.0000 13000.000  0.300000 58846.148 7.4000E+5
0.200000
$    eps1T     eps1C     mSigf        Yt        Yc       S12     theta
crv1
$#      p1        p2        p3        p4        p5        p6        p7
p8
  0.017600  0.010300  1.100000 62.700001 231.20000 76.300003 51.000000
11.000000
$     crv2
$#      p1        p2        p3        p4        p5        p6        p7
p8
 12.000000     0.000     0.000     0.000     0.000     0.000     0.000
0.000
*DEFINE_CURVE_SMOOTH_TITLE
displacement
$#    lcid      sidr      dist    tstart      tend     trise        v0
         1         0  1.000000     0.000  2.000000  0.100000     0.000
*DEFINE_CURVE_TITLE
Forskyvning steg for steg
$#    lcid      sidr       sfa       sfo      offa      offo    dattyp
         2         0  1.000000  1.000000     0.000     0.000         0
$#                a1                  o1
               0.000               0.000
           0.1000000           0.0100000
           1.5000000           1.0000000
           1.6000000           1.0000000
*DEFINE_CURVE_TITLE
Swich impl/expl
$#    lcid      sidr       sfa       sfo      offa      offo    dattyp
         3         0  1.000000  1.000000     0.000     0.000         0
$#                a1                  o1
               0.000           1.0000000
           0.4000000           1.0000000
           0.4100000               0.000
           2.0000000               0.000
*DEFINE_CURVE_TITLE
```

```
compression
$#    lcid      sidr       sfa       sfo      offa      offo    dattyp
        11         0  1.000000  1.000000     0.000     0.000         0
$#              a1                  o1
           0.0209320               0.000

          ...

*DEFINE_CURVE_TITLE
tensile
$#    lcid      sidr       sfa       sfo      offa      offo    dattyp
        12         0  1.000000  1.000000     0.000     0.000         0
$#              a1                  o1
           0.0209320               0.000

           ...

*DAMPING_FREQUENCY_RANGE
$#   cdamp      flow     fhigh      psid
  0.100000 1.0000E-6  1.000000         0
*ELEMENT_SHELL
$#   eid     pid      n1      n2      n3      n4      n5      n6      n7
n8
    4801       1    5005    5026    5027    5006       0       0       0
0

           ...

*NODE
$#   nid               x               y               z      tc      rc
    5005      76.0000000      56.0000000           0.000       0       0

          ...

*END
*COMPONENT
$#    clid    color1    color2    color3    color4
         1  0.769000  0.004000  0.110000     0.000         0         0
0
$# name
Part 1
*COMPONENT_PART
$#     pid      clid
         1         1
*COMPONENT_END
```